UPPSALA
UNIVERSITET

Digital Comprehensive Summaries of Uppsala Dissertations from the Faculty of Science and Technology 1062

Structural, Electronic and Mechanical Properties of Advanced Functional Materials

MUHAMMAD RAMZAN

ACTA
UNIVERSITATIS
UPSALIENSIS
UPPSALA
2013

ISSN 1651-6214
ISBN 978-91-554-8723-2
urn:nbn:se:uu:diva-205243

Dissertation presented at Uppsala University to be publicly examined in Polhemsalen, Ångströmlaboratoriet, Lägerhyddsvägen 1, Uppsala, Friday, September 27, 2013 at 10:15 for the degree of Doctor of Philosophy. The examination will be conducted in English.

Abstract
Ramzan, M. 2013. Structural, Electronic and Mechanical Properties of Advanced Functional Materials. Acta Universitatis Upsaliensis. *Digital Comprehensive Summaries of Uppsala Dissertations from the Faculty of Science and Technology* 1062. 98 pp. Uppsala. ISBN 978-91-554-8723-2.

The search for alternate and renewable energy resources as well as the efficient use of energy and development of such systems that can help to save the energy consumption is needed because of exponential growth in world population, limited conventional fossil fuel resources, and to meet the increasing demand of clean and environment friendly substitutes. Hydrogen being the simplest, most abundant and clean energy carrier has the potential to fulfill some of these requirements provided the development of efficient, safe and durable systems for its production, storage and usage.

Chemical hydrides, complex hydrides and nanomaterials, where the hydrogen is either chemically bonded to the metal ions or physiosorbed, are the possible means to overcome the difficulties associated with the storage and usage of hydrogen at favorable conditions. We have studied the structural and electronic properties of some of the chemical hydrides, complex hydrides and functionalized nanostructures to understand the kinetics and thermodynamics of these materials.

Another active field relating to energy storage is rechargeable batteries. We have studied the detailed crystal and electronic structures of Li and Mg based cathode materials and calculated the average intercalation voltage of the corresponding batteries. We found that transition metal doped MgH_2 nanocluster is a material to use efficiently not only in batteries but also in fuel-cell technologies.

MAX phases can be used to develop the systems to save the energy consumption. We have chosen one compound from each of all known types of *MAX* phases and analyzed the structural, electronic, and mechanical properties using the hybrid functional. We suggest that the proper treatment of correlation effects is important for the correct description of Cr_2AlC and Cr_2GeC by the good choice of Hubbard 'U' in DFT+U method.

Hydrogen is fascinating to physicists due to predicted possibility of metallization and high temperature superconductivity. On the basis of our ab initio molecular dynamics studies, we propose that the recent claim of conductive hydrogen by experiments might be explained by the diffusion of hydrogen at relevant pressure and temperature.

In this thesis we also present the studies of phase change memory materials, oxides and amorphization of oxide materials, spintronics and sulfide materials.

Keywords: DFT, Hydrogen storage, Rechargeable batteries, Amorphization, Electronic structure, Crystal strcuture, Molecular dynamics, Diffusion, Intercalation voltage, High pressure, MAX phases, Mechanical properties, Optical properties, Phase change memory, Spintronics, Magnetism, Correlation effects, Band structure

Muhammad Ramzan, Uppsala University, Department of Physics and Astronomy, Materials Theory, Box 516, SE-751 20 Uppsala, Sweden.

ISSN 1651-6214
ISBN 978-91-554-8723-2
urn:nbn:se:uu:diva-205243 (http://urn.kb.se/resolve?urn=urn:nbn:se:uu:diva-205243)

To my daughter Fatima, for completing my life

Cover illustration: *An illustration of the melting curve of hydrogen [1]. The circles represent the melting P-T points computed in this study by the Z method. The sharp P changes at 852 K, 652 K, 567 K and 482 K, for C2c at 210 GPa, Cmca-12 at 260 GPa, Cmca-12 at 305 GPa, and Cmca-12 at 350 GPa, respectively. Already and recent measured and/or calculated data is also included for comparison taking from literature when available.*

List of papers

This thesis is based on the following papers, which are referred to in the text by their Roman numerals.

I **Structural and energetic analysis of the hydrogen storage materials $LiNH_2BH_3$ and $NaNH_2BH_3$ from *ab initio* calculations**
Muhammad Ramzan, Fredrik Silvearv, Andreas Blomqvist, Ralph H. Scheicher, Sèbastien Lebègue and Rajeev Ahuja
Phys. Rev. B **79**, 132102 (2009).

II **High pressure phase determination and electronic properties of lithiumamidoborane**
Muhammad Ramzan, Tanveer Hussain and Rajeev Ahuja
Appl. Phys. Lett. **101**, 111902 (2012).

III **High pressure and temperature study of hydrogen storage material BH_3NH_3 from *ab initio* calculations**
Muhammad Ramzan and Rajeev Ahuja
J. Phys. Chem. Solid. **71**, 1137 (2010).

IV **Electronic Structure from First-Principles of $LiBH_4.NH_3$, $Sr(NH_2BH_3)_2$ and $Li_2Al(BH_4)_5{\cdot}6NH_3$ for Hydrogen Storage Applications**
Muhammad Ramzan, Fredrik Silvearv, Sèbastien Lebègue and Rajeev Ahuja
J. Phys. Chem. C **115**, 20036 (2011).

V **Hybrid Density Functional and Molecular Dynamics Study of Promising Hydrogen Storage Materials: Double Metal Amidoboranes and Metal Amidoborane Ammoniates**
Muhammad Ramzan and Rajeev Ahuja
J. Phys. Chem. C **116**, 17351 (2012).

VI *Ab initio* **molecular dynamics study of the hydrogen-deuterium exchange in bulk lithiumborohydride ($LiBH_4$)**
Muhammad Ramzan and Rajeev Ahuja
Appl. Phys. Lett. **94**, 141903 (2009).

VII *Ab initio* **molecular dynamics study of the hydrogen diffusion in sodium and lithium hydrides**
Muhammad Ramzan and Rajeev Ahuja
J. Appl. Phys. **106**, 016104 (2009).

VIII **Hydrogen diffusion in bulk and nanoclusters of MgH_2 and the role of catalysts on the basis of *ab initio* molecular dynamics**
Muhammad Ramzan, Tanveer Hussain and Rajeev Ahuja
Appl. Phys. Lett. **94**, 221910 (2009).

IX **Transition metal doped MgH_2: A material to potentially combine fuel-cell and battery technologies**
Muhammad Ramzan, Sèbastien Lebègue and Rajeev Ahuja
Int. J. Hydrogen Energy **35** 10373 (2010).

X **Calcium doped graphane as a hydrogen storage material**
T. Hussain, B. Pathak, Muhammad Ramzan, T. A. Maark, and R. Ahuja
Appl. Phys. Lett. **100**, 183902 (2012).

XI **Functionalization of graphane with alkali and alkaline-earth metals: An insulator-to-metallic transition**
T. Hussain, B. Pathak, T. A. Maark, Muhammad Ramzan and R. Ahuja
Eur. Phys. Lett. **99**, 47004 (2012).

XII **Electronic structure and metalization of a silane-hydrogen system under high pressure investigated using density functional and GW calculations**
Muhammad Ramzan, Sèbastien Lebègue and Rajeev Ahuja
Phys. Rev. B **81**, 233103 (2010).

XIII **Semimetallic dense hydrogen above 260 GPa**
Sèbastien Lebègue, C. Moysés Araújo, D. Y. Kim, Muhammad Ramzan, H.-K. Mao and Rajeev Ahuja
Proc. Natl. Acad. Sci. USA (PNAS) **109**, 9766 (2012).

XIV **Atomic Diffusion in Solid Molecular Hydrogen**
Anatoly B. Belonoshko, Muhammad Ramzan, Ho-kwang Mao and Rajeev Ahuja
Nature Sci. Rep. **3**, 2340 (2013).

XV *Ab initio* **study of lithium and sodium iron fluorophosphate cathodes for rechargeable batteries**
Muhammad Ramzan, Sèbastien Lebègue and Rajeev Ahuja
Appl. Phys. Lett. **94**, 151904 (2009).

XVI **Ferromagnetism in the potential cathode material $LiNaFePO_4F$**
Muhammad Ramzan and Rajeev Ahuja
Eur. Phys. Lett. **87**, 18001 (2009).

XVII **Structural, magnetic, and energetic properties of Na_2FePO_4F, Li_2FePO_4F, $NaFePO_4F$, and $LiFePO_4F$ from *ab initio* calculations**
Muhammad Ramzan, Sèbastien Lebègue, Peter Larsson and Rajeev Ahuja
J. Appl. Phys. **106**, 043510 (2009).

XVIII **Crystal and electronic structures of lithium fluorosulphate based materials for lithium-ion batteries**
Muhammad Ramzan, Sèbastien Lebègue, and Rajeev Ahuja
Phys. Rev. B **82**, 125101 (2010).

XIX **Hybrid Density Functional Calculations and Molecular Dynamics Study of Lithium Fluorosulphate, A Cathode Material for Lithium-Ion Batteries**
Muhammad Ramzan, Sèbastien Lebègue, Tae W. Kang and Rajeev Ahuja
J. Phys. Chem. C **115**, 2600 (2011).

XX **The electronic structure and the metal-insulator transition of $Mg_2Mo_6S_8$**
T. Kaewmaraya, Muhammad Ramzan, J. M. Osorio Guillén, and Rajeev Ahuja
(*In manuscript*)

XXI **Electronic structure of $MgCuMo_6S_8$**
Muhammad Ramzan and Rajeev Ahuja
(*In manuscript*)

XXII **Hybrid exchange-correlation functional study of the structural, electronic, and mechanical properties of the *MAX* phases**
Muhammad Ramzan, Sèbastien Lebègue, and Rajeev Ahuja
Appl. Phys. Lett. **98**, 021902 (2011).

XXIII **$M_{N+1}AX_N$ (M=Ti, A=Al, X=H) phase class materials with hydrogen: Ti_4AlH_3 and Ti_3AlH_2**
Muhammad Ramzan and Rajeev Ahuja
Appl. Phys. Lett. **96**, 261906 (2010).

XXIV **Correlation effects in the electronic and structural properties of Cr_2AlC**
Muhammad Ramzan, Sèbastien Lebègue, and Rajeev Ahuja
Phys. Stat. Sol. (RRL) **5**, 122 (2011).

XXV **Electronic and mechanical properties of Cr_2GeC with hybrid functional and correlation effects**
Muhammad Ramzan, Sèbastien Lebègue, and Rajeev Ahuja
Solid. Stat. Commun. **152**, 1147 (2012).

XXVI **Anomalous temperature dependence of elastic constant c_{44} in V, Nb, Ta, Pd, and Pt**
L. Huang, Muhammad Ramzan, L. Vitos, B. Johansson and R. Ahuja
J. Phys. Chem. Solid. **71**, 1065 (2010).

XXVII **Probing temperature-induced ordering in supersaturated $Ti_{1-x}Al_xN$ coatings by electronic structure**
C. Århammar, J. L. Endrino, Muhammad Ramzan, D. Horwat, Andreas Blomqvist, J-E. Rubensson, J. Andersson and R. Ahuja
(*Submitted to CVD-Journal Special Issue*)

XXVIII **Structural characterization of amorphous $YCrO_3$ from first principles**
Raquel Lizàrraga, Muhammad Ramzan, Carlos Moysés Araújo, Andreas Blomqvist, Rajeev Ahuja and Erik Holmström
Eur. Phys. Lett. **99**, 57010 (2012).

XXIX **Disorder-induced Room Temperature Ferromagnetism in Glassy Chromites**
Carlos Moysés Araújo, Sandeep Nagar, Muhammad Ramzan, R. Shukla, O. D. Jayakumar, A. K. Tyagi, Yi-Sheng Liu, Jeng-Lung Chen, Per-Anders Glans, Chinglin Chang, Andreas Blomqvist, Raquel Lizàrraga, Erik Holmström, Lyubov Belova, Jinghua Guo, Rajeev Ahuja and K. V. Rao
(*Under review in APL*).

XXX **Electronic density of states of amorphous vanadium pentoxide films: Electrochemical measurements and density functional theory calculations**
Iliana Lykissa, Shu-Yi Li, Muhammad Ramzan, Rajeev Ahuja, Claes G. Granqvist and Gunnar A. Niklasson
(*In manuscript*).

XXXI **Optical reflectivities of $Gd_3Ga_5O_{12}$ at $\sim$ TPa (10 Mbar) shock pressures**
W. J. Nellis, N. Ozaki, T. Mashimo, Muhammad Ramzan, T. Kaewmaraya, and R. Ahuja
(*In manuscript*).

XXXII **Electronic, mechanical and optical properties of Y_2O_3 with hybrid density functional (HSE06)**

Muhammad Ramzan, Y. Li, R. Chimata and R. Ahuja
Comput. Mater. Sci. **71**, 19 (2013).

XXXIII **Electronic structure, mechanical and optical properties of In_2O_3 with hybrid density functional (HSE06)**
Muhammad Ramzan, Yunguo Li, and R. Ahuja
(*Accepted for publication in SSC*).

XXXIV **Surface states and ferromagnetism in crystalline $YCrO_3$**
Muhammad Ramzan, Y. Li, C. Moysés Araújo and R. Ahuja
(*In manuscript*).

XXXV **High Pressure Phase Transition and Electronic, Mechanical Properties of Ferroelectric Material: $PbTiO_3$**
Muhammad Ramzan, P. Liu and R. Ahuja
(*In manuscript*).

XXXVI **Atomistic study of promising catalyst and electrode material for memory capacitors: Platinum Oxides**
T. Kaewmaraya, Muhammad Ramzan, W. Sun, M. Sagynbaeva and Rajeev Ahuja
(*Accepted for publication in Comput. Mater. Sci.*).

XXXVII **High pressure, mechanical, and optical properties of ZrW_2O_8**
Muhammad Ramzan, W. Luo and R. Ahuja
J. Appl. Phys. **109**, 033510 (2011).

XXXVIII **Molecular dynamics study of amorphous Ga-doped In_2O_3: a promising material for phase change memory devices**
Muhammad Ramzan, T. Kaewmaraya, and R. Ahuja
Appl. Phys. Lett. **103**, 072113 (2013).

XXXIX **Hybrid density functional study of electronic and optical properties of phase change memory material: $Ge_2Sb_2Te_5$**
Thanayut Kaewmaraya, Muhammad Ramzan, H. Löfås, and Rajeev Ahuja.
J. Appl. Phys. **113**, 033510 (2013).

XL **Pressure-Induced and Mn Content Driven Phase Transitions in Ternary Chalcopyrite**
A. Yu. Mollaev. K. Kamilov, R. K. Arslanov, L. Kilanski, S. López-Moreno, Muhammad Ramzan, P. Panigrahi, R. Ahuja, I. O. Troyanchuk, V. M. Trukhan, V. M. Novotortsev, S. F. Marenkin, and T. R. Arslanov.
(*In manuscript*)

XLI **Role of correlation effects in the superconducting material: InV_6S_8**
Muhammad Ramzan and Rajeev Ahuja
Appl. Phys. Lett. **99**, 221904 (2011).

The following papers are co-authored by me but are not included in this thesis.

- **Tweaking the magnetism in MoS_2 nanoribbon with hydrogen and carbon passivation**
  M. Sagynbaeva, P. Panigrahi, Y. Li, Muhammad Ramzan and R. Ahuja
  (*In manuscript*).

- **Electronic, mechanical and optical properties of Cr_2O_3 with hybrid functional**
  Muhammad Ramzan, Y. Li, and R. Ahuja
  (*In manuscript*)

- **Study of the high pressure phase transitions and electronic structure of CeRuPO**
  Muhammad Ramzan, T. Kaewmaraya, M. Sagynbaeva and R. Ahuja
  (*In manuscript*).

- **Band gap closure in NiO at extreme pressures**
  Muhammad Ramzan, Y. Li and R. Ahuja
  (*In manuscript*).

- **Structural and electronic properties of high pressure phases of Co_2O_3**
  T. Kaewmaraya, P. Panigrahi, Muhammad Ramzan, M. Sagynbaeva and R. Ahuja
  (*In manuscript*) .

- **Structural and electronic properties of stable phases of PdO**
  W. Sun, T. Kaewmaraya, Muhammad Ramzan, and Rajeev Ahuja
  (*In manuscript*).

- **Metallization of carbon at very high pressures**
  Muhammad Ramzan, Y. Li and R. Ahuja
  (*In manuscript*).

- **Insight into BiI_3 surfaces from first principles calculations**
  T. Kaewmaraya, Wei Luo, Muhammad Ramzan and R. Ahuja
  (*In manuscript*).

- **Structural and electronic properties of high pressure phases of $BiFeO_3$**
  Muhammad Ramzan, Thanayut Kaewmaraya and Rajeev Ahuja
  (*In manuscript*).

- **The study of the underlying physics of light induced spin-crossover magnet with the use of hybrid functionals**
  Muhammad Ramzan, S. Lebegue and R. Ahuja
  (*In manuscript*)

- **Molecular dynamics study and electronic structure of lithium based superionic conductor promising for rechargeable batteries**
  Muhammad Ramzan, Thanayut Kaewmaraya and Rajeev Ahuja
  (*In manuscript*).

- **Mechanical and optical properties of CrN**
  Muhammad Ramzan, Thanayut Kaewmaraya, M. Sagynbaeva and Rajeev Ahuja
  (*In manuscript*).

Details of my contributions

In those papers where I am the first author, I took the main responsibility to design the research, perform calculations, analyzing the data and writing the papers. However, my contribution is being indicated by the following table.

Papers	designing research	performing calculations	analyzing data	writing the paper
I	x	x	x	x
II	x	x	x	x
III	x	x	x	x
IV	x	x	x	x
V	x	x	x	x
VI	x	x	x	x
VII	x	x	x	x
VIII	x	x	x	x
IX	x	x	x	x
X			x	x
XI			x	x
XII	x	x	x	x
XIII	x	x	x	x
XIV	x	x	x	x
XV	x	x	x	x
XVI	x	x	x	x
XVII	x	x	x	x
XVIII	x	x	x	x
XIX	x	x	x	x
XX	x	x	x	x
XXI	x	x	x	x
XXII	x	x	x	x
XXIII	x	x	x	x
XXIV	x	x	x	x
XXV	x	x	x	x
XXVI			x	x
XXVII		x	x	x
XXVIII	x	x	x	x
XXIX	x	x	x	x
XXX	x	x	x	x
XXXI	x	x	x	x
XXXII	x	x	x	x
XXXIII	x	x	x	x
XXXIV	x	x	x	x
XXXV	x	x	x	x
XXXVI	x	x	x	x
XXXVII	x	x	x	x
XXXVIII	x	x	x	x
XXXIX	x	x	x	x
XL		x	x	x
XLI	x	x	x	x

Contents

1. Introduction

The discovery, design and development of new materials is important for the progress of mankind because of the close and strong connection between the historical evolution of manhood and materials which demands a comprehensive understanding of the nature of matter. A network of computers to perform quantum mechanical calculations and simulations is one of the tools to enhance and improve our knowledge about materials. Being a fundamental tool for materials research because theoretical interpretations are needed to explain the experimental measurements as well as the limitations of contemporary experimental techniques to obtain certain required conditions, such as extreme pressure and/or temperature and/or to obtain the crystal and electronic structures of some materials, the interest in computational materials science is increasing rapidly in the scientific and industrial communities.

In condensed matter theory, an independent and reliable source of data, can be provided by means of first principles calculations. At the quantum mechanical level, density functional theory (DFT) is playing an important role to perform much more accurate simulations of materials than previous approximate theories, such as calculations of structural, electronic, mechanical, magnetic, and optical properties of solids. Therefore, it has become a popular demand of the time to acquire much more accurate results comparable with experiments by means of state of the art theoretical predictions.

Hydrogen, being the most abundant, lightest and simplest element (consisting of one electron and one proton only) in the universe, due to the predicted possibility of dissociation of solid hydrogen into an atomic metal around 25 GPa by Wigner and Huntington [2] and that the metallic hydrogen might be a promising material for high temperature superconductivity [3], is one of the most studied material, theoretically and experimentally [4, 5, 6, 7, 8, 9, 10, 11, 12, 13, 14, 15]. Recently, conductive hydrogen at room temperature and around 260-270 GPa has been reported by Eremets *et al.* [16], however they could not identify the crystal structure of hydrogen and suggested the need for further comprehensive study of their findings, proposing that it might be the Cmca-12 phase of Pickard and Needs [14]. In contrast, some very recent studies could not confirm these findings [17, 18, 19]. In such a complicated situation, computational studies become important to investigate the possible causes of difference between these findings. Therefore, we have employed density functional theory and GW approximation to explore the phase seen by Eremets *et al.* [16], by considering the four phases ($C2/c$, $Cmca$-12, $C2$, and $Pbcn$) found by Pickard and Needs for the 200-300 GPa range of pressure [14]

and compared the values of their band gaps closure under pressure. We have also performed *ab initio* molecular dynamics simulations to study the impact of temperature on the structures predicted to be stable at relevant pressure and zero temperature. For this purpose, the phases relevant to the range of pressures in recent experiments ($C2/c$, $Cmca$-12) were chosen for our studies.

The search for alternate, renewable, safe, and environment friendly energy resources are required to meet the recent and future demands of energy because of the depletion of conventional fossil fuel resources, rapid increase in world population, and luxurious life style of the people of developed countries [20]. Hydrogen being the most abundant and simplest element in universe can serve this purpose if it can be produced, stored and used efficiently [20]. In this thesis, we are going to present our studies on hydrogen storage materials. The required hydrogen storage system should have high gravimetric and volumetric hydrogen density, a reversible hydrogen uptake/release at around ambient conditions, and fast reaction kinetics, to meet the requirements of mobile applications [21]. The candidates for hydrogen storage materials can be classified as: conventional metal hydrides, chemical hydrides, complex hydrides, and sorbent materials [21]. Complex hydrides like, $LiBH_4$, generally have high gravimetric and volumetric capacities and are potential candidates for hydrogen storage systems, whereas, chemical hydrides have high gravimetric capacities but low volumetric capacities, although the NH_3BH_3 has modest volumetric capacity [21]. The search for new materials with improved hydrogen capacities and with favorable hydrogen reaction thermodynamics has been the main focus of research in chemical and complex hydrides [21]. Recently, new chemical hydrides like, amidoboranes, $LiBH_4.NH_3$ and $NaLi(NH_2BH_3)_2$ have been synthesized, which have high gravimetric and volumetric capacities. Catalysts can be used to improve the kinetics of chemical and complex hydrides. Reducing particle size/nanosizing has also been proved an effective way to improve the hydrogen reaction kinetics, decreasing the hydrogen desorption temperatures and to eliminate the unwanted species in complex hydrides [22]. *Ab initio* molecular dynamics simulations can be performed to analyze and understand the chemistry of bond breaking and formation, and hydrogen dissociation and recombination at materials surfaces in these systems [23]. The sorbent systems have excess gravimetric capacity depending upon the specific surface area of the sorbent, however, high volumetric capacity is difficult to prove in these systems [21]. We have analyzed the crystal and electronic structures and/or diffusion of hydrogen in the following promising materials for hydrogen storage applications: BH_3NH_3, $LiNH_2BH_3$, $NaNH_2BH_3$, $LiBH_4.NH_3$, $Sr(NH_2BH_3)_2$, $Li_2Al(BH_4)_5{\cdot}6NH_3$, $Na_2Mg(NH_2BH_3)_4$, $NaLi(NH_2BH_3)_2$, $Mg(NH_2BH_3)_2{\cdot}NH_3$, $Ca(NH_2BH_3)_2{\cdot}2NH_3$, $LiBH_4$, LiH, NaH, bulk and nanoclusters of MgH_2, calcium doped graphane, and $SiH_4(H_2)_2$.

Rechargeable batteries is another active area of research related to energy storage solution. Because of the rapid increase in the usage of portable electronic devices, this technology is growing exponentially. Rechargeable lithi-

um ion batteries have become more attractive for research because of the wide range of applications and the development of the portable electronic devices, such as cell phones, laptops, digital cameras and medical equipment due to small size and light weight than other types of batteries [24, 25, 26, 27, 28]. They are also promising to use as important power sources for future electric, hybrid vehicles and developing smart grids and it can lead us to electric vehicle revolution [29, 30, 31, 32]. The main challenge for electrochemistry research is the development of such type of environment friendly batteries, which can store sustainable energy with long term stability and have prolonged cycle life [33]. Hence, nowadays, the primary focus of the research is to develop new materials for rechargeable batteries.

Silicates and phosphates are considered suitable materials for rechargeable batteries, namely lithium iron phosphate has been known one of the most promising cathode material [34, 35]. Good safety features, low cost, low environmental impact, around 170 mAh/g theoretical capacity and 3.5 Volts intercalation voltage makes them advantageous over other cathode materials [36]. However, one dimensional lithium ion transport and two phase redox reaction are the limits of this material [37, 38, 39, 40]. As a step forward, Eliss *et al.* have reported sodium iron fluoro-phosphate and lithium iron fluoro-phosphate to be promising cathode materials for Na-ion and Li-ion batteries [41]. Recently, Recham *et al.* [42] have explored an other promising cathode material namely, $LiFeSO_4F$ for a lithium-ion battery and measured that the corresponding battery can deliver a slightly higher voltage (3.6 Volts) than the one made with $LiFePO_4$. Carbon coating or nanosizing was also not necessary for this material to obtain an efficient battery. We have presented our results obtained by means of ab-initio calculations concerning the ground-state properties and the crystal structures of Na_2FePO_4F, Li_2FePO_4F, $LiNaFePO_4F$, $NaFePO_4F$, $LiFePO_4F$, $LiFeSO_4F$ and $FeSO_4F$ in order to obtain the corresponding electronic structure, magnetic order, and the intercalation voltage of these materials, as well as, a study of the related materials [43, 44] $LiCoSO_4F$ and $LiNiSO_4F$. We have also studied Mg based cathode materials promising for rechargeable batteries namely, $Mg_2Mo_6S_8$ and $MgCuMo_6S_8$. Following some recent experiments [45], we have studied the Li diffusion in the clusters of MgH_2. In an effort to combine battery and fuel-cell technologies, we have analyzed the diffusion properties of Li in (Fe, Ni, Ti, and V) doped nanoclusters of MgH_2. We have found that the presence of the transition metals, that decrease the desorption energy of hydrogen in MgH_2, does not affect the diffusion properties of Li in the cases of Fe and V doping, and thus the device remains suitable for the batteries technology, as well as being a promising material for hydrogen storage.

The discovery of light weight and such promising materials that are able to tolerate high temperatures, readily machinable, electrically and thermally conductive, helpful to increase the fuel burning engines efficiency and reduce the energy consumption and cost, is strongly needed [46, 47]. *MAX* phases are

unique compounds that have the potential to fulfill all these demands, resembling both metallic and ceramic properties at the same time [47]. Generally, *MAX* phase compounds are denoted by the formula $M_{n+1}AX_n$, where *M* is an early transition metal, *A* is IIIA or IVA group element and *X* is either C and /or N and n=1, 2, or 3 [46, 47]. In literature (to the best of our knowledge), more than 50 compounds with n=1 (211- type *MAX* phases), five compounds with n=2 (312- type *MAX* phases) and five compounds with n=3 (413- type *MAX* phases) have been reported to date. Previously, the properties of the MAX phases have been analyzed by means of density functional theory with the use of conventional exchange-correlation potentials namely, the local density approximation (LDA) and/or the generalized gradient approximation (GGA). However, on the overall, these approximations could not reproduce well the structural parameters, the electronic structure and the mechanical properties measured by experiments for a large range of MAX phases. Thus, these approximations have a limited capability to predict more properties for the same family of compounds. We have used HSE06 hybrid functional to calculate the electronic, structural, and mechanical properties of Ti_2AlN, Ti_2AlC, V_2AlC, Nb_2AlC, Ta_2AlC, V_2GeC, Ti_3SiC_2 and Ti_4AlN_3, that are comprises on each class, i.e.; 211, 312, and 413 of the *MAX* phases and our results are presented in this thesis. We have predicted a new type of *MAX* phase consisting of hydrides in their composition as a substitute for C or N. We have also studied the other *MAX* phase materials namely, Cr_2AlC and Cr_2GeC.

Amorphous materials are attaining growing interest of scientific and industrial communities because of their electronic, mechanical, optical, and magnetic properties which are mostly superior to their crystalline counterparts. Altering multifunctional physical-chemical properties of oxide thin films is another growing, and challenging area of interest in materials science [48]. Search for multiferroic materials with co-existing room temperature ferromagnetism and ferroelectricity is one of the most interesting area of research activity nowadays to develop devices which can be controlled by both magnetic and electric potentials [49]. To explore the effects of amorphization on the magnetic structure of a material is important because many physical properties of solids, especially, magnetism are closely related to the local atomic structure of the material. The crystalline $YCrO_3$ is a well known antiferromagnetic insulator with Neel temperature, TN $\approx$ 140 K, but in this thesis, we report a robust soft ferromagnetism above room temperature in amorphized $YCrO_3$ films obtained by Pulsed Laser deposition and we have combined advanced spectroscopic techniques with density functional theory calculations to investigate the underlying physics of this unusual phenomenon. In oxide films, disorder induced room temperature ferromagnetism is a novel effect, which deserves a special attention and might lead to many multifunctional technological applications.

The growing interest in thin films of V_2O_5, is due to the wide range of its applications [50], such as: the layered structure of vanadium pentoxide makes it an important intercalation material to use as a cathode material in Li-ion bat-

teries [51]; V_2O_5 and mixed V_2O_5-TiO_2, films can be used in electrochromic devices for smart windows [52, 53, 54]; Nanostructured films of vanadium pentoxide have shown high optical contrast between colored and bleached states [55]; gas sensors [56]; and detectors for infrared radiation [57]. We have measured the electron DOS of sputtered amorphous V_2O_5 thin films by a chronopotentiometry technique using intercalation of Li^+ ions. Then we have performed *ab initio* molecualr dynamics simulations to model the amorphous structure of V_2O_5 and calculated the density of states (DOS) of this amorphous structure. We have compared the measured DOS with theoretical calculated DOS for amorphized V_2O_5.

$Gd_3Ga_5O_{12}$ (GGG) has a cubic garnet structure at ambient. Mao *et al.* found that GGG becomes amorphous in a DAC at 88 GPa and transforms to a new high-pressure phase at the same pressure on laser heating to 1500 K. The high pressure phase in a DAC is cubic, consistent with a perovskite structure and stoichiometry of $(Gd_{0.75}Ga_{0.25})GaO_3$, and persists up to 180 GPa at 1500 K. High power laser shock waves were generated to measure Hugoniot points and optical reflectivity of $Gd_3Ga_5O_{12}$ (GGG) at shock pressures from 0.7 to 2.6 TPa. We also performed *ab initio* molecular dynamics simulations to construct the amorphous structures of $Gd_3Ga_5O_{12}$ (GGG) at extreme pressures and we have calculated and compared the corresponding electronic and optical properties of these amorphous structures with our experimental observations.

Oxide materials are very important because of several industrial applications. They can be used in optoelectronics, optics, microelectronics, solar cells, liquid crystal displays, light emitting diodes etc. Some oxides have a negative thermal expansion (NTE) and they can be used for electronic, defence, aerospace, automotive, and medical applications. Therefore, we have studied In_2O_3, Y_2O_3, $PbTiO_3$, ZrW_2O_8, PtO and PtO_2, $YCrO_3$ and our calculated results are presented in this thesis.

Phase change materials are generally exist in two structurally distinct solid phases namely, amorphous and crystalline phases [58]. Due to large differences in structure between the amorphous and the crystalline phases, mostly the amorphous and crystalline phases contain very different optical and electrical properties [58]. The data storage process is accompanied by rapid and reversible phase switching from an ordered crystalline state to a disordered amorphous state. Phase change memory (PCM) materials are potential candidates for rewritable data storage devices such as, CD-RW, DVD-RW and DVD-RAM. We have employed *ab initio* molecular dynamics simulations to construct the amorphous structure of gallium doped indium oxide and calculated the corresponding electronic properties of amorphous and crystalline structures. We have found that the band gap closure in amorphous structure corresponds to a semiconductor to metal transition in this material upon amorphization. We have also carried out density functional theory calculations to study the structural and electronic properties of another well known phase change memory material, i.e; $Ge_2Sb_2Te_5$.

The search for ferromagnetic ordering in dilute magnetic semiconductors (DMS) has also become another intensive area of research in recent years [59, 60, 61]. The main focus of this field is accompanied by possible spin transport properties having interesting device applications. Logic devices, spin light emitting diodes, optical isolators, non volatile memory, ultrasoft optical switches, and spin volve transistors are some examples of spintronic devices to familiarize the ferromagnetic properties in semiconductors at room temperature. DMS, semiconductors II-IV-V_2 doped with Mn, having chalcopyrite structure are considered promising material for the possibility of room temperature ferromagnetism. Therefore, we have studied the pressure induced and Mn content driven phase transitions in ternary chalcopyrite (Mn doped $CdGeP_2$) and our results have been discussed in the present thesis.

Because of unique physical and structural properties, binary vanadium sulfur compounds that are isostructural with the niobium chalcogenides and lie between the localized and delocalized d-electron materials, have also become more interesting materials in research community. We have performed high pressure calculations to analyze the structural parameters, electronic structure and band structures of superconducting material InV_6S_8. We find that the correct choice of Hubbard like correction is necessary to take into account the correlation effects in this material, which are important for the complete description of this compound. Furthermore, we could not find any anomaly in the lattice constants of InV_6S_8 in the high pressure calculations at extended range of pressures.

2. Density functional theory

The non relativistic Schrödinger equation is the basis of the electronic structure of matter for the many electron wave function: $\Psi(\mathbf{r}_1, \mathbf{r}_2, ..., \mathbf{r}_n)$, where the position and the spin of the particle i are represented by $\mathbf{r}_i$. Typically in a solid, we are dealing with 10^{23} particles, and we will have to solve Schrödinger equation for a number of electrons interacting with each other in the order of 10^{23}. If we work with only crystalline structures in solids and consider the symmetries like; translational, rotational, invertional, etc.; we still have to do a large number of calculations and it makes the problem very difficult.

An alternative technique to study the electronic structure of matter is density functional theory (DFT). The electron density distribution $n(\mathbf{r})$, depending only on three spatial coordinates and spin instead of the many electron wave function, plays an important role in the density functional theory (DFT). The theorems formulated by Hohenberg and Kohn (HK) [62], which were derived from the n-particle Schrödinger equation and finally expressed in terms of the electron density $n(\mathbf{r})$, are the foundations of density functional theory (DFT). However, later in Kohn and Sham formalism [63], it was expressed in terms of $n(\mathbf{r})$ and single particle wave function $\varphi(\mathbf{r})$. The much more accurate simulations of materials at the quantum mechanical level, compare with previous theories, can be performed using the density functional theory (DFT). Especially, in solid state physics, density functional theory (DFT) can be used to calculate the ground state energies, high pressure characteristics, and corresponding properties like; structural, electronic, optical, elastical, mechanical, magnetic properties and phase transitions, etc. The DFT will be introduced briefly here, a complete report can be found elsewhere [64].

2.1 The many body problem

The solution of Schrödinger equation in solid state theory is important to study the interacting electron-nucleus system, containing *n* electrons and *t* nuclei,

$$H_t \Psi(\mathbf{r}_1, \mathbf{r}_2, ..., \mathbf{r}_n, \mathbf{R}_1, \mathbf{R}_2, ..., \mathbf{R}_t) = E_{tot} \Psi(\mathbf{r}_1, \mathbf{r}_2, ..\mathbf{r}_n, \mathbf{R}_1, \mathbf{R}_2 ... \mathbf{R}_t) \quad (2.1)$$

with the Hamiltonian

$$H_t = -\sum_i \frac{h^2}{2m} \nabla_i^2 - \sum_I \frac{h^2}{2M_I} \nabla_I^2 + \frac{1}{2} \sum_{i \neq j} \frac{e^2}{|\mathbf{r}_i - \mathbf{r}_j|} - \sum_{i,I} \frac{Z_I e^2}{|\mathbf{r}_i - \mathbf{R}_I|} + \frac{1}{2} \sum_{I \neq J} \frac{Z_I Z_J e^2}{|\mathbf{R}_I - \mathbf{R}_J|}. \quad (2.2)$$

The Ist and 2nd terms in (2.2) denote the kinetic energy operators for the electrons and nuclei, respectively, whereas the 3rd, 4th and 5th terms correspond to the potential operators that describe the electron-electron, electron-nucleus and nucleus-nucleus interactions, respectively. The Eq.(2.1), with the Hamiltonian (2.2), can only be solved exactly for the hydrogen atom. For a helium atom, we will have to use approximation methods based on either the variational principle or perturbation theory. The solution of the Eq.(2.1), with the Hamiltonian (2.2) for solids, having a complex many-body problem, is very difficult and requires more levels of approximations.

2.2 Born-Oppenheimer approximation

The Born-Oppenheimer approximation is used to perform calculations in solid state physics. In this approximation, the nuclei and electrons are treated separately. Having much larger masses and much slower motion than electrons, the nuclei are considered frozen at their equilibrium positions. Therefore, the nuclei are taken as an external potential exerted on the electrons. By implementing the Born-Oppenheimer approximation, the total wave function is the product of the electronic and ionic wave functions and the electronic part can be achieved by solving the following Schödinger equation:

$$H_e\psi_e(\mathbf{r}_1, \mathbf{r}_2..., \mathbf{r}_n; \mathbf{R}_1, \mathbf{R}_2....\mathbf{R}_m) = E_e\psi_e(\mathbf{r}_1, \mathbf{r}_2..., \mathbf{r}_n; \mathbf{R}_1, \mathbf{R}_2....\mathbf{R}_m), \tag{2.3}$$

and the electronic Hamiltonian can be written as:

$$H_e = -\sum_i \frac{h^2}{2m}\nabla_i^2 + \frac{1}{2}\sum_{i\neq j}\frac{e^2}{|\mathbf{r}_i - \mathbf{r}_j|} - \frac{1}{2}\sum_{i,I}\frac{Z_I e^2}{|\mathbf{r}_i - \mathbf{R}_I|}. \tag{2.4}$$

The Born-Oppenheimer approximation is helpful to reduce the complexity of the system, but still there is problem to solve the electron-electron interaction, which is represented by the 2nd term of the Hamiltonian in (2.4). Thus, further approximations are required to solve the Eq.(2.3). To resolve such problems, many approaches like, Hartree-Fock method and the density functional theory (DFT) have been developed. But in this thesis, we will focus only on the density functional theory (DFT) in the following sections, as we have worked only with it.

2.3 The Hohenberg-Kohn theorems

As we have stated earlier, density functional theory (DFT) is based on the theorems introduced by Hohenberg and Kohn (HK) [62]:

Theorem 1: Every system of interacting particles has a one-to-one correspondence between the potential and the ground-state particle density $\rho_0(\mathbf{r})$ in

an external potential $V_{ext}(\mathbf{r})$. So, the ground-state expectation value of any observable is a unique functional of the ground-state particle density $\rho_0(\mathbf{r})$:

$$< \psi|A|\psi >= A[\rho_0(\mathbf{r})]. \tag{2.5}$$

The proof of this theorem can be found elsewhere [64]. However, this theorem can be explained as; the reconstruction of the system Hamiltonian is possible if the ground-state particle density is known and by solving the Schrödinger equation, to calculate the many body wave function. Thus, all observable quantities can be achieved in a unique way i.e; from the particle density only, which means that the density has enough information to replace the wave function.

Theorem 2: A universal total energy functional of the particle density can be defined for any external potential applied to an interacting particle system,

$$E[\rho(\mathbf{r})] = E_{HK}[\rho(\mathbf{r})] + \int V_{ext}(\mathbf{r})\rho(\mathbf{r})d\mathbf{r}, \tag{2.6}$$

where the term $E_{HK}[\rho(\mathbf{r})]$ consists of all internal energies of the interacting particle systems. The global minimum of the functional in (2.6) is the exact ground-state total energy of the system E_0 and the particle density which minimizes this functional is the exact ground-state density $\rho_0(\mathbf{r})$, i.e.;

$$\frac{\delta}{\delta\rho}E[\rho(\mathbf{r})]|_{\rho=\rho_0} = 0, \tag{2.7}$$

with

$$E_0 = E[\rho_0(\mathbf{r})]. \tag{2.8}$$

The first part of this theorem describes the universality of total energy functional. By construction, the term E_{HK}, has no information about the type of nuclei or their positions, representing a universal functional for the interacting electron system. Moreover, the contribution from the external potential to the total energy can also be calculated exactly, as the density operator is known. Variational principle is probably the most important part of this theorem. In this part, the total energy functional has a global minimum, which is the exact total energy of the ground-state. Furthermore, among the many possible electron densities, the one which minimizes the total energy functional is the exact ground-state density corresponding to the external potential. By implementing this theorem, the original formulation of the many-body problem (Eq.(2.3)) is possible to replace by something which can be solved easily. However, it's uses depends only on the known functional E_{HK} or a good approximation for it.

2.4 The Kohn-Sham equations

The Hohenberg-Kohn (HK) theorems can be applied within the formalism of Kohn and Sham (K-S) equations [63]. The central idea is to replace the interacting many-body problem with a corresponding non-interacting particle

system, in an appropriate external potential. In the Kohn and Sham (K-S) formalism, the total energy functional in atomic units can be described as:

$$E[\rho(\mathbf{r})] = T_0[\rho] + \frac{1}{2}\int\int \frac{\rho(\mathbf{r})\rho(\mathbf{r}')}{|\mathbf{r}-\mathbf{r}'|} d\mathbf{r}d\mathbf{r}' + \int V_{ext}(\mathbf{r})\rho(\mathbf{r})d\mathbf{r} + E_{xc}[\rho(\mathbf{r})] + E_{II}, \tag{2.9}$$

which is called the Kohn-Sham functional. The first, second and third terms in (2.9) represent the functionals for the kinetic energy of a non-interacting electron gas, the classical Coulomb contribution (Hartree term) for the electron-electron interaction and the external potential contribution because of nuclei and any other external potential, respectively. The term $E_{xc}[\rho(\mathbf{r})]$ consisting of all many-body effects of exchange and correlation, is called the exchange-correlation functional. Because of unknown analytical expression of this term, the implementation of the K-S functional depends on our capability to find a good approximation for it. The energy contribution from the interaction between the nuclei is represented by the term E_{II}. In the Kohn-Sham (K-S) functional the exact ground-state density is assumed to be same as the ground state density of non-interacting particle system. Therefore, it can be explained as the total energy functional of a non interacting particle system subject to two potentials: the external potential V_{ext} and an exchange correlation potential, V_{xc}.

It is deduced from the second theorem that the solution of the Kohn-Sham auxiliary system can be considered as the minimization problem of the K-S functional with respect to density $\rho(\mathbf{r})$, which can be written in the following Schrödinger-like equation, [63]:

$$\Big[-\frac{1}{2}\nabla^2 + V_{eff}(\mathbf{r})\Big]\psi_q(\mathbf{r}) = \epsilon_q\psi_q(\mathbf{r}), \tag{2.10}$$

consisting of the eigenvalues, ϵ_q, the K-S orbitals, $\psi_q(\mathbf{r})$ and the effective potential, $V_{eff}(\mathbf{r})$. The effective potential, $V_{eff}(\mathbf{r})$ can be defined as:

$$V_{eff}(\mathbf{r}) = V_{ext} + \int \frac{\rho(\mathbf{r}')}{|\mathbf{r}-\mathbf{r}'|} d\mathbf{r}' + V_{xc}, \tag{2.11}$$

and the exchange-correlation potential, V_{xc} can be described as:

$$V_{xc} = \frac{\delta E_{xc}[\rho]}{\delta\rho(\mathbf{r})}. \tag{2.12}$$

The exact ground-state density of a N-electron system by construction is defined by

$$\rho(\mathbf{r}) = \sum_q |\psi_q(\mathbf{r})|^{\mathbf{2}}. \tag{2.13}$$

The solution of the single-particle Kohn-Sham (K-S) equations can provide the exact ground-state density and energy of the many-body electron problem, by the assumption that the exchange-correlation potential defined in (2.12) is known.

2.5 Exchange-correlation functional approximations

The Kohn-Sham (K-S) equations have to be solved self consistently to obtain an accurate ground state electron density. The only unknown part in these equations is the exchange-correlation functional, $E_{xc}[\rho(\mathbf{r})]$. This unknown part must be approximated and in this section, we are going to discuss such approximations for the exchange correlation term.

2.5.1 Local density approximation

In atomic, molecular and solid state physics, different approximations have been used for the exchange-correlation functional, $E_{xc}[\rho(\mathbf{r})]$. One of the most popular and commonly used approximation is known as Local Density Approximation (LDA) [63];

$$E_{xc}[\rho(\mathbf{r})] = \int \rho(\mathbf{r})\epsilon_{xc}[(\rho(\mathbf{r}))]d\mathbf{r}, \tag{2.14}$$

where $\epsilon_{xc}[(\rho(\mathbf{r}))]$ is the exchange-correlation energy density of a jellium (homogeneous electron gas) with the density $\rho = \rho(\mathbf{r})$. Therefore, by assuming this approximation, the only requirement is the exchange-correlation energy of the jellium as a function of density. The exchange energy is a simple analytical form [65] and the correlation energy can be calculated very accurately with Quantum Monte Carlo method [66]. The Local Density Approximation (LDA) is considered to give reasonable results for slow varying density systems like; nearly-free-electron metals. It is also found to work well with semiconductors and insulators, however, the LDA tends to overestimate the ground state energy and bulk modulus; and underestimate the band gap values for these systems as compared to experimental data.

2.5.2 Generalized gradient approximation

Another important approximation, which is used to improve the deficiencies of Local Density Approximation (LDA), is known as the Generalized Gradient Approximation (GGA). The Generalized Gradient Approximation (GGA) is used to take into account the exchange-correlation energy density, consisting of density $\rho(\mathbf{r})$ and its gradient $\nabla\rho(\mathbf{r})$. The widely used GGA-functional are the ones of Perdew and Wang (PW91) [68] and Perdew, Burke and Enzerhof (PBE) [69]. The Generalized Gradient Approximation (GGA), usually give the more accurate results of the ground state energies, bulk modulus and band gap values than the Local Density Approximation (LDA). However, still further improvements are needed to get the correct results comparable with experimental values.

2.5.3 DFT+U

In strongly correlated materials, the Local Density Approximation (LDA) and/or the Generalized Gradient Approximation (GGA) are unable to take into account the Coulomb interaction correctly during the calculation of V_{xc} potential. Within these approximations, *d* and *f* electrons cannot be treated properly because of insufficient electron correlations. The Mott Hubbard insulators and 4f rare earth materials are predicted metals wrongly by using the LDA and GGA. To overcome this deficiency, the Hubbard parameter U is used to improve the description of the localized 3d or 4f states. This scheme is generally known as the DFT+U method, where U represents the Coulomb interaction term. A good choice of U parameter is important for the correct description of these correlated electron systems.

2.5.4 Hybrid density functional

The DFT+U method is efficient to treat the correlated electron systems, provided that a suitable value of U is chosen. An alternate approach to address this problem is the use of hybrid functionals. The hybrid method can be described by using a mixing coefficient a=1/4, derived from perturbation theory [70].

$$E_{xc}^{PBE0} = aE_x^{HF} + (1-a)E_x^{PBE} + E_c^{PBE}, \tag{2.15}$$

where E_{xc}^{PBE0} denotes the PBE0 exchange-correlation, E_x^{PBE}, PBE exchange part, E_c^{PBE}, PBE correlation part and E_x^{HF}, the HF exchange.

The PBE0 exchange functional can be written as

$$E_x^{PBE0} = aE_x^{HF} + (1-a)E_x^{PBE} \tag{2.16}$$

Furthermore, each component of exchange functional can be divided into short range and long range terms as:

$$\begin{aligned} E_x^{PBE0} &= aE_x^{HF,SR}(\omega) + aE_x^{HF,LR}(\omega) \\ &+ (1-a)E_x^{PBE,SR}(\omega) + E_x^{PBE,LR}(\omega) - aE_x^{PBE,LR}(\omega) \end{aligned} \tag{2.17}$$

Now using $\omega = 0.15$, which is a numerical tests based a realistic ω value, the long range PBE and HF exchange contributions become very small and tend to cancel each other. By neglecting these terms and assuming that this approximation may be compensated by other terms in the functional, we can obtain a Heyd, Scuseria and Ernzerhof (HSE) functional [71, 72, 73], which can be written as:

$$E_{xc}^{HSE} = aE_x^{HF,SR}(\omega) + (1-a)E_x^{PBE,SR}(\omega) + E_x^{PBE,LR}(\omega) + E_c^{PBE} \tag{2.18}$$

Hybrid density functional performs well to calculate the ground state, electronic, structural and optical properties for transition metals and rare earth f electron materials.

3. Electronic structure calculations

3.1 The Bloch electrons and plane wave basis set

The self consistent Kohn-Sham equations are useful to calculate the ground state electron density and ground state energy of the interacting electron system. In a K-S equation (2.10), the effective potential is periodic for a crystal, therefore the K-S orbitals can be defined as:

$$\psi^n_{\mathbf{k}}(\mathbf{r}) = u^n_{\mathbf{k}}(\mathbf{r})e^{i\mathbf{k}\cdot\mathbf{r}}, \tag{3.1}$$

which is known as Bloch theorem [74]. In the equation (3.1), **k** is a vector in the first Brillouin zone, whereas $u^n_{\mathbf{k}}(\mathbf{r})$ and $e^{i\mathbf{k}\cdot\mathbf{r}}$ represent the periodicity of the crystalline lattice and a plane wave, respectively. Thus, it is appropriate to find the wave function in the primitive cell. To solve the Kohn-Sham equation (3.1), the periodic function, $u^n_{\mathbf{k}}(\mathbf{r})$ can be expanded in a plane wave basis set, which will be the sum over plane waves of same periodicity. These plane waves are correspond to the reciprocal lattice vectors. Therefore, $\psi^n_{\mathbf{k}}(\mathbf{r})$ in this basis set can be expanded as:

$$\psi^n_{\mathbf{k}}(\mathbf{r}) = \frac{1}{\sqrt{\Omega_{cell}}} \sum_j c^n_j(\mathbf{k}) e^{i(\mathbf{k}+\mathbf{K_j})\cdot\mathbf{r}}, \tag{3.2}$$

where Ω_{cell} denotes the volume of the primitive cell, $\mathbf{K}_j$ are the reciprocal lattice vectors and n is the band index. If the plane wave basis set are limited by setting all **K** with $\mathrm{K} \leq \mathrm{K}_{max}$, the corresponding cut-off energy can be specified as:

$$E_{cut} = \frac{h^2 K^2_{max}}{2m}. \tag{3.3}$$

A finite number of electrons are required to take into account as each K point will occupy a finite number of energy levels. Although, there are an infinite number of k- points, but a few waves are appropriate to obtain the ground state energy of a solid, because: (i) The periodicity of the crystalline lattice needs to consider the k- points in the first Brillouin zone (BZ) only. (ii) Due to the rotational and inversion symmetries, the k- point subspace inside the BZ can be reduced. (iii) Therefore, a discrete number of k- points are enough to calculate the total energy. However, a higher energy cut-off and/or a denser k-points mesh are required to get the efficient results.

3.2 Pseudopotentials

In a periodic crystal of a solid, it is convenient to construct the wave function by using plane waves. The valence electrons are involved in the chemical bonding while the core electrons, being lower in energy, remain comparatively unchanged as compared to the rapid changes of the valence electrons. Thus, the "frozen core approximation" is implemented, in which the core electrons are considered stationary and in a plane wave basis set, the Kohn-Sham equations are solved for the valence states. Many plane waves, necessary to describe the atomic orbital like cores can be eliminated by replacing the true potential close to the core with a pseudopotential, which is effective to enhance the speed of the calculations.
The pseudopotentials should be soft, which allows the expansion of the valence wave functions by using a few plane waves. If the potentials for crystals and atoms are different, then the good transferability of the potential is very important for reliable calculations.

3.3 PAW method

One commonly used method to calculate the electronic structure calculations is projector augmented wave (PAW) method, which was developed by Blöchl [75] as implemented in the Vienna *ab initio* simulation package (VASP) [76, 77]. The projector augmented wave (PAW) method is a unique method which combines the properties of the ultrasoft pseudopotential approach [78] with the linear augmented plane wave (LAPW) method [79]. If plane wave and atomic orbital expansions are complete then the PAW approach is capable to calculate the density functional total energy efficiently. In the Vienna *ab initio* simulation package (VASP) [76, 77], for the PAW scheme, the "frozen core approximation" is implemented, which provides the correct densities and wave functions, facilitating us to calculate the other parameters of the system. Therefore, the PAW method can be efficiently used to study the solids, molecules and surfaces. Thus, we have used the projector augmented wave (PAW) approach in our most of the studies presented in this thesis to perform the electronic structure calculations and the geometry optimizations of different materials. The PAW method can be expressed as a linear transformation τ, of all electron wave functions ψ to the smooth functions $\widetilde{\psi}$:

$$|\psi >= \tau|\widetilde{\psi} >. \tag{3.4}$$

In which, the pseudo wave function can be expanded into pseudo partial waves, as given by:

$$|\widetilde{\psi} >= \sum_i C_i \mid \widetilde{\phi}_i > . \tag{3.5}$$

The all electron wave functions can be expanded by the relation:

$$|\psi >= \sum_i C_i \mid \phi_i > . \tag{3.6}$$

The solution of the radial Schrödinger equation for the isolated atom provides the all electron partial waves ϕ_i. The pseudo partial waves and all electron partial waves are equal outside the augmented region. Since the transformation in (3.4) is linear, so the pseudo partial waves $|\widetilde{\phi}_i >$ should be dual to a projector function $< \widetilde{p}_i|$, fulfilling the condition:

$$< \widetilde{p}_i|\widetilde{\phi}_j >= \delta_{i,j}. \tag{3.7}$$

We can obtain the transformation τ by combining the (3.5), (3.6) and (3.7):

$$\tau = \widehat{\mathbf{1}} + \sum_i (|\phi_i > -|\widetilde{\phi}_i >) < \widetilde{p}_i|. \tag{3.8}$$

Now, we can write the equation (3.4), in the following form:

$$|\psi >= |\widetilde{\psi} > + \sum_i (|\phi_i > -|\widetilde{\phi}_i >) < \widetilde{p}_i|\widetilde{\psi} > . \tag{3.9}$$

Thus, the Kohn-Sham equation can now be transformed as:

$$\tau^\dagger \widehat{H} \tau |\widetilde{\psi}_i >= \epsilon_p \tau^\dagger \tau |\widetilde{\psi}_i > . \tag{3.10}$$

Now the less plane waves will be enough for the correct description of the Kohn-Sham orbitals which will reduce the computational cost, provided that, we just use the plane waves basis set to solve the problem.

3.4 Optical properties

The electronic structures of materials can be well defined with the help of optical properties. In solid state physics, the optical properties like, absorption, reflection and transmission can be observed in solids. In bulk materials, the complex dielectric function is associated with band structures. The complex imaginary dielectric function $\varepsilon_2(\omega)$ can be obtained by summing over conduction bands [80]:

$$\varepsilon^{(2)}_{\alpha\beta}(\omega) = \frac{4\Pi^2 e^2}{\Omega} \frac{1}{q^2} \lim_{q\to 0} \sum_{c,v,k} 2w_k \delta(\epsilon_{ck} - \epsilon_{vk} - \omega) \times \langle u_{ck+e_\alpha q}|u_{vk}\rangle \langle u_{ck+e_\alpha q}|u_{vk}\rangle^* \tag{3.11}$$

In which the transitions are based on occupied to non-occupied states within the Ist Brillouin zone while the wave vectors are kept fixed **k**. In Kramers-Kronig relation, the real and imaginary parts of the dielectric function are coupled with each other in the following way:

$$\varepsilon_{\alpha\beta}^{(1)}(\omega) = 1 + \frac{2}{\Pi}\mathbf{P}\int_0^{\infty} \frac{\varepsilon_{\alpha\beta}^{(2)}(\omega')\omega'}{\omega'^2 - \omega^2 + i\eta} d\omega' \tag{3.12}$$

The reflectivity can be expressed as:

$$R\left(\omega\right) = \left|\frac{\sqrt{\varepsilon\left(\omega\right)} - 1}{\sqrt{\varepsilon\left(\omega\right)} + 1}\right|^2 \tag{3.13}$$

Now the Energy-loss spectrum, Refractive index and extinction coefficient formulas can be expressed as:

$$L\left(\omega\right) = \frac{\varepsilon_2(\omega)}{\varepsilon_1^2(\omega) + \varepsilon_2^2(\omega)} \tag{3.14}$$

$$n = \left[\frac{\sqrt{\varepsilon_1^2 + \varepsilon_2^2} + \varepsilon_1}{2}\right]^{\frac{1}{2}} \tag{3.15}$$

$$k = \left[\frac{\sqrt{\varepsilon_1^2 + \varepsilon_2^2} - \varepsilon_1}{2}\right]^{\frac{1}{2}}. \tag{3.16}$$

3.5 Molecular dynamics

Molecular dynamics (MD) is used to study the change in positions and velocities of particles in solids, liquids and gases with time and temperature. In condensed matter physics, molecular dynamics simulations are employed to compute the dynamical properties of materials at particular temperature and to calculate the time dependent properties such as mean square displacement and radial distribution function.

During molecular dynamics calculations, the second law of Newton is employed to study the motions of atoms:

$$\mathbf{F}_i = m_i \mathbf{a}_i, \tag{3.17}$$

where m_i is the mass of the atom, $\mathbf{a}_i$ is the acceleration and $\mathbf{F}_i$ is the force acting upon that atom for each item i in a system of *N* atoms.

Classical and *ab initio* molecular dynamics are the two main types of molecular dynamic simulations. The only difference in two methods is that in the classical molecular dynamics (CMD), the force is calculated through the generation of a model potential to simulate the manner of actual atoms, whereas, in *ab initio* molecular dynamics calculations the density functional theory calculations are employed to calculate such forces. In classical molecular dynamics

(CMD), large systems can be studied due to the consideration of simple interactions between atoms but the correct description of all the underlying physics such as charge transfer is very difficult due to the limitation in the correct modeling of potentials. However, in *ab initio* molecular dynamics (AIMD), the long computational time is required which limits the simulations to a few hundreds of atoms due to the computational cost, which is the only limitation of this method. There are two common methods to implement *ab initio* molecular dynamics (i) Car-Parinello MD (ii) Born-Oppenheimer MD. In Car-Parinello MD, the same algorithm is used to solve the dynamics of nuclei and quantum electronic problems, whereas in Born-Oppenheimer MD, the problem is divided into two parts i.e; the motion of the nuclei and the self consistent solution of Kohn-Sham equations for electrons.The advantages and disadvantages between the implementation of these two approaches can be found somewhere else [65]. In this thesis, the Born-Oppenheimer MD approach has been used to simulate the molecular dynamics calculations, which has been implemented in Vienna *Ab initio* Simulation Package (VASP). The molecular dynamics simulations are used to calculate the macroscopic properties and explore the dynamics of molecular systems. The system is initially equilibrated to perform the molecular dynamics calculations. The microcanonical ensemble (N, V and E), canonical ensemble (N,V and T), grand ensemble (μ,V, and T) and isothermal isobaric ensemble (N, P, and T) are used to fix the thermodynamic state, where N (the number of particles), V (volume of simulation box), E (total energy), T (temperature) and μ (chemical potential) represent the environmental variables. The data calculated from the molecular dynamics simulations can be analyzed through the use of some following tools. The radial distribution function (RDF) is an important *static* property of materials, which is usually extracted from the X-ray and neutron diffraction measurements, can also be simulated by MD calculations. The radial distribution function (RDF) can be computed by simulating the individual atomic positions as a function of time, which can be used to study the changes in the local atomic environment, number of nearest neighbours and to distinguish the molten, amorphous or crystalline systems. For example, in a liquid system, the RDF will be smoother. The following expression can be used to evaluate the RDF for the uniform substances:

$$g(r) = \frac{1}{N}\sum_{l=1}^{N} N_l(r)\rho 4\pi r^2(\Delta r), \tag{3.18}$$

where ρ is the average density of the system, N and $N_l(r)$ are the total number of atoms and number of atoms in the spherical cell having the radius larger than r and smaller than $r + \Delta r$ centered on atom l, respectively.

The dynamical properties of the system can also be obtained by simulating the individual atomic positions as a function of time by using the following

expression to evaluate the mean square displacement (msd):

$$msd = \Big\langle \sum_{i}^{N} [r_i(t) - r_i(0)]^2 \Big\rangle. \tag{3.19}$$

The msd is related to the diffusion coefficient D through the Einstein equation, which can be expressed as:

$$D = \frac{1}{6N} \lim_{t\to\infty} \frac{d}{dt} \Big\langle \sum_{i}^{N} [r_i(t) - r_i(0)]^2 \Big\rangle, \tag{3.20}$$

where N is the number of particles in the simulation box.

The bond angle distribution (BAD) can be used to analyze the local atomic structures of the systems. The angles between the nearest neighbours can be found by bond angle distribution (BAD) as given by:

$$g(\Theta) = \sum_{n=1}^{N} [N_n(\Theta), \tag{3.21}$$

where $N_n(\Theta)$ represent the number of atoms with the an angle Θ between the nearest neighbours. By increasing the temperature of the system, the sharp peaks become broaden and if there will be phase transition, it can be analyzed by the corresponding change in the band angle distribution (BAD) peaks.

4. Hydrogen and hydrogen storage materials

Solid hydrogen is an interesting material expecting to have unusual properties like: a sea of free electrons and superconductor at room temperature [3, 81], superfluidity at low temperatures [12, 13], uses as a rocket fuel [82] and/or a metallic conductor at ambient conditions [3]. On the other hand, hydrogen can also be used as energy carrier for alternate energy source and even for renewably, if it is obtained from water, however the efficient storage of hydrogen for mobile applications is the big challenge for scientific and industrial community [20].

In this chapter, we are going to present the summaries of our studies on these issues. In the first three sections the summaries of our studies on some forms of hydrogen storage and the possible solutions of the issues associated with these storage techniques are presented whereas the fourth section consists of the summaries of our studies on the metallization of hydrogen.

4.1 Light weight compounds for hydrogen storage

Chemical and complex hydrides typically have high gravimetric and volumetric capacities for instance NH_3BH_3 and $LiBH_4$ respectively, possess more than 10 wt% of hydrogen [83]. However, the poor thermodynamics, the poor kinetics of hydrogen uptake/release and reversibility are the major issues associated with this class of materials [20, 83]. Generally, the chemical hydrides having high gravimetric and volumetric density of hydrogen are produced by chemical reactions but these materials are not reversible for on board hydrogen systems [20, 83]. In the similar way, most of the complex hydrides, in which the hydrogen is covalently bonded with central atoms of complex anions, are reversible and also contain high gravimetric and volumetric capacities, but the poor hydrogenation/dehydrogenation kinetics are troublesome for these materials [20, 83]. In this section, we shortly address some possible techniques to understand and improve the thermodynamics and kinetics of these types of materials.

Ammonia borane (NH_3BH_3) is one of the promising chemical hydride that can release 19.6 wt% hydrogen depending on the conditions chosen for release, but the co-production of trace amounts of borazine, ammonia and diborane, during desorption process is the main hindrance of this material for practical application [84, 85]. These deficiencies can be improved either by substituting the one hydrogen atom by alkali metals or alkaline earth metals in the NH_3

group of ammonia to form the metal amidoboranes such as: $LiNH_2BH_3$ [86, 87], $NaNH_2BH_3$ [86, 88], $Ca(NH_2BH_3)_2$ [87, 89], KNH_2BH_3 [90, 91], $Y(NH_2BH_3)_3$ [92], $Sr(NH_2BH_3)_2$ [93] etc.; or by synthesizing the ammine metal borohydrides, such as: $LiBH_4{\cdot}NH_3$ [94], $Ca(BH_4)_2{\cdot}2NH_3$ [95], $Mg(BH_4)_2{\cdot}2NH_3$ [96], $Al(BH_4)_3{\cdot}6NH_3$ [96], $Li_2Al(BH_4)_5{\cdot}6NH_3$ [97] etc.. The release of NH_3BH_3 instead of hydrogen, during the decomposition of $LiBH_4{\cdot}NH_3$ and $Ca(BH_4)_2{\cdot}2NH_3$ [94, 95] is the limitation of these materials, but the release of small amount of ammonia in the dehydrogenation of $Al(BH_4)_3{\cdot}6NH_3$ and $Mg(BH_4)_2{\cdot}2NH_3$ [96], make them more attractive for hydrogen storage applications. Recently, some new types of chemical hydride compounds: the double metal amidoboranes, i.e.; $Na_2Mg(NH_2BH_3)_4$ [98], $NaLi(NH_2BH_3)_2$ [99] and/or metal amidoborane ammoniates like: $Mg(NH_2BH_3)_2{\cdot}NH_3$ [100] and $Ca(NH_2BH_3)_2{\cdot}2NH_3$ [101] have also been reported as promising hydrogen storage compounds in terms of high hydrogen storage capacity and improved dehydrogenation kinetics.

Amidoboranes ($LiNH_2BH_3$ and $NaNH_2BH_3$) can provide high storage capacity (10.9 wt% and 7.5 wt%, respectively) of hydrogen at moderate temperatures. In paper I [102], we present a detailed theoretical analysis of the structural and energetic properties of lithium amidoborane ($LiNH_2BH_3$) and sodium amidoborane ($NaNH_2BH_3$) using density functional theory. We study the ground state properties and crystal structures of $LiNH_2BH_3$ and $NaNH_2BH_3$, including the atomic positions in their respective unit cells and confirm that an atomic arrangement with symmetries given by the $Pbca$ space group yields the lowest total energy structure among all other possible candidate structures. The dynamical stability is tested by calculating the vibrational spectrum at the Γ-point and no imaginary frequencies were found. A schematic representation of the computationally determined crystal structure of $LiNH_2BH_3$ is shown in Figure 4.1. We study the internal structure of the $LiNH_2BH_3$ crystal by calculating the Li--N and N--B bond lengths and Li-N-B bond angle (the corresponding steps in our investigations are carried out for $NaNH_2BH_3$ as well). The hydrogen removal energies are also calculated to analyze the energy that is required to remove hydrogen from the system. Our calculated hydrogen removal energies for these two systems were found to be in good qualitative agreement with the similar hydrogen desorption temperatures measured by experiments. Then we explore the electronic structures of these compounds by calculating the corresponding density of states (DOS) and partial density of states (PDOS), charge densities following Bader's theory of atoms in molecules [103, 104, 105] and electron localization function (ELF) [106]. Both $LiNH_2BH_3$ and $NaNH_2BH_3$ are found to be wide band gap insulators. The strong bonding between the nitrogen and its two neighboring hydrogen atoms is understood based on the calculated PDOS and the same behavior is seen between the boron and its neighboring three hydrogen atoms, whereas a predominantly ionic character of lithium/sodium is found. This analysis is supported by the electron localization function (ELF). From Fig. 4.2, it is evi-

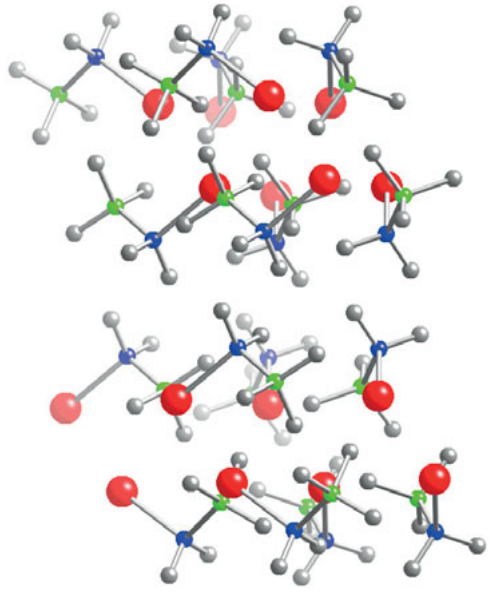

Figure 4.1. The fully relaxed crystal structure of $LiNH_2BH_3$, as obtained from our density functional theory calculations. Li is shown as red spheres, N in blue, B in green, and H in grey. [102].

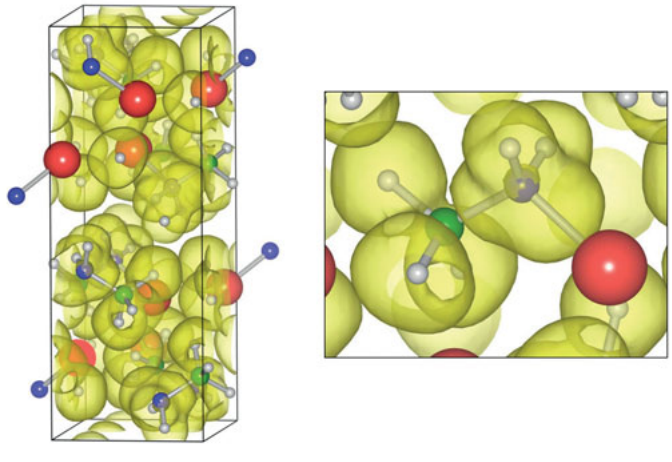

Figure 4.2. The left panel shows the calculated electron localization function for the unit cell of $LiNH_2BH_3$ plotted as yellow-colored transparent isosurfaces at a level of 0.5. The right panel presents a zoomed-in view showing more details. Li in red, N in blue, B in green, and H in grey. [102].

dent that Li is forming ionic bonds with adjacent negatively charged molecular units, whereas the NH_2 and BH_3 are held together by covalent bonds, as can be seen from the connected ELF isosurfaces. The Bader charge analysis also supports these findings. However, the two groups of hydrogen atoms (two hydrogen atoms bonded with nitrogen atom and three hydrogen atoms bonded with boron atom) differ by a charge of approximately one electron, reflecting the different electronegativity of nitrogen and boron atoms (which themselves carry charges of around -1.4 and $+1.9$ e, respectively). The calculated difference in hydrogen removal energies, when taking away one hydrogen atom bonded either with boron or with nitrogen from the supercell of $LiNH_2BH_3$, is speculated to be due to these differences in the charge states. Analogous findings also hold true for $NaNH_2BH_3$.

To fully understand and improve the absorption and desorption kinetics of hydrogen storage materials, the correct information of the crystal structure is important. High Pressure studies are thus very important to investigate the possibility of the new structures at high pressures in the same material, showing better kinetic and hydrogen storage properties [107]. In paper II [108], we take the five candidate structures of $LiNH_2BH_3$ namely: $Pbca$, $Pbcn$, $Pcca$, $Pnma$ and $Pnnm$ and perform the high pressure calculations. At first, we fully optimize all the candidate structures of $LiNH_2BH_3$ at ambient pressure. Then we take these optimized structures at different chosen volumes to perform the high pressure calculations. We relax the corresponding structures with respect to fractional atomic coordinates and cell parameters. Then with the use of fully self-consistent *ab initio* electronic structure calculations, we calculate the equilibrium parameters and total energies. The comparison of total energies versus volume reveals the phase transition of $LiNH_2BH_3$ as shown in Fig. 4.3. Then we calculate the structural parameters, density of states, Bader charge analysis and corresponding electron density of this phase.

In paper III [109], we present the high pressure and temperature based phase transition of BH_3NH_3. Our calculated phase transition of BH_3NH_3 from body-centered tetragonal to orthorhombic at ≈ 220°K is in accordance with the recent and earlier studies [110, 111]. We also calculate the phase transformation of BH_3NH_3 at ≈ 11.5 GPa, which supports the experimental findings available in literature [112].

In paper IV [113] and V [114], we focus on the very recently synthesized compounds, namely; the $LiBH_4.NH_3$ [94], $Sr(NH_2BH_3)_2$ [93], $Li_2Al(BH_4)_5{\cdot}6NH_3$ [97], $Na_2Mg(NH_2BH_3)_4$ [98], $NaLi(NH_2BH_3)_2$ [99], $Mg(NH_2BH_3)_2{\cdot}NH_3$ [100] and $Ca(NH_2BH_3)_2{\cdot}2NH_3$ [101], to explore the hydrogen desorption mechanism in these materials, which are all relevant for hydrogen storage applications. We calculate the crystal and electronic structures of these materials and our calculated structural parameters are in good agreement with experimental measurements, when available. We analyze the electronic structures of these compounds by calculating the density of states (DOS), partial density of states (PDOS), Bader charges and corresponding charge den-

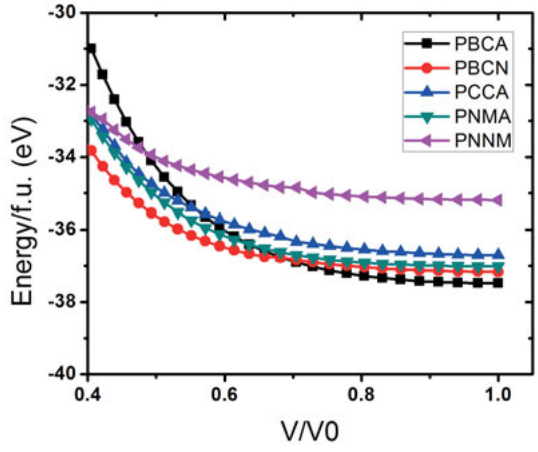

Figure 4.3. Computed variations in the total energies with volume compression for the candidate structures of $LiNH_2BH_3$. [108].

sity in the given planes. As expected, all these materials appeared to be wide band gap insulators.Although these compounds present some significant differences in their crystal structures and chemical composition, the metal cations have never been completely ionized and some covalent nature of bonding is found between metal cations and corresponding anions as shown in Fig. 4.4. However, the bonding between Mg cation and N (NH_3) in $Mg(NH_2BH_3)_2{\cdot}NH_3$

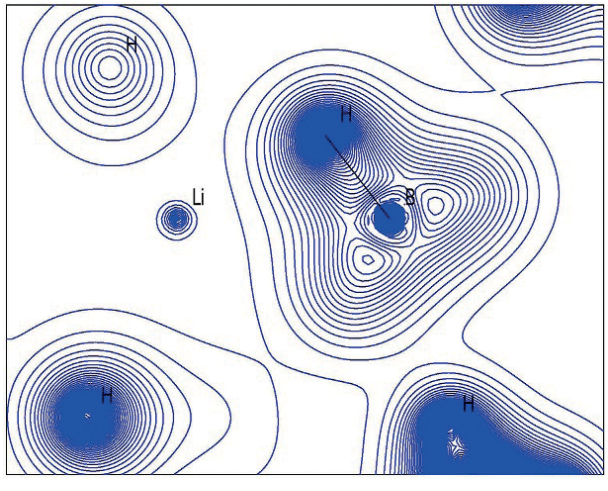

Figure 4.4. Calculated electron density in the plane of Li-B-H. The contours are 0.05 e/Å^3. [113].

is mainly covalent, which facilitates the direct initiate of dehydrogenation process instead of the deammoniation unlike the deammoniation rather dehydrogenation in $Ca(NH_2BH_3)_2{\cdot}2NH_3$ at low temperatures in which the chemical bonding between Ca cations and corresponding nitrogen atoms is mainly ionic. Our calculated Bader's charge for the nitrogen atom is between 6.2 and 6.63 electrons, and the corresponding number of electrons for boron is in the range 1.17-1.44. We suggest further experiments on these compounds because if the electronic structure factors could be measured at high resolution, it would be possible to get the corresponding Bader's charges from the experimental electron density and to compare them with our calculated data. We also calculate the hydrogen removal energies, which correspond to the binding strength of hydrogen at the respective sites (B-site and N-site). Our calculated hydrogen removal energies fall in the range from 5.23 eV to 5.63 eV for hydrogen atoms bonded with B and in the range from 5.32 eV to 6.02 eV for hydrogen atoms bonded with N, in the six compounds studied here, except $Ca(NH_2BH_3)_2{\cdot}2NH_3$, in which the hydrogen removal energy for B site is 2.62 eV and for N site is 3.30 eV, which supports the decomposition of this material at low temperature as reported by experiments. We find that N--H bonds are stronger than the B--H bonds, which follow the same trend as we have already observed in the study of ammonia borane (NH_3BH_3) and amidoboranes ($LiNH_2BH_3$ and $NaNH_2BH_3$).

For an efficient fuel cell, the sufficient mobility of the hydrogen specie is also important among other parameters. Therefore, we perform *ab initio* molecular dynamics simulations to get deeper insight concerning the mobility of the hydrogen atoms in these compounds. We observe that, for a given compound, the diffusion properties of the different hydrogen atoms which belong to that material are roughly similar. However, we observe that diffusion of hydrogen in $LiBH_4.NH_3$ is faster than other compounds studied here, since at the end of our simulation the MSD value of hydrogen atoms in $LiBH_4.NH_3$ is clearly larger than the corresponding MSD values in other compounds. The MSD of hydrogen atoms in $LiBH_4.NH_3$ and $Li_2Al(BH_4)_5{\cdot}6NH_3$ is shown in Fig. 4.5 and Fig. 4.6 respectively. Thus, depending upon solely diffusion properties, $LiBH_4.NH_3$ is more promising candidate than other materials, which are under discussion here, to get an efficient fuel cell. We can explain it partly by the fact that the crystal structures are different: geometries which are less compact are more favorable for hydrogen transport. The environment of the hydrogen atoms is different, as can be seen by our calculated hydrogen removal energies, which can play a role on the MSD values, especially at the beginning of the simulations when the hydrogen atoms are still located close to their equilibrium position.

Complex metal hydrides such as $LiBH_4$ and $NaAlH_4$ can also be considered promising candidates for hydrogen storage [118, 119, 120], especially, $LiBH_4$ is reported to have 18.5 wt% volumetric density of hydrogen [121, 122, 123]. The thermodynamic stability and sorption rates are key features of hydrogen

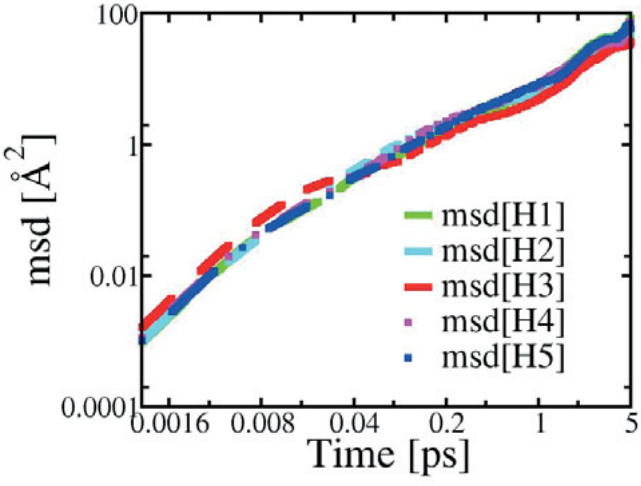

Figure 4.5. Diffusion of hydrogen atoms in $LiBH_4.NH_3$. [113].

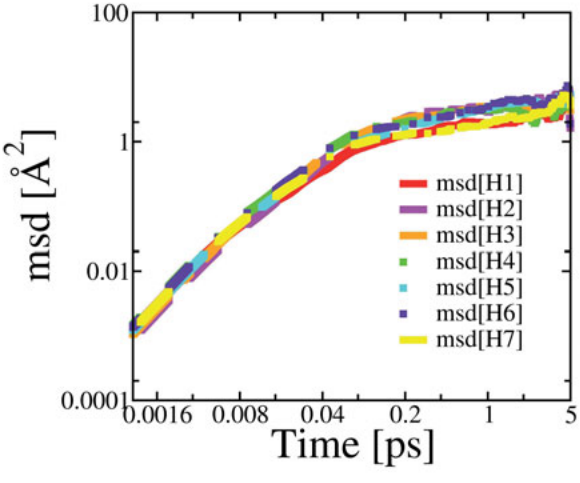

Figure 4.6. Diffusion of hydrogen atoms in $Li_2Al(BH_4)_5{\cdot}6NH_3$. [113].

storage materials but the slow sorption mechanism of complex hydrides is controversial [125]. In hydrogen sorption, diffusion of hydrogen is one of the important mechanism. The diffusion of hydrogen in solids is well known but only limited knowledge is available for the dynamics of hydrogen in complex hydrides because of the different electronic structures of metal hydrides. In most of transition metals, hydrogen occupies interstitial site and hydrogen can jump easily from interstitial to interstitial due to small covalent contribution to the hydrogen- metal bond [124]. In contrast, in complex compounds hydro-

gen is covalently bounded and remained in subunits [125]. Borgschulte *et al.* [126] have reported an alternative method by labeling the diffusive atoms in the study of specific diffusion process to measure the exchange rate and estimate the self-diffusion coefficient in hydrogen-deuterium exchange during the decomposition of $LiBH_4$ [126]. In paper VI [127] and VII [128], we perform ab initio molecular dynamics simulations to study the diffusion of hydrogen in lithiumborohydride ($LiBH_4$), lithiumhydride (LiH) and sodiumhydride (NaH). We study the deuterium - hydrogen exchange in these materials and calculate the diffusion constants of deuterium in lithiumborohydride ($LiBH_4$), lithiumhydride (LiH) and sodiumhydride (NaH). The diffusion of deuterium in lithiumborohydride ($LiBH_4$) through MSD is shown in Fig. 4.7.

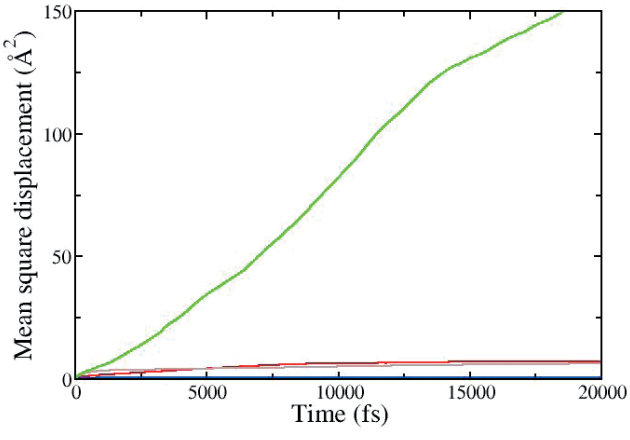

Figure 4.7. The diffusion of deuterium in $LiBH_4$ obtained from our molecular dynamics calculations. Deuterium is shown in green colour, Lithium in red, Boron in blue, and Hydrogen in brown. [127].

4.2 Clusters and low dimensional materials for hydrogen storage

As we have mentioned in the previous section, complex metal hydrides are promising for hydrogen storage due to their large gravimetric density. However, the poor kinetics and thermodynamics due to strong metal- hydrogen bonding in these materials are the limitations to use them for mobile applications. The intensive research is going on to improve the kinetics and thermodynamics of these materials by weakening the metal- hydrogen bond. In the recent years, MgH_2 and Mg-H based composites are being considered as promising candidates, due to their high gravimetric density (7.7 wt%) and low cost of easily available magnesium. The bonding strength of metal- hydrogen bond in MgH_2

can be weakened either by using the catalysts or by nanostructuring of this material. It is reported that the large surface areas, grain boundaries and defects can improve the kinetics and thermodynamics of hydrogen sorption with the reduction of $\approx$ 10 nm particle size by mechanical ball milling [129]. It has also been shown that the hydrogen sorption kinetics can also be improved by the ball milling with transition metal additives [130, 131, 132]. In the search of another possibility, functionalized carbon nanostructures are also considered promising for hydrogen storage applications. However, carbon nanostructures in their pristine form are chemically very inert which make them unsuitable candidate for hydrogen storage purposes. To overcome these limitations, functionalized carbon nanostructures can be doped by foreign atoms on the surface or in the interior of the nanostructures. In this section, we are going to discuss the nanostructuring of metal hydrides and effect of catalysts in these materials as well as the doping of foreign elements in functionalized carbon nanostructures to make them suitable candidates for hydrogen storage applications.

Recently, Larsson *et al.* [133] have presented a 31 formula unit MgH_2 nanocluster model to study the effect of doping in nanostructures, on the basis of systematic studies of electronic structure and desorption energies of $Mg_{31}H_{62}$ cluster. It has already been shown with the systematic studies of Mg_nH_{2n} nanocluster, as a function of n, that the properties can be converged with n$\approx$ 30 [134, 135, 136]. The surface effects of transition metals in the cluster model have been described by presenting the evidence of iron diffusion during dehydrogenation. It has also been predicted that iron and other transition metals may reside in the MgH_2/Mg interface region to catalyze the continuous dehydrogenation.

In paper VIII [137], we perform *ab initio* molecular dynamics (MD) simulations, based on density functional theory, to study the hydrogen-deuterium exchange in bulk and nanoclusters of MgH_2. We reveal the important role of catalysts to improve the kinetics and thermodynamics of MgH_2 by showing the diffusion of hydrogen atoms at low temperatures and increase in the diffusion rate. We calculate the diffusion constants, $< D >$ of deuterium, and show the single hydrogen-deuterium exchange in bulk and nanoclusters of MgH_2. In Table 4.1, we present that the edge site doping of catalysts play an important role in the fast diffusion of hydrogen.

Table 4.1. *Diffusion constant values of hydrogen in $Mg_{31}H_{62}$ nanocluster at 300 K with Ni as a catalyst, on the basis of ab initio molecular dynamics (MD) calculations. [137].*

catalytic atom	site	Diffusion constant
Ni	surface	$< D > \approx 1.39 \times 10^{-8} m^2 s^{-1}$
	edge	$< D > \approx 7.80 \times 10^{-8} m^2 s^{-1}$
	center	$< D > \approx 2.22 \times 10^{-8} m^2 s^{-1}$

Besides the attractive features of MgH_2 (as well as other metal hydrides) for the storage and production of hydrogen, Oumellal *et al.* [45] have reported a new concept for Li-ion batteries by demonstrating the reactivity of MgH_2 versus Li ions through a conversion reaction, and obtained an average voltage of 0.5 Volts. Therefore, MgH_2 is at the cross point between battery and fuel-cell research. Following these experiments [45], in paper IX [138], we investigate the metal hydride MgH_2 and calculate the average voltage of Li-ion and Na-ion cells. Our calculated value for the Li-ion battery using MgH_2 as the negative electrode is ≈ 0.58 Volts, which confirms the experimental value of 0.5 Volts [45], and supports our computational procedure. Furthermore, using the same methodology, we predict a value of 0.4 Volts for the corresponding Na-ion cell, which makes it slightly less interesting than the corresponding Li-ion battery, although this can eventually be compensated in practice by the cheaper price of Na in comparison with Li. We have simulated the nanosized composite material by doping with a Li atom at different sites (center, edge, and surface) in the $Mg_{31}H_{62}$ nanocluster to study the mobility of Li. As described earlier [133], a "surface" site is a 6-H coordinated atom, and an "edge" site is 4-H coordinated atom, both at the surface of the cluster, while a "center" site has a bulk environment. To characterize which site has the best diffusion properties, we calculate from the mean square displacement (MSD), the corresponding diffusion constant values in a MgH_2 cluster. We find that the diffusion reaches its highest value ($22.7 \times 10^{-9} m^2 s^{-1}$) when the dopant is at the edge of the magnesium hydride nanocluster due to the less coordinated environment (only 4 H are neighbouring it). Then, we study the diffusion properties of Li in (Fe, Ni, Ti, and V)-doped nanoclusters of MgH_2 and do an effort to combine battery and fuel-cell technologies. We find that in the presence of the transition metal, which lowers the desorption energy of hydrogen in MgH_2, does not alter significantly the diffusion properties of Li in the cases of Fe and V doping, and therefore the device is still efficient for the batteries technology, while being also a suitable material for hydrogen storage. Our calculated diffusion constant values of Li are presented in Table 4.2.

Table 4.2. *Diffusion constant values of Li in a cluster of MgH_2 doped with transition metals (Fe, Ni, Ti and V), on the basis of ab initio molecular dynamics. [138].*

Atom	site	Transition metal	site	Diffusion constant
Li	edge	Fe	surface	$< D > \approx 21.0 \times 10^{-9} m^2 s^{-1}$
	surface	Ni	edge	$< D > \approx 13.3 \times 10^{-9} m^2 s^{-1}$
	edge	Ti	surface	$< D > \approx 16.2 \times 10^{-9} m^2 s^{-1}$
	edge	V	surface	$< D > \approx 20.2 \times 10^{-9} m^2 s^{-1}$

Graphane is the material prepared by attaching hydrogen atoms on both sides of graphene and first of all (according to best of our knowledge) predicted by Sofo *et al.* [139] and later on confirmed experimentally by Elias *et al.* [140].

Graphane is prepared by exposing pure graphene to a hydrogen plasma and the hydrogen atoms are attached on each carbon atom on both sides of graphene sheet alternatively. In contrast of graphene, the structure of graphane is no more planar, rather a crumpled one because each hydrogen atom attached to carbon pulls it a small distance out of the plane. Graphane having stable structure and small size, if doped with alkali metals (AM) and/or alkaline-earth-metals (AEM), can become a promising candidate for hydrogen storage purposes. AEMs, particularly Ca binds more strongly on defective graphene than on pristine graphene [141]. In paper X [142], we study the stability, electronic structure, and hydrogen storage capacity of a monolayer calcium doped graphane (CHCa). The higher binding energy of Ca on graphane sheet than its bulk cohesive energy, calculated by us, indicates the stability of CHCa. In Fig. 4.8, we have shown (a) front view, (b) top view of the optimized structure of pure graphane as well as (c) side and (d) top views of Ca doped graphane. In the fully optimized structure, the C-C bond distance is 1.53 Å and C-H bond length is 1.12 Å. These values are in good agreement with the previous study, where CHLi was reported as a potential hydrogen storage material [143]. We calculate that 6 wt.% of hydrogen storage capacity can be attained with a doping concentration of 11.11% of Ca atoms on graphane sheet.

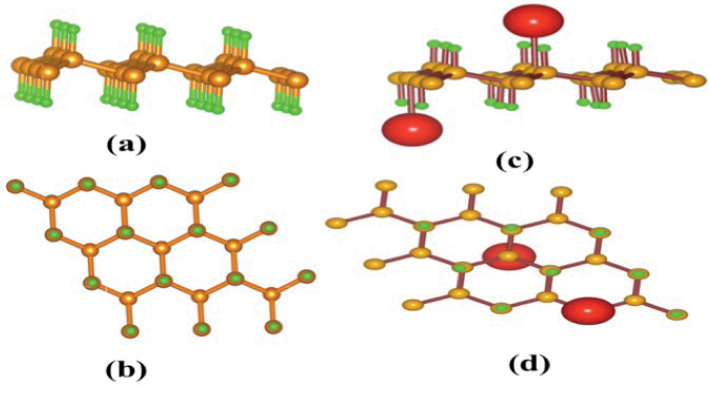

Figure 4.8. (a) and (b) are the side and top view of the optimized structures of pure CH, respectively, (c) and (d) show the side and top views of the optimized structures of CHCa, respectively. [142].

In paper XI [144], we study the interaction of the first four elements of both alkali (Li, Na, K, Rb) and alkaline (Be, Mg, Ca, Sr) earth metals (adatoms) on a CH sheet. Fig. 4.9 shows the optimized geometries of the side and top views of adatom doped CH. Different doping concentrations of adatoms ranging from 3.125% to 50% are employed to calculate the effects of adatom elements on the CH sheet. The binding energy, bond length, charge transfer, and band gap of each adatom element is investigated. In the case of alkali metal adatoms,

the binding energies decrease monotonically with the increase of atomic numbers as well as with the increase of doping concentrations. A similar pattern is calculated in the case of charge transfer, which decreases as we go down the group with the increase of doping concentrations. All the elements of alkali metals studied here show the semi-conducting behavior at lower doping concentrations (3.125%, 5.55%), whereas, at higher doping than this, the metallic behavior is shown. In case of alkaline earth metals, we can not find any regular trend in terms of binding energies of adatoms, such as Be at 50% has the highest and Ca at 25% has the lowest binding strength to the CH sheet. For elements having higher size in both the groups (alkali and alkaline-earth metals) the positive value of binding energies indicates the instability, the endothermic adsorption process. All the elements of alkaline-earth metals at all doping concentrations present a metallic transition in the adatoms doped CH sheet.

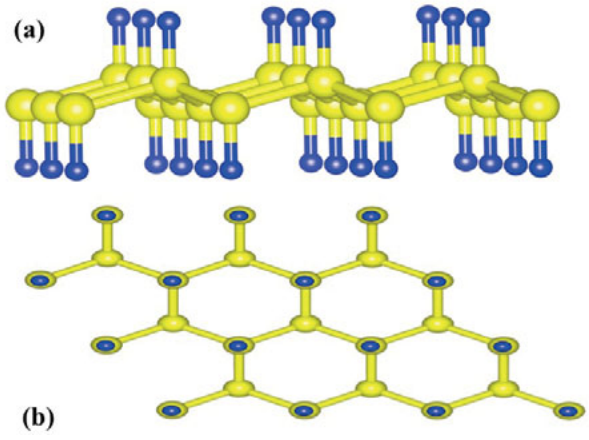

Figure 4.9. (a) and (b): side and top views of the optimized structure of adatom doped CH, respectively. [144].

4.3 Silane hydrogen system

The study of hydrogen-rich systems at extreme conditions not only provide the insight into the metallization and superconductivity of these materials but it can also contribute a lot in the applied research areas, which can lead to design and development of much efficient hydrogen storage systems [145]. CH_4, SiH_4, GeH_4, and SnH_4 are the hydrides belonging to IVa group and are promising for the hydrogen storage applications because of the highest hydrogen content (80%) of hydrogen among elemental hydrides [146]. These materials have also been predicted to be metallized at lower pressures compared with pure hydrogen [146]. Silane (SiH_4) has been reported to be metallized

by synchrotron infrared reflectivity and electrical conductivity measurements indicate at around 50-60 GPa [147, 148], whereas SiH_4 has been reported to become superconducting at a transition temperature of 17 K at 96 GPa [148]. At high pressures, the interactions between elemental hydrides and additional molecular hydrogen at high pressure is one of the rapidly growing area of research [149, 150]. Recently, Strobel *et al.* [151] have reported the $SiH_4(H_2)_2$, to have a highly symmetrical and well-ordered structure with one formula unit per cell, and presented the phase diagram of this material mentioning that the H_4 bond weakening occurs at an unusual low pressure. They also observed a darkening of the sample at a pressure around 35 GPa, which can be associated with a metal-insulator transition. Approximately, at the same time, Wang et al. [145] also reported a study on the same compound and measured a strong interaction between the SiH_4 and H_2 components.

Keeping in view the above scenario, in paper XII [152], we present a theoretical counterpart of these experimental studies of $SiH_4(H_2)_2$. We set up a crystal structure with a fcc lattice containing one $SiH_4(H_2)_2$ formula per unit cell, with a volume of 66.5 $Å^3$ [151] and the calculated pressure of our relaxed structure is found to be 6.5 GPa, in a very good agreement with the experiments (6.8 GPa). Then, we perform a series of similar calculations for different values of the volume to get the metallization in this material by an overlap of the valence and conduction bands as shown in Fig. 4.10. Our calculated corresponding value of the pressure of metallization (the electronic band gap is equal to zero) with the GGA is $\approx$ 145 GPa.

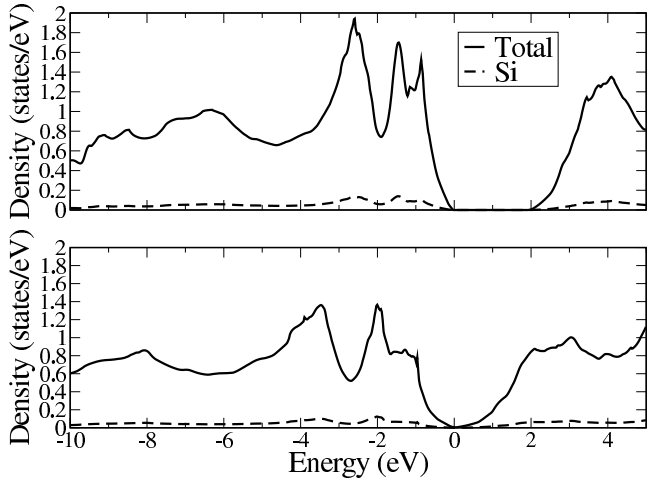

Figure 4.10. Calculated total (full line) and partial (dashed line) density of states of $SiH_4(H_2)_2$ for 84 GPa (upper plot) and 145 GPa (lower plot). [152].

It is well konw that GGA underestimate the band gap values. Therefore, we have performed a series of GW calculations in order to get the correct value of pressure of metallization and the corresponding results are shown in Fig. 4.11.

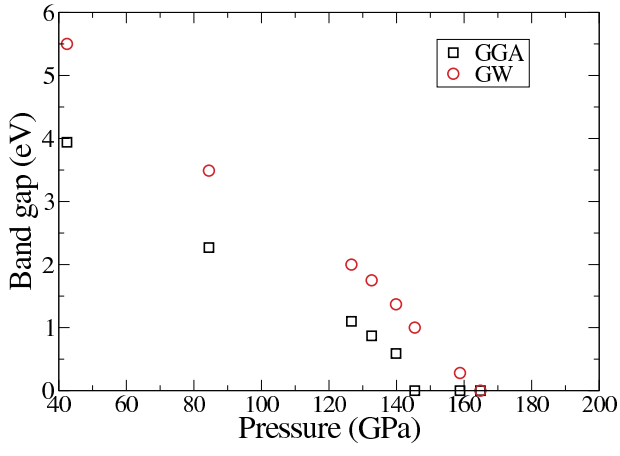

Figure 4.11. Pressure variation of the minimum electronic band gap of $SiH_4(H_2)_2$, computed with the GGA (black squares) and the GWA (red circles). Using the GGA, the insulator-metal transition is found to occur at 145 GPa, while with the GWA the corresponding pressure is 164 GPa. [152].

The band gap decreases almost linearly with the pressure, and it is found that the pressure of metallization is about 164 GPa. From our calculations, it appears that the calculated pressure of metallization is much higher than the one noticed in ref. [151], who observed a darkening of the sample around 35 GPa. The phase transitions or an interaction between the sample and the gasket material during the experiment, may be the reason for these differences in the measured and calculated values of transition pressure of this material.

4.4 Solid hydrogen

Hydrogen is one of the most fascinating material to physicist because of the most abundant and lightest material as well as the conditions of its metallization associated with a possible superconducting state at high temperature. Recently, Eremets *et al.* [16] reported the metallization of hydrogen at room temperature and around 260-270 GPa using the conductivity measurements, and claimed it to be accompanied by a first-order structural transition. However, recently Nellis et al.[17] analyzed this work and could not find clear evidence

for metallic hydrogen in the experiments of Eremets *et al.*. Even more recently, Zha et al.[18] studied hydrogen samples above 300 GPa and from 12 to 300 K using the synchroton, infrared and optical absorption techniques. In contrast to Eremets *et al.*, they concluded that the properties measured correspond to the ones of a semi-metal and that this phase persists over a broad range of temperature and pressure. However, they could not measure the possible crystal structure of this phase. At the same time, Howie *et al.* did measurements at 300 K and up to 310 GPa, and observed the transformation to a new phase (phase IV) at 220 GPa and identified this phase as the $Pbcn$ phase obtained by Pickard *et al.* [14]. With the use of density functional theory (DFT) and a random search method, Pickard and Needs[14] have studied the stability of various phases of solid hydrogen in function of pressure for a temperature equals to zero kelvins. They have found that the most stable phases are the $C2/c$ for pressures between 105 GPa and 270 GPa, and the $Cmca$-12 phase for pressures between 270 GPa and 385 GPa, which are also in our pressure range of interest (from 200 GPa to 300 GPa). By including the zero point effects (ZPE), the transition between the two phases occurs at 240 GPa instead of 270 GPa without ZPE. They also suggested the $C2$ and $Pbcn$ phases to be relevant for this range of pressures, although these structures are slightly higher in enthalpy.

In paper XIII [153], we study the four phases ($C2/c$, $Cmca$-12, $C2$, and $Pbcn$) found by Pickard and Needs for the 200-300 GPa range of pressure, to compare the value of their band gaps and how it closes under pressure. To calculate the reliable values for the pressure of metallization by band-gap closure of the different phases, we use the GW approximation in which it is possible to overcome the difficulties of standard functionals to predict the correct values of the band gap. We find the band gap closure of $C2/c$ and $Pbcn$ phases around 350 GPa, the $C2$ phase around 300 GPa, whereas the $Cmca$-12 has the lowest pressure of band closure among all the phases we investigate here, with a metallization that occurs already for a pressure of about 260 GPa, which is in agreement with the experiments of Eremets et al.[16], in which hydrogen transformed to a metal at 260-270 GPa. Therefore the $Cmca$-12 phase may be the phase observed during these experiments. They have also mentioned [16] that for pressure above 240 GPa, the band gap should be smaller than 0.7 eV because of the absence of illumination. This is also in agreement with our calculated minimum band-gap of 0.25 eV at 240 GPa. However, the scenario that we propose is partly different by these experiments, which stated that the transformation to a metal is accompanied by a first-order structural transition. Then the band structures, picturing the metallization of the Cmca-12 phase, with the GGA and GW approximations are calculated. As shown in Fig. 4.12, from the band structures, we conclude that this phase is a semi-metal as no direct overlap occurs between the valence and the conduction band in the range of our studied pressures.

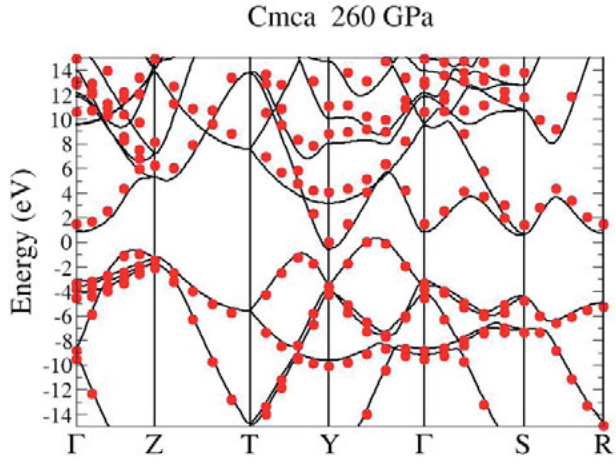

Figure 4.12. Calculated band structure for the $Cmca$-12 phase of hydrogen with GW approximation at 260 GPa. [153].

Therefore, the mechanism that we propose for the transition to a metal is different from the one of Eremets *et al.* [16], but the nature of the phase (a semi-metal) is in agreement with the work of Zha *et al.* [18]. Then from the phonon calculations, we demonstrate it to be dynamically stable but our calculated electron-phonon coupling is rather weak and therefore this phase is not expected to be a high-temperature superconductor.

Proceeding to re-conciliate and in search of the possible explanation in the different interpretations about the conductive hydrogen, in paper XIV [1], we study the impact of temperature on the structures predicted to be stable at relevant P and zero temperature. Therefore, we chose to investigate the C2c and Cmca-12 phases, relevant to the range of pressures in recent experiments. These phases were found stable above 200 GPa by Pickard and Needs [14]. Since the impact of temperature is expected to be critical (no metallization according to Loubeyre *et al.* [11] at 77 K and metallization according to Eremets and Troyan [16] at 300 K), we employ molecular dynamics (MD) method that allows to account for temperature impact. We perform MD simulations for the constant volume starting with the C2c and Cmca-12 (12 atoms in a primitive unit cell) structures. The cell parameters are obtained from the relaxation calculations at pressures of 210 GPa, 260 GPa, 305 GPa and 350 GPa, respectively. Then for a number of temperatures we performed MD simulations. The drop in pressure on melting, indicates negative volume of melting in accordance with previous studies. Our melting curve, computed at 200 to 350 GPa, compares well with available data in literature. We have computed our P-T points, where the sharp P changes at 852 K, 652 K, 567 K and 482 K, for

C2c and Cmca-12 phases, representing the melting transitions at these temperatures.

Hydrogen melts at a much higher temperatures than the ambient temperature in the Eremets and Troyan experiment [16]. The hydrogen melting curve bends down but not fast enough to become liquid at 260 GPa. Our hydrogen melting points at 652 K and 261 GPa and 567 K and 288 GPa are in good agreement with the melting curve depicted in Fig. 1 of ref. [19] and the melting point very recently calculated by Liu *et al.* [154]. The diffusive state might be an intermediate between the Cmca-12 and the Ibam structure [19] and/or Cmca-4 structure [154]. It is possible that these structures have actually formed in our MD simulations (see Fig. 4.13).

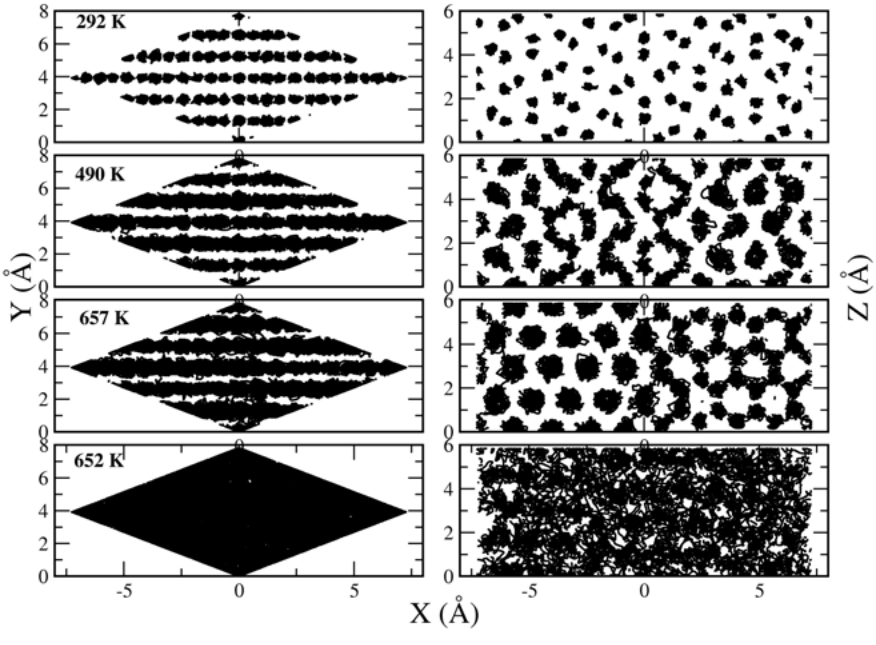

Figure 4.13. Trajectories of atoms for Cmca-12 at 260 GPa. The left panels show XY (along Z) projections of all 216 atoms computed at the last 4000 timesteps of MD runs at the temperatures (from top to bottom) 292, 490, 657, and 652 K. All runs show layered structure of hydrogen except the last one which is a liquid structure. The right panels show the XZ projections of the central (the longest) layer in the computational cell for the run on the left. At T=292 K there is no diffusion, all atomic positions during the run are confined to the close neighborhood of the original crystallographic positions. At T=490 K one can see formation of connected patterns indicating the ionic diffusion of hydrogens. At T=657 K this formation is fully developed in the computational cell. At T=652 K in the liquid state the lattice is gone and the atoms homogeneously fill the cell. [1].

We analyzed the charge that diffusing H atom can carry (Fig. 4.14). By performing Bader analysis [103, 104], we computed charges on H atoms at a number of temperatures (Fig. 4.14). One can see that below the diffusion threshold the charge is close to 1 e., interesting that the charge distribution is asymmetric as predicted by Baranowski [155]. The charge distribution becomes much wider in diffusing state and similar to the distribution in the liquid state. Considering that the liquid monatomic state is metallic it is possible that the diffusing state is also conductive. Also, considering that in these experiments hydrogen might recrystallize and that the diffusion proceeds along the 001 direction, different experiments might lead to different observations due to the different grains orientation.

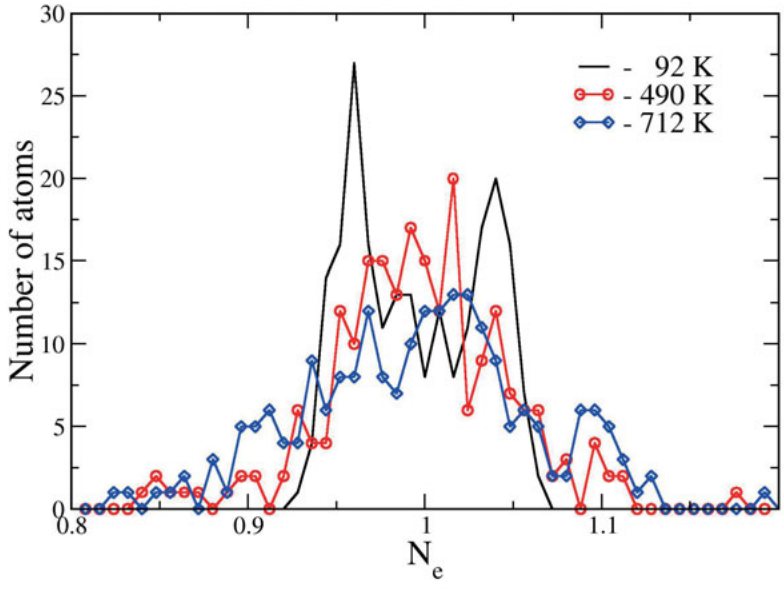

Figure 4.14. Density of states for the charge distribution according to Bader procedure for Cmca-12 at 260 GPa. The DOS at 92 K in non-diffusive state is narrow and asymmetric. The DOS in diffusive and liquid states are wide and similar implying similar electronic structure. [1].

5. Cathode materials for rechargeable batteries

Nowadays, the world is facing an energy crisis due to depletion of fossil fuel supplies and at the same time, related issues, like environmental pollution and global warming, are also requiring the alternate green energy resources and the replacement of the present oil-based provisions [156, 157]. A possible solution is to produce electricity from sustainable energy resources instead of burning fuel and to move towards more intensive use of electric vehicles (EV's) other than the vehicles driven by internal combustion engines (ICE's) [33]. However, the availability of appropriate technology for energy storage, like batteries, because of the fluctuation of the sources of sustainable energy, is the main issue associated with this solution [33]. Thus, the development of long term sustainable energy storage and environment friendly batteries along with elongated cycle life is a key challenge for scientific and industrial communities [33].

In this chapter, we present our studies to explore the characteristics of energy storage materials. In the first section, we focus on the lithium phosphate and lithium sulphate based cathode materials for rechargeable batteries, whereas, in the second section of this chapter, we present our studies on magnesium based materials for rechargeable batteries.

5.1 Lithium phosphate and sulphate based materials

As we have described earlier, the search for environment friendly and sustainable low-cost energy conversion and storage systems with prolonged cycle life, is a need of the modern society. Because of high energy density and prolonged cycle life, there is a growing demand for lithium-ion batteries, which are commonly used in portable electronic devices for aerospace, defence and automotive applications as well as for medical devices [158]. In the search of promising candidate materials, phosphates and silicates have become attractive because of good electrochemical properties at useful redox potential as well as safety advantages over the commonly used metal oxides, especially, the good electrochemical and thermal stability along with high theoretical capacity and reversibility of lithium transition metal phosphates, make them promising candidates as positive electrodes for Li-ion rechargeable batteries [159, 160]. However, the study of only a few lithium transition-metal fluorophosphates is available in the literature [161, 162, 163].

Keeping in view the environmental and economic advantages of the Li-ion rechargeable batteries over disposable batteries, the search of new improved materials and the comprehensive study of these systems is of great importance. In papers XV [165], XVI [166] and XVII [167], we present the

theoretical study of Na_2FePO_4F, Li_2FePO_4F, $LiNaFePO_4F$, $NaFePO_4F$ and $LiFePO_4F$, which were recently synthesized by Ellis *et al.* [164]. In paper XV [165], we determine the crystal structures, electronic and magnetic properties of Na_2FePO_4F, Li_2FePO_4F, $NaFePO_4F$ and $LiFePO_4F$, respectively and we predict the atomic positions of Li_2FePO_4F. The corresponding voltages of Li-ion cell and Na-ion cell are also calculated, as shown in table 5.1([165]).

Table 5.1. *Calculated intercalation voltages of Na_2FePO_4F and Li_2FePO_4F batteries. The experimental value is from Ref. [164].*

Composition	Approximation	Voltage (Volts)
Li_2FePO_4F	GGA	2.98
	GGA+U	3.38
	Expt	3.50
Na_2FePO_4F	GGA	2.64
	GGA+U	3.04

We reproduce the experimental value of the voltage of Li-ion cell, however, our predicted average intercalation voltage of Na-ion cell is slightly lower than for the Li-ion cell. Thus, in term of voltage, the Li-ion battery appears to be more promising than the Na-ion battery, but the depletion of lithium resources and the low cost and the vast availability of sodium, makes it a favorable candidate for rechargeable batteries.

In paper XVI [166], we focus on the structural, electronic and magnetic properties of another promising cathode material for Na-ion rechargeable batteries: $LiNaFePO_4F$. We find the ferromagnetic ordering of iron atoms to be the ground state of this material at 0 K. We also predict around 5.0 V of average intercalation voltage of this material for sodium ion batteries as shown in Table 5.2. The low cost of sodium iron fluorophasphate and more than 5.0 V average intercalation voltage of $LiNaFePO_4F$, makes it advantageous over other cathode materials for rechargeable batteries.

Table 5.2. *Calculated intercalation voltages of $LiNaFePO_4F$ battery with different approximations. [166].*

Approximation	Voltage (V)
LDA	5.24
LDA+U	4.90
GGA(PAW-91)	5.57
GGA(PAW-91)+U	5.09
GGA(PAW-PBE)	5.12
GGA(PAW-PBE)+U	5.28

In paper XVII [167], we present the detailed study of Na_2FePO_4F, Li_2FePO_4F, $NaFePO_4F$ and $LiFePO_4F$ by using the different approximations, like, LDA, GGA, PBE, LDA+U, GGA+U and PBE+U and compare our results with available experimental data. We find that DFT+U performs well to reproduce the experimental data, provided the correct choice of the U parameter. We predict the atomic positions of $LiFePO_4F$, and $NaFePO_4F$ and we also calculate the average intercalation voltages of Li-ion cell and Na-ion cell, respectively by use of all these methods along with non spin polarized and spin polarized ordering of iron atoms (see Table 5.3). The Bader charge analysis [103] and electron localization function (ELF) [106] are also calculated for these cathode materials.

Table 5.3. *Calculated Intercalation Voltages of Na_2FePO_4F and Li_2FePO_4F batteries, NSP stands for non spin polarized and SP for spin polarized. [167].*

Composition	Approximation	*NSP/SP*	Voltage (V)
	LDA	*NSP*	2.35
		SP	3.04
	LDA+U	*NSP*	3.72
Na_2FePO_4F		*SP*	3.19
	GGA-91	*NSP*	2.12
		SP	2.62
	GGA-91+U	*NSP*	3.54
		SP	2.98
	*GGA-PBE***	*NSP*	2.17
		SP	2.64
	*GGA-PBE+U***	*NSP*	3.58
		SP	3.04
	*Expt**.		3.50
	LDA	*NSP*	2.71
		SP	3.38
	LDA+U	*NSP*	4.05
Li_2FePO_4F		*SP*	3.54
	GGA-91	*NSP*	2.43
		SP	3.06
	GGA-91+U	*NSP*	3.83
		SP	3.41
	*GGA-PBE***	*NSP*	2.38
		SP	2.98
	*GGA-PBE+U***	*NSP*	3.78
		SP	3.38
	*Expt**.		3.50

*From Ref. [164].
**From Ref. [165].

In the search of more promising materials, very recently, Recham *et al.* [168] have explored an other direction, by synthesizing the $LiFeSO_4F$ to be used as positive electrode for lithium-ion batteries. The corresponding device of Lithium fluorosulphate was reported to deliver a slightly higher voltage (3.6 Volts)

than the one prepared by $LiFePO_4$, and there was no need to use carbon coating or nanosizing to obtain an efficient battery. In paper XVIII [169], we use the GGA and GGA+U method to calculate the crystal structure of $LiFeSO_4F$ and predict the correct position of lithium ion, which was not confirmed by experimentalists. We also obtain the crystal structure of $FeSO_4F$, which was not completely determined by experiments. Then we explore the electronic structures of $LiFeSO_4F$ and $FeSO_4F$. Our calculated value of average intercalation voltage of $LiFeSO_4F$ battery is in good agreement with experiments as shown in Table 5.4 ([169]). We find that GGA+U method corresponds well with the experimental findings. Then we also calculate the crystal structures of related materials [43, 44], i.e.; $LiCoSO_4F$ and $LiNiSO_4F$, which are found to share a similar crystal structures with $LiFeSO_4F$.

Table 5.4. *Calculated intercalation voltages of $LiFeSO_4F$ battery. NSP stands for non spin polarized and SP for spin polarized calculations. The experimental value is from Ref. [168].*

Composition	Method	Voltage (V)
$LiFeSO_4F$	GGA (NSP)	2.74
	GGA (SP)	3.08
	GGA+U (NSP)	4.27
	GGA+U (SP)	3.69
	Expt	3.6

To further explore the corresponding characteristics of $LiFeSO_4F$ and $FeSO_4F$, in paper XIX [170], we use the Heyd-Scuseria-Ernzerhof (HSE06) hybrid functional to calculate the crystal and electronic structures of these materials. Recently, Chevrier *et al.* [171] have used this functional to calculate the redox reaction and formation energies of transition metal compounds of interest for Li-ion batteries. Then we calculate the intercalation voltage of $LiFeSO_4F$ battery with the use of this method and our results are in good agreement with experimental data (see Table 5.5 ([170])).

Table 5.5. *Calculated intercalation voltages of $LiFeSO_4F$ battery. The GGA+U value is from Ref. [169] and the experimental value is from Ref. [168].*

Composition	Method	Voltage (Volts)
$LiFeSO_4F/FeSO_4F$	HSE06	3.54
	GGA+U	3.69
	Expt	3.6

We conclude that the hybrid functional (HSE06) performs as well to calculate the structural properties as the DFT+U method and there is no need to adjust the U and J parameters like in DFT+U method. Thus, we believe that

the corresponding properties of Li-ion batteries can be explored and predicted efficiently by the use of HSE06 functional. We also calculate the electron density distribution in the $LiFeSO_4F$ and $FeSO_4F$ crystals with the use of Bader's charge analysis. Olivine ($LiFePO_4$) is also considered promising material for Li-ion batteries, but the development of the corresponding technology is now limited because of the one dimensional Li-ion transport in olivine [37, 38, 39, 40]. To explore the Li-diffusion and transport properties of lithium in $LiFeSO_4F$, we performed *ab initio* molecular dynamics simulations. As shown in Fig. 5.1, we find that it is three-dimensional, which is a clear advantage over other cathode materials promising for Li-ion batteries, such as $LiFePO_4$.

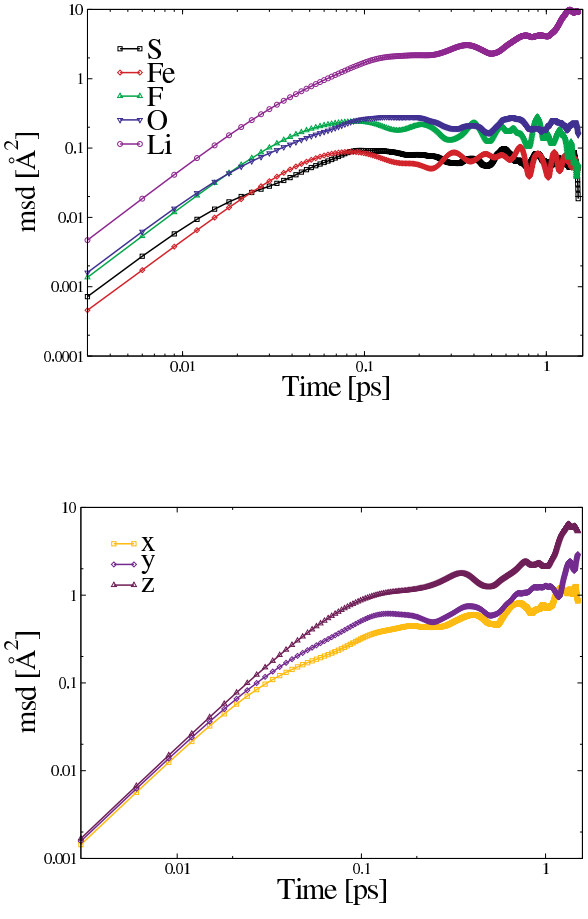

Figure 5.1. Up: Mean square displacements of all the species of $LiFeSO_4F$ computed by molecular dynamics calculations at 1200 Kelvins. Down: Mean square displacement of Li in $LiFeSO_4F$ projected on each cartesian axis.([170]).

5.2 Electronic structure of Mg based cathode materials

Magnesium is comparatively more abundant i.e.; cheaper than lithium and its divalent character (Mg^{2+}) is theoretically able to serve a higher volumetric energy density (3833 $mAhcm^{-3}$) than lithium (2061 $mAhcm^{-3}$) [172, 173, 174, 175]. Magnesium metal anodes have been reported to deliver superior cycle life and efficiency [176]. In addition, Singh *et. al.* [177] recently performed experiments by using low-cost Sn as an anode material, Mo_6S_8 as a cathode material and conventional battery electrolyte i.e.; $Mg(N(SO_2CF_3)_2)_2$ and they have attained superior operating voltages and capacity for rechargeable Mg-ion batteries. This work does not only highlight the enhanced performances of Mg-ion batteries, but it also guides a crucial issue that Mg-ion batteries can be conveniently manufactured by the same procedures as Li-ion batteries, further strengthening possibilities of magnesium ion batteries in the near future.

In paper XX, we present the density functional theory calculations of the crystal and electronic structures of $Mg_2Mo_6S_8$, a promising material to use for magnesium rechargeable batteries using the PBE and HSE06 functionals. Our calculated structural parameters are in good agreement with the experimental values and the corresponding optimized crystal structure is shown in Fig. 5.2. The mechanical stability of this material is verified by calculating the phonon

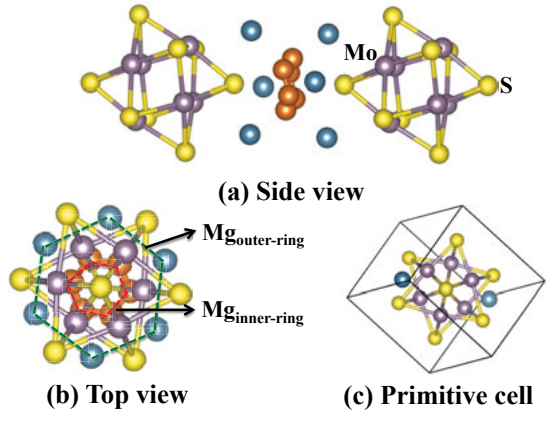

Figure 5.2. Crystal structure (side view (**a**) and top view (**b**) of $Mo_xMo_6S_8$ (space group $R\bar{3}$) where Mg atoms can be accommodated between Mo_6S_8 cages. Color coding is Mo (purple), S (yellow), Mg in the inner ring (orange) and Mg in the outer ring (blue). **(c)**: The representative primitive cell employed in this study where 2 Mg atoms are occupied in the outer ring.

band structure as shown in Fig. 5.3, which confirms the dynamical stability of this material. We have explored the electronic structure of $Mg_2Mo_6S_8$, by calculating the total density of states (DOS), partial density of states (PDOS)

and Bader charge analysis. The electron localized function (ELF) and the corresponding charge distributions results are presented in Figure 5.4.

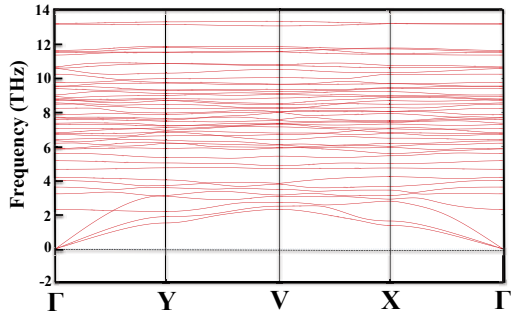

Figure 5.3. Phonon band structure of $Mg_2Mo_6S_8$.

Then, we calculate the average intercalation voltage derived for the system $Mg/Mg_2Mo_6S_8$. Our calculated value for this quantity is in good agreement with experimental value. We also find that the insertion of Mg into Mo_6S_8 transforms the trigonal symmetry to a triclinic one and shifts the Fermi level, leading to a metal-insulator transition when two Mg ions are accommodated in each Mo_6S_8 cluster.

Similarly, in paper XXI, we present the crystal and electronic structures of $MgCuMo_6S_8$ with the use of hybrid functionals. The corresponding density of states are shown in Fig. 5.5. Indeed the density of states of $MgCuMo_6S_8$ (Fig. 5.5) are very similar to that of $Mg_2Mo_6S_8$, however, in this case there is no metal-insulator transition and the Fermi level is always shifted to the edge of the conduction band. We have also calculated the average intercalation voltage of $Mg/MgCuMo_6S_8$ battery system and the results are listed in Table 5.6.

Table 5.6. *Average intercalation voltage of $Mg/MgCuMo_6S_8$ battery systems (inner sites,[1] outer sites[2]).*

	XC	Average voltage (V)
[1]$Mg/MgCuMo_6S_8$	PBE	0.88
	HSE06	1.22
	PBE0	1.26
[2]$Mg/MgCuMo_6S_8$	PBE	0.86
	HSE06	1.22
	PBE0	1.24

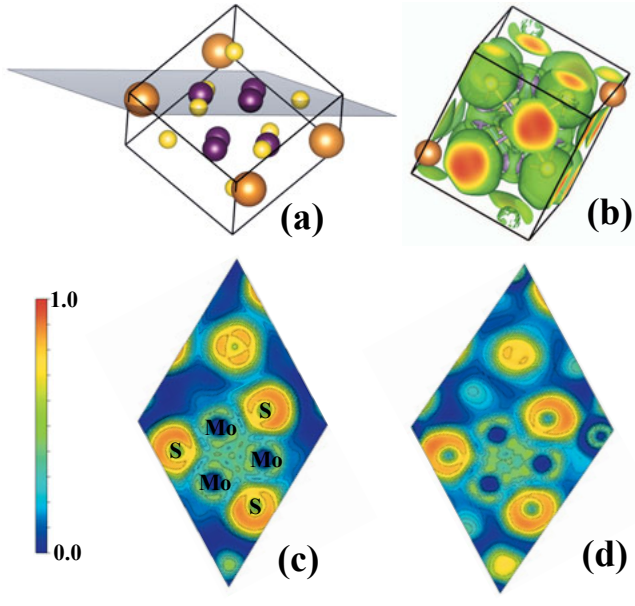

Figure 5.4. (a) The cross section of (111) plane where Mg, Mo and S atoms are resided (b) 3-dimensional ELF of $Mg_2Mo_6S_8$ where the isosurface (green) corresponds to ELF of 0.4 (c) and (d) 2-dimensional ELF of Mo_6S_8 and $Mg_2Mo_6S_8$.

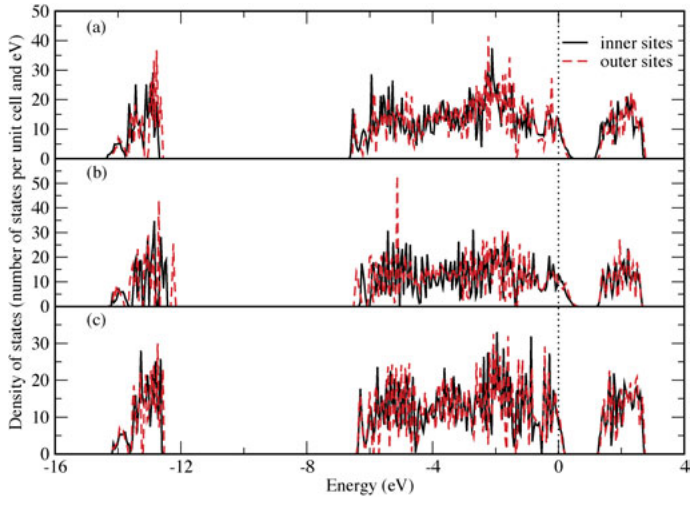

Figure 5.5. Electronic density of states for $MgCuMo_6S_8$ with (a) PBE (b) HSE06 (c) PBE0 . The Fermi level is set at 0 eV.

6. Electronic structure and mechanical properties of *MAX* phases and related materials

The consumption of fuel can be saved by making the engines and/or internal combustion engines with efficient, lighter and higher temperature tolerant materials [47]. This class of materials, having a combination of properties of ceramics and metals, is known as *MAX* phases [47]. The *MAX* phases usually behave like ceramics, i.e.; stiff, lightweight, resistant to oxidation and tolerant to high temperatures as well as metal like properties e.g.; electrical and thermal conduction, readily machinable and resistance to thermal shock [46, 47]. Thus, these compounds can be used to enhance the efficiency of fuel burning engines and to reduce the energy consumption and cost [46, 47],which can eventually lead to improve the world economy. The *MAX* phases with all these properties are playing an important role in the advancement of science and technology and are interesting materials for not only automotive, aerospace, defence, and medical applications, as well as for portable electronic devices. Being the more advantageous than most of other common materials, technologically and economically, the continuous search and detailed study of such type of materials (*MAX* phases) is a need of our time.

The *MAX* phases are generally denoted by $M_{n+1}AX_n$, because of their composition, where *M* is an early transition metal, *A* is a IIIA or IVA group element and *X* is either C or N, and n=1-3 [46, 47, 178, 179, 180, 181, 182, 183]. The *MAX* phases are classified into three types, i.e.; 211-type (with n=1), 312-type (with n=2) and 413-type (with n=3). In paper XXII [184], we present the comprehensive description of each type, i.e.; 211, 312, and 413 of the *MAX* phases by calculating the electronic, structural and mechanical properties of: Ti_2AlN, Ti_2AlC, V_2AlC, Nb_2AlC, Ta_2AlC, V_2GeC, Ti_3SiC_2 and Ti_4AlN_3, with the use of hybrid density functional and we compare our results with the experimental data available in the literature as shown in Table 7.5. We are studying TiC because of its simple crystal structure (cubic) and having similar electronic structure like *MAX* phases due to the presence of Ti and C, however, is not a member of the *MAX* phase family. In the past years, the properties of the *MAX phases* have been studied by density functional theory with the use of standard exchange-correlation potentials namely, the local density approximation (LDA) and/or the generalized gradient approximation (GGA), but on the overall, these approximation could not succeed to reproduce the experimental electronic and mechanical properties and structural parameters of such type

of materials, which reveal the limitation of these functionals. However, our calculated results with the use of hybrid density functional (HSE06), are in accordance with experimental data, which makes us confident to conclude that hybrid density functional can be used as a predictive tool to study the properties of most of the *MAX* phase materials.

Table 6.1. *Calculated and experimental values of the lattice constants, volumes and bulk moduli of TiC, Ti_2AlN, Ti_2AlC, V_2AlC, Nb_2AlC, Ta_2AlC, V_2GeC, Ti_3SiC_2 and Ti_4AlN_3, determined from our ab initio calculations. NSP stands for non spin polarized, while SP-AFM stands for spin-polarized anti-ferromagnetic. [184].*

Compound	Method	a_0 (Å)	c_0 (Å)	V_0 (Å^3)	B_0 (GPa)
TiC	*HSE* (NSP)	4.31		80.1	273
	Expt.	4.327[h]		80.48[a]	272[b]
Ti_2AlN	*HSE* (NSP)	2.97	13.54	103.3	170
	Expt.	2.986±0.003[c]	13.60±0.02[c]	105.0±0.5[c]	169±3[c]
Ti_2AlC	*HSE* (NSP)	3.05	13.67	109.8	149
	Expt.	3.065±0.004[c]	13.71±0.03[c]	111.6±0.6[c]	144[j]
V_2AlC	*HSE* (NSP)	2.88	13.03	93.3	196
	Expt.	2.914±0.003[f]	13.19±0.03[f]	97.0±0.7[f]	201±3[f]
Nb_2AlC	*HSE* (NSP)	3.11	13.86	116.4	191
	Expt.	3.103±0.004[f]	13.93±0.03[f]	116.2±0.7[f]	209±2[f]
V_2GeC	*HSE* (SP-AFM)	3.01	11.95	93.6	153
	Expt.	3.038±0.005[g]	12.112±0.009[g]	96.6±0.9[g]	165±2[g]
Ta_2AlC	*HSE* (NSP)	3.08	13.90	114.5	206
	Expt.	3.086±0.006[f]	13.85±0.04[f]	114.4±0.7[f]	251±3[f]
Ti_3SiC_2	*HSE* (NSP)	3.05	17.67	142.2	202
	Expt.	3.06[i]	17.66[i]	143.50[a]	206±6.0[d]
Ti_4AlN_3	*HSE* (NSP)	2.97	23.27	177.5	223
	Expt.	2.9905[e]	23.380[e]	181.08[e]	185[b]

[a]From Ref.[185], [b]From Ref.[186], [c]From Ref.[187], [d]From Ref.[188], [e]From Ref.[189], [f]From Ref.[190], [g]From Ref.[191], [h]From Ref.[192], [i]From Ref.[193], [j]From Ref.[194].

In paper XXIII [195], we introduce a new type of *MAX* phase materials namely, Ti_4AlH_3 and Ti_3AlH_2, which contains hydrides in their composition rather than carbides/nitrides. We find the electronic and mechanical properties of these materials similar to other well known *MAX* phases, i.e.; our calculated bulk moduli 142 GPa and 138 GPa of Ti_4AlH_3 and Ti_3AlH_2 respectively, are comparable with Ti_3SiC_2 and $Ti_3Si_{0.5}Ge_{0.5}C_2$.

In paper XXIV [196], we are presenting the electronic and mechanical properties of another potential *MAX* phase material Cr_2AlC, which was studied a lot experimentally and theoretically, but a correct theoretical description of this material was lacking. We succeeded to obtain the correct values of bulk modulus and volume of this material, comparable with experimental data by taking into account the correlation between the d electrons of Cr atoms with the use of GGA+U method, which was not considered so far by other researchers. Our results are summarized in Table 6.2. We find that the treatment of the correlated electrons is important to explore the electronic structure of Cr_2AlC, provided that a correct value of U is chosen carefully.

Table 6.2. *Calculated and experimental values of the lattice constants, equilibrium volume and bulk modulus of Cr_2AlC. NM stands for non-magnetic, while FM refers to a ferromagnetic ordering the magnetic moments on the Cr atoms. The GGA+U results were obtained with U=1.95 eV and J=0.95 eV. [196].*

Method	a (Å)	c (Å)	V_0 (Å^3)	B_0 (GPa)
GGA (NM)	2.85	12.71	89.1	185
GGA+U(NM)	2.86	12.64	89.5	188
GGA+U(FM)	2.86	12.78	90.3	164
Expt.[a]	2.857±0.002	12.81±0.002	90.6±0.5	165±2

[a]From Ref.[190].

Similarly, in paper XXV [197], we investigate the electronic, magnetic and mechanical properties of another well known *MAX* phase material Cr_2GeC. We find the anti-ferromagnetic ordering to be the ground state for this material. Again, we find that it is important to take into account the correlated electrons with the GGA+U approximation for the correct understanding of this *MAX* phase material. Our calculated results with different approximations are presented in Table 7.5. As you can see from Table 7.5 that our calculated results with GGA+U method are comparable with available experimental values.

Table 6.3. *Calculated and experimental values of lattice constants, volumes and bulk modulus of Cr_2GeC, determined from our ab initio calculations. [197].*

Method	a (Å)	c (Å)	V_0 (Å^3)	B_0 (GPa)
GGA (NM)	2.95	12.08	91.08	197
GGA+U(AFM)	2.97	12.16	91.21	150
HSE (AFM)	3.05	12.65	102.46	168
Expt.[a]	2.950±0.006	12.086±0.008	91.1±0.8	182±2
Expt.[b]	2.958	12.249	92.817±0.1	169±3

[a]From Ref.[191], [b]From Ref.[198].

In paper XXVI [199], we present the anomalous temperature dependence of elastic constant c_{44} for elements V, Nb, Ta, Pd, and Pt. We find that the variation of elastic constant for simple elements can be approximated as the sum of thermal expansion and electronic components. We also calculate the equilibrium volume V_0, bulk modulus B, elastic constant c_{44}, and the thermal expansion coefficient α as shown in Table 6.4 [199]. Our calculated results are in good agreement with experimental values [200].

$Ti_{1-x}Al_xN$ is one of the most common coating material, which can be used as a protective layer on cutting tools. The spinodal decomposition of $Ti_{1-x}Al_xN$ leads to an increase in both hardness and indentation modulus at the temperatures 600-1000°C. In paper XXVII, we construct the 216 atoms SQS model

Table 6.4. *Theoretical and experimental [200] equilibrium volume V_0, bulk modulus B, shear elastic constant c_{44}, and thermal expansion coefficient α.*

		V_0 (Å^3)	B(GPa)	c_{44}(GPa)	α(x10^{-6}K^{-1})
V	EMTO	13.47	175	35.69	6.6
	Exp.	13.77	162	45.87	7.8
Nb	EMTO	18.13	161	37	6.0
	Exp.	17.98	170	30	7.1
Ta	EMTO	18.41	185	95.8	4.6
	Exp.	18.13	200	87.6	6.3
Pd	EMTO	15.48	165	85.15	12.59
	Exp.	14.72	181	71.17	11.6
Pt	EMTO	15.84	244	98.72	8.13
	Exp.	15.06	230	77.4	8.9

structure of cubic $Ti_{0.35}Al_{0.65}N$ and probe the local ordering in c-$Ti_{0.35}Al_{0.65}N$ up to and above the temperature of decomposition using the X-ray spectroscopy and density functional theory calculations. Our results reveal the gradual segregation of, Al and N and Ti and N vacancies in c-$Ti_{0.35}Al_{0.65}N$, which will eventually decompose into cubic domains. We find that nitrogen is favoring an Al surrounding whereas N vacancies are attracted to Ti at the studied concentration of 0.92 % vacancies on the N lattice.

7. Oxides and amorphization of oxide materials

7.1 Amorphous materials

Because of the superior mechanical and magnetic properties in most cases, amorphous materials are drawing the increasing interest of researchers for industrial and scientific applications. Generally, the interpretation of experiments becomes difficult due to the lack of periodicity and symmetries in amorphous structures. In experiments, the structural information can be obtained through radial distribution function (RDF), which is an averaged quantity over the structure, but in amorphous structures the detailed local environment information is missing, therefore, it is not possible to uniquely identify a structure through RDF, although it can be done in crystals. However, an amorphous model structure can be produced to get the local environment information and its radial distribution function (RDF) can be compared with measurements. Other properties namely: the X-ray photoemission spectrum (XPS) [201, 202], nuclear magnetic resonance (NMR) spectra [203], the electronic density of states (DOS) [204] and thermodynamic properties [205] can also be compared with experiments. Thus a reliable amorphous structure can be obtained by comparing its properties with the independently measured properties.

In paper XXVIII [206], we construct amorphous structures of $YCrO_3$ with the use of *ab initio* molecular dynamics simulations and stochastic quenching (SQ) method to perform a detailed analysis by calculating the radial distribution functions (RDFs), angle distribution functions (ADFs), bond lengths and average coordination numbers of these structures. We compare all these parameters of the structures obtained by both independent first principles density functional theory methods to predict the reliable structure of amorphous $YCrO_3$. The small differences in the calculated RDFs and ADFs of both structures are too small to distinguish from statistical fluctuations. We also find by our calculated properties that the Cr^{3+} local environment of the $YCrO_3$ crystal is almost preserved in the amorphous structure, which indicate that interesting properties in the crystalline structure of this material may also be presented in the amorphous structure.

In paper XXIX, we present the combined results from XAS, XES and density functional theory calculations to predict the room temperature ferromagnetism in thin films of $YCrO_3$. We find that upon amorphization, an insulator to metal transition affects the magnetic coupling between local spin moments on Cr

atoms. Based on our results it can be speculated that the short range ferromagnetic coupling is accompanied by disorder in the system, which permeates in the sample. We also find that the high-spin solution for the local moments is energetically favored in amorphous $YCrO_3$. Our first principles calculated results are shown in Figure 7.1.

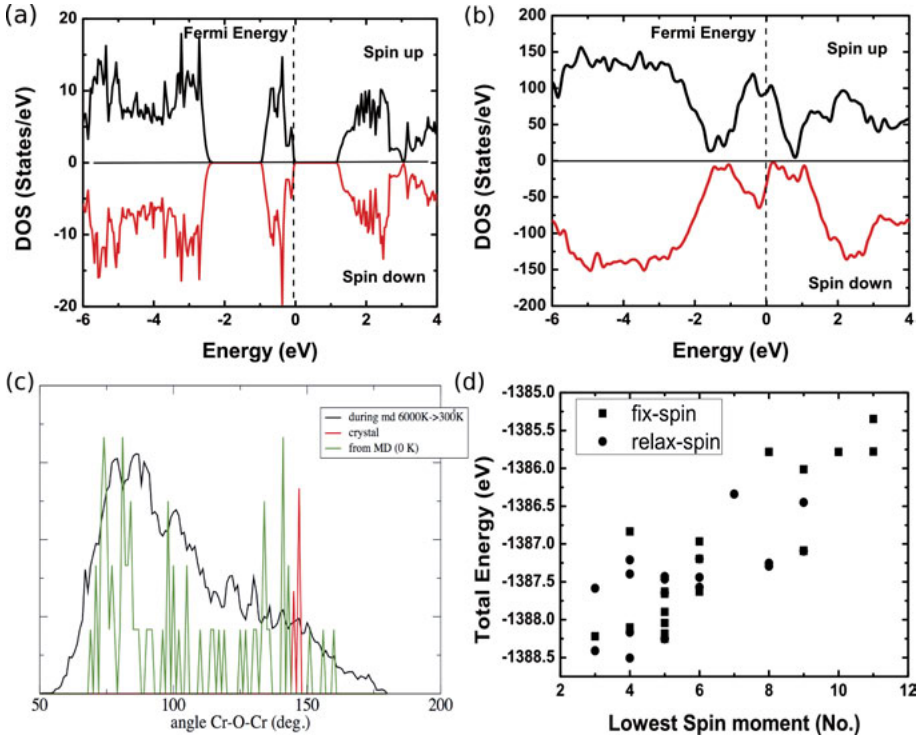

Figure 7.1. (a) Total DOS of crystalline phase of $YCrO_3$, (b) Total DOS of amorphous $YCrO_3$; (c) Cr-O-Cr bond angle distribution; and (d) total energy as a function of the number low spin states (local moment close to 1μB) on Cr atoms in the amorphous cell.

Here we are presenting the results of $YCrO_3$ only, but amorphizing of $YbCrO_3$ also reveals the same results, and we believe that our results are more general, that can be applied for a wide range of antiferromagnetic oxides, which may become metallic in the amorphous phases.

To explore and understand the electronic density of states (DOS) of V_2O_5 is important because of several of the potential applications [50] like: intercalation material to use as cathode material in Li-ion batteries [51], mixed V_2O_5-TiO_2 films, used in electrochromic devices for smart windows [52, 53, 54], gas sensors [56], and detectors for infrared radiation [57]. The electronic density of states of intercalation materials can be measured by simple electrochemical measurements [207, 208]. During the intercalation of ions in a thin film ma-

terial, empty states are filled by electrons which are inserted from the external circuit to maintain charge neutrality however, the rigid-band approximation should be valid during the intercalation [208]. During this process, we obtain an image of the DOS in the lower part of the conduction band from the energy distribution of the inserted ions.

In paper XXX, we employ a chronopotentiometry technique using intercalation of Li^+ ions to measure the electron DOS of sputtered amorphous V_2O_5 thin films. *Ab initio* molecular dynamics (MD) calculation are also simulated to get the amorphous structure of V_2O_5. We calculate the electronic density of states of amorphous V_2O_5. Then we compare the measured DOS with theoretical computations for amorphous V_2O_5, and find them in good agreement. The characteristics of the optical properties of as-deposited and ion intercalated V_2O_5 films are qualitatively interpreted with the use of measured EDOS. On the basis of our observed significant similarities between experimental EDOS and computed DOS, we conclude that the general methodology that we opt in our measurements is a promising way to investigate the characteristics of amorphous oxide thin films.

In paper XXXI, we present the characteristics of cubic $Gd_3Ga_5O_{12}$ (GGG), having an extensive experimental database and is an excellent simulant for a geological material, like $MgSiO_3$. We have demonstrated by our laser-driven shock compression experiments that a transparent, electrically-insulating strong oxide at ambient becomes optically reflective and a poor metal at sufficiently high shock pressures. Then we perform *ab initio* molecular dynamics simulations to construct the amorphous structures of $Gd_3Ga_5O_{12}$ (GGG) at high pressures and calculate the corresponding electronic and optical properties of these amorphous structures. As we can see from Figures 7.2 and 7.3 , $Gd_3Ga_5O_{12}$ (GGG) remains semiconductor at d= 14.16 g/cm^3 whereas the bandgap is closed and it becomes optically reflective at d = 16.18 g/cm^3 with R=0.105, that continues up to d = 17.3 g/cm^3 with R=0.095, which supports our experimental findings.

7.2 Oxide materials

In paper XXXII [211], we present the detailed study of electronic and mechanical properties of Y_2O_3 with the use of GGA-PBE and hybrid functional (HSE06). We calculated the elastic constants, the shear and Young's modulus, and Poisson's ratio with GGA-PBE method and find them in good agreement with experimental values available in literature, but the GGA-PBE method overestimates our calculated value of bulk modulus of Y_2O_3 with elastic constants. Then we employ the Birch–Murnaghan EOS to calculate the lattice parameters and corresponding bulk modulus value of Y_2O_3 using the GGA-PBE and HSE06 functional. We find that GGA-PBE method is underestimating the bulk modulus of Y_2O_3, however, hybrid functional (HSE06) performs well to

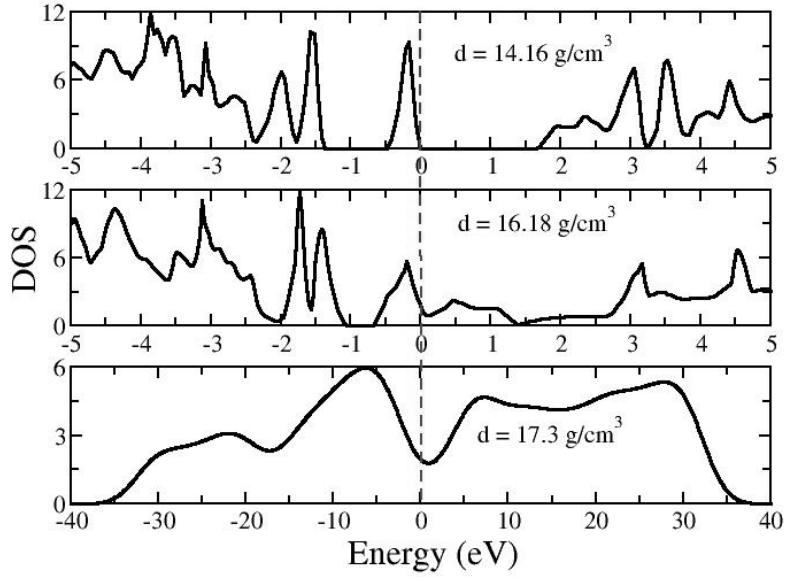

Figure 7.2. Total density of states (DOS) of amorphous structures of GGG.

reproduce the experimental bulk modulus value of Y_2O_3. Furthermore, our calculated lattice constant, equilibrium volume and band gap values of Y_2O_3 (see Table 7.1 and 7.2), as well as optical properties, with hybrid functional (HSE06) are also in good agreement with experimental data [209, 210].

Table 7.1. *The calculated bulk modulus and equilibrium lattice parameters of Y_2O_3 with the use of Birch Murnaghan equation of state. [211].*

methods	B0 (GPa)	a0 (Å)	V0/atom (Å^3)
GGA-PBE	136.81	10.71	15.34
HSE06	150.64	10.60	15.03
Expt. [209]	149.5±1.0	10.6018	14.904514

Similarly, in paper XXXIII, we investigate the electronic, mechanical and optical properties of In_2O_3 using the hybrid functional. We successfully reproduce the bandgap value of In_2O_3 and our calculated values of lattice constant, equilibrium volume and bulk modulus of In_2O_3, as shown in Table 7.3, are in good agreement with the available experimental data in the literature. On the basis of our systematic studies, we can say that the hybrid functional (HSE06)

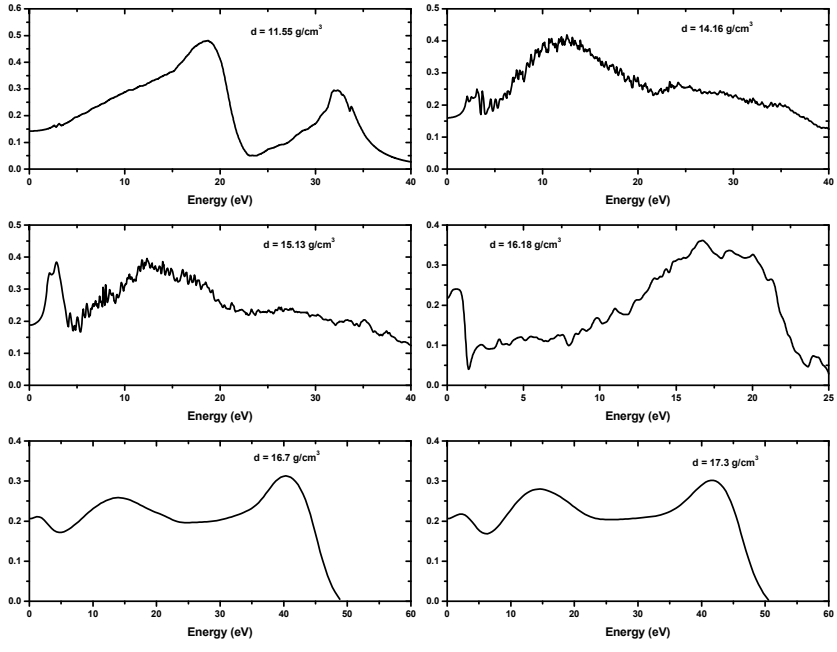

Figure 7.3. Optical properties (reflectivity) of amorphous structures of GGG.

Table 7.2. *The calculated and experimental band gap values of Y_2O_3. [211].*

Method	bandgap (eV)
GGA-PBE	4.3
HSE06	6.0
Expt. [210]	5.5

may play an important role for the accurate and comprehensive description of the electronic, optical and mechanical properties of oxide materials.

Table 7.3. *The calculated bulk modulus and equilibrium lattice parameters of In_2O_3.*

method	B0 (GPa)	a0 (Å)	V0/f.u. (Å^3)
HSE06	192.66	10.232	66.96
Expt. [212]	194.24	10.121	64.80

In paper XXXIV, we study the surface states of $YCrO_3$ using first-principles calculations by constructing the three surfaces of $YCrO_3$ namely: 001, 010 and 100 surfaces. We calculate the surface energies of all these three surfaces of

$YCrO_3$ and it is found that, (001) surface is the lowest in surface energy, followed by (100) and (010) surfaces respectively as shown in Table 7.4. We also find that the ferromagnetic ordering is the ground state (energetically favorable) for all the three surfaces in our slab calculations.

Table 7.4. *The calculated surface energies of $YCrO_3$ surfaces.*

surface	surface energy (J/m^2)
001	1.84
010	2.57
100	2.10

In paper XXXV, we use the hybrid functional (HSE06) to study the phase transition of $PbTiO_3$, which is one of the most extensively studied material due to its ferroelectric properties [213, 214, 215] and wide range applications [216, 217]. Our calculated transition pressure from tetragonal to cubic structure is found to be around 13.2 GPa, as shown in Figure 7.4, which is in good agreement with experiments [218]. Then we calculate the structural parameters, electronic and mechanical properties of the tetragonal and cubic phases of $PbTiO_3$. We also calculate the bulk modulus and elastic constants using LDA and hybrid functional (HSE06). Our calculated results are in good agreement with experimental data available in literature.

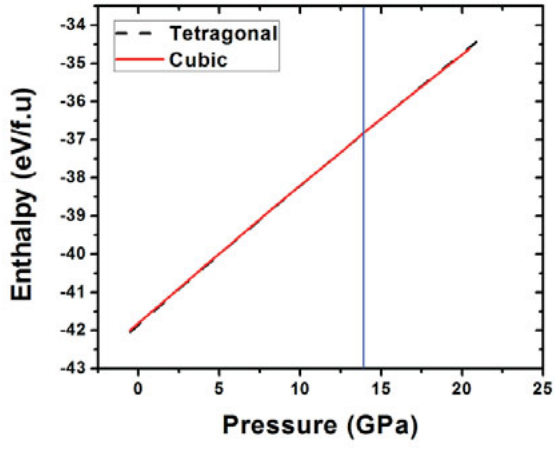

Figure 7.4. Pressure vs Enthalpy plot of $PbTiO_3$.

Because of a variety of technological applications of platinum oxides, like: an important constituent in Adam's catalyst [219], a superficial phase for oxidizing carbon compounds [220] and electrode materials for memory capaci-

tors [221, 222], a lot of research work both theoretically and experimentally has been carried out concentrating on the crystal structures to attain the clear atomistic understanding of platinum oxides, but the controversy exists between the experimental and theoretical studies [223, 224, 225, 226, 227, 228, 229, 230, 231, 232, 233, 234].

Therefore, in paper XXXVI [235], we use the hybrid functional (HSE06) to study the proper atomic geometries, electronic structures and optical properties with the predictions of the most energetically stable phases of PtO and PtO_2. We perform theoretical calculations of PtO (PtS and GeS structures) and orthorhombic PtO_2 ($CaCl_2$, $PbCl_2$ and ZrO_2 structures) within the framework of DFT by using the approach of hybrid functional. We also employ the conventional GGA for our calculations to compare the results acquired from two different methods. We determine the structures having the lowest energy for both PtO and PtO_2 and find that PtS-type structure of PtO and $CaCl_2$-type structure of PtO_2 are the most stable structures of these materials on the basis of hybrid density functional and they appear to be semiconductors. The phonon band structures are calculated to ensure the mechanical stability of these structures (see Figure 7.5). We calculate the corresponding structural parameters, electronic structure, Bader charge analysis and optical properties of these phases.

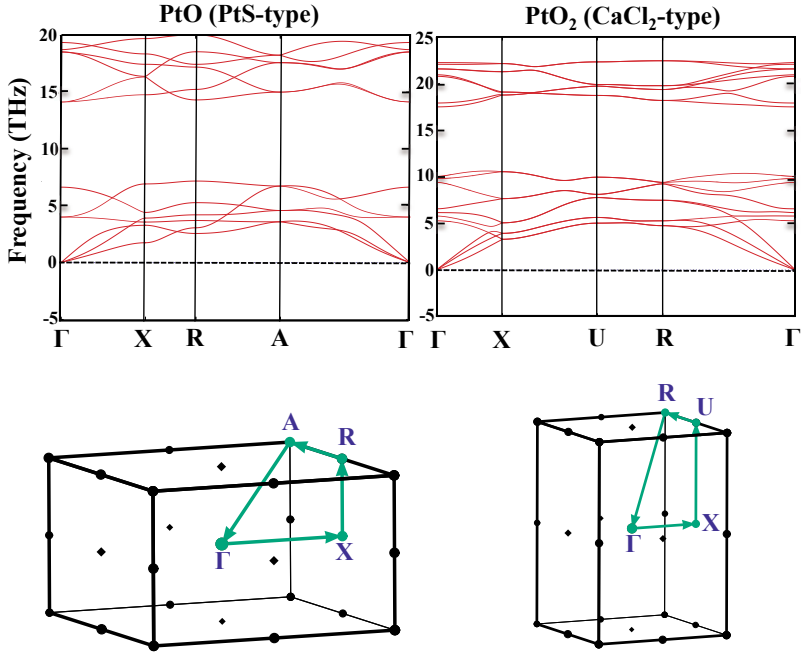

Figure 7.5. Phonon band structures and corresponding first brillouin zones of PtO in PtS-type structure (left) and PtO_2 in $CaCl_2$-type structure (right). [235].

ZrW_2O_8 with a unique property of isotropic contraction over a wide temperature range of 0-1050 K, is a well known negative thermal expansion material [238], which has been studied a lot in the literature [236, 237, 238, 239, 240, 241, 242, 243, 244, 245, 246, 247, 248, 249]. However, the detailed theoretical counterpart of this potential candidate material for industry and technology is still lacking. Thus, in paper XXXVII [250], we present a comprehensive study of structural parameters and high pressure characteristics of ZrW_2O_8. We use the generalized gradient approximation (GGA) and local gradient approximation (LDA) methods to calculate the structural parameters, mechanical and optical properties of this material. The corresponding properties such as: bulk, shear and Young's moduli, Poisson's ratio, and Debye temperature of this material are also calculated. We find that our results obtained with LDA method are in good agreement with the available experimental data in the literature, as shown in Table 7.5 ([250]). We determine the transition pressure of α to γ-ZrW_2O_8 and compare it with the experimental data. Furthermore, we calculate the optical properties of this material and explain them through the electronic structure of ZrW_2O_8.

Table 7.5. *Calculated and experimental elastic constants (C_{ij}), bulk modulus B, Young modulus E, shear modulus G, Poisson ratio ν, and Debye temperature θ_D for α-ZrW_2O_8. The experimental values are from Ref. [238].*

Method	T (K)	C_{11} (GPa)	C_{12} (GPa)	C_{44} (GPa)	B (GPa)	E (GPa)	G (GPa)	ν	θ_D
Calc.(GGA)	0	144.8	65.6	22.6	92.0	79.7	29.4	0.356	314
Calc.(LDA)	0	157.7	78.7	30.5	105.0	92.3	34.1	0.354	335
Expt.	0	161.8	75.5	29.4	104.3	98.8	36.8	0.342	333
Expt.	300	128.4	47.5	27.4	74.5	88.3	33.9	0.303	321

8. Phase change memory, chalcopyrite, and sulfide materials

8.1 Phase change memory materials

The technology of rewritable data storage devices such as CD-RW, DVD-RW, DVD-RAM is currently dominated by the phase change memory (PCM) materials because of several key benefits [251, 252, 253, 254]. The rapid and reversible phase switching from an ordered crystalline state to a disordered amorphous state is used for data storage process and such type of phase transformation is a temperature-driven process, which can be repeated by applying external stimuli, such as: electrical pulse to generate heat. This process can be initiated by taking an as-deposited thin-film of amorphous phase and then the sample is heated up to its glass-transition temperature, which is called set operation, during which atoms have higher mobility and can be energetically rearranged to stabilize in the crystalline state. Similarly, during the reset operation, the crystalline state is further heat up above to its melting temperature by applying an other electrical pulse of higher magnitude to liquefy and then suddenly it is cooled down to obtain again an amorphous state. Because of pronounced contrast of electrical resistance between crystalline and amorphous states, the recorded data can be easily read.

Gallium doped indium oxide is recently reported to be a promising phase change memory material due to its considerable contrast (two order of magnitude) in electrical resistivity between a high-resistance amorphous and low-resistance crystalline states during a reversible temperature-dependent phase switching, if the important requirements for practical PCM like, stability and energy density can be appropriately fulfilled [255]. In paper XXXVIII [256], we investigate the atomic structures of amorphous and crystalline phases and transition mechanisms of Ga:In_2O_3 to insight into atomistic understanding of this material that may lead to its practical use for phase change memory (PCM) devices. We construct and characterize the amorphous structure of gallium-doped indium oxide by means of *ab-initio* molecular dynamics (MD) simulations, within the framework of density functional theory (DFT) calculations. We calculate the density of states (DOS), as shown in Figure 8.1 to explore the electronic properties of amorphous and crystalline structures of Ga:In_2O_3 and find the band gap closure in amorphous structure that is corresponded to semiconductor to metallic transition in this material on amorphization.

We investigate the characteristics of amorphous and crystalline phases of Ga:In_2O_3 by calculating the other properties like radial distribution function

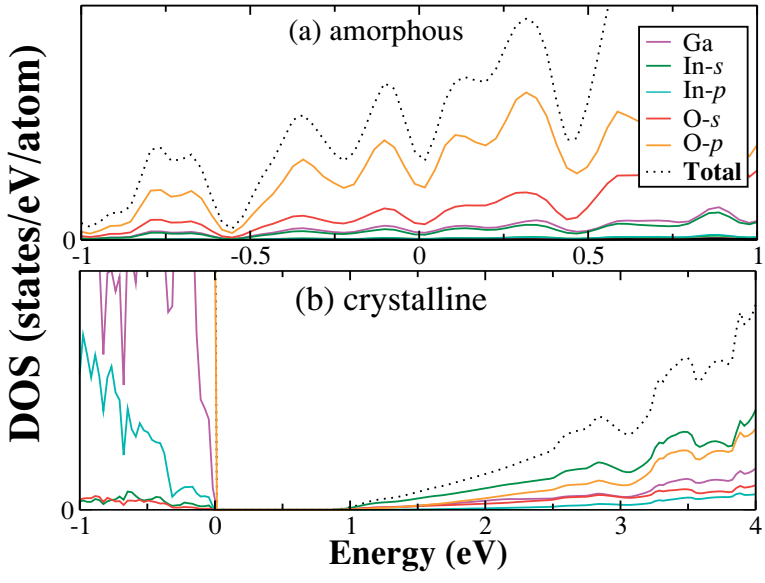

Figure 8.1. Total density of state (DOS) of (a) a-$GaIn_2O_3$ equilibrating at 300 K and (b) optimized c-$GaIn_2O_3$. Fermi level is set to zero. [256].

(RDF), bond angle distribution (BAD) and Bader charge analysis. We find the similarities between the Ga:In_2O_3 and other well known PCM materials available in literature. Therefore, on the basis of our density functional theory (DFT) calculations, we suggest it a promising material for phase change memory (PCM) devices.

In paper XXXIX [257], the crystal and electronic structures and optical properties of well known phase change memory material $Ge_2Sb_2Te_5$ are investigated by means of GGA and hybrid functional (HSE06). We initiate our study by taking three stable structures namely: A, B and C, of this material and calculate the structural parameters, band gaps and dielectric functions. Our calculated electronic band gap values of this material with HSE06 method are in good agreement with the available experimental data in the literature (see Table 8.1).

Table 8.1. *The calculated bandsgap energy of the stable* $Ge_2Sb_2Te_5$ *phase. [257].*

Proposed structures	PBE (eV)	HSE06 (eV)
A	0.00	0.26
B	0.24	0.37
C	0.22	0.48
Experiments	0.57 (Ref. [258]), 0.50 (Ref. [259])	

We also analyze the electronic charge distribution using the Bader's theory of charge analysis. We find that our results calculated by means of hybrid functional (HSE06) are on average, very close to available experimental values than calculated with the use of PBE functional. We also find that all the calculated characteristics of stable phase B of $Ge_2Sb_2Te_5$ are more closer to available experimental results than other stable phases namely, A and C, which makes phase B, the promising candidate for $Ge_2Sb_2Te_5$ material.

8.2 Chalcopyrite materials

In spintronics, diluted magnetic semiconductors (DMS) and related materials play an important role, where the materials science and traditional solid state physics are strongly linked with each other [260, 261, 262, 263, 264]. DMS are extremely sensitive to external disorders, which can directly affect the magnetic nature. In such cases, pressure can also provide an additional opportunity to manipulate and expand the fundamental properties. A transition towards a ferromagnetic state in the initial paramagnetic alloy (In,Mn)Sb can be induced by applying the pressure [265]. This transition directly affects the wave functions overlap, setting up the exchange interaction, and also allows to control the degree of magnetic scattering [266]. In an other example, the hydrostatic pressure in (Ga,Mn)As, pushes TC on the order of 1 K/GPa and opposite for the two samples with different degree of hole localization [267].

In the above materials, the effect of pressure was mainly taken into account on the intrinsic magnetic coupling. In our paper XL, we present our study of hydrostatic pressure induced magnetic phase transitions, which occurs in ternary compound $CdGeP_2$:Mn with the cluster ferromagnetism. We show on the basis of high-pressure measurements of volume, transport and magnetic properties as well as with ab initio methods that a simple external pressure and RT occur two FM-PM transition caused by the second phase in $CdGeP_2$:Mn, that can be controlled by varying degrees of Mn content. We find that the observed transitions are realized under pressure at RT regime, which can also be controlled at low temperature regime, in contrast with early findings [265, 267]. We also present a detailed study of the effect of pressure up to 10 GPa, and further to 20 GPa, where the magnetic moment collapsed by means of density functional theory (DFT) calculations. Our results can lead towards a new opportunities in the field of spintronic functionality as pressure induced FM-PM switches by using ferromagnetic chalcopyrite and beyond.

8.3 Sulfide materials

Sulfides, specifically, the binary vanadium sulfur compounds that lie between the localized and delocalized d-electron materials and are isostructural with

the niobium chalcogenides, are growing interest in the scientific and industrial communities because of their unusual unique physical and structural properties [268, 269, 270, 271]. In InV_6S_8 structure, In atoms are mainly one dimensional statically disordered and the large hexagonal channels parallel to the c axis are occupied by In atoms, is important feature of this compound resembling with other niobium chalcogenides, NB_3X_4 structures. In such type of compounds, high pressure study is an excellent tool to analyze the charge and spin density wave instabilities [272, 273].

In paper XLI [274], we have presented the high pressure studies of InV_6S_8 with the use of LDA, GGA and LDA+U approximations. We performed a series of calculations and used the third order Birch-Murnaghan equation of state (EOS) and extracted the equilibrium volume and bulk modulus values of this compound. Our calculated results are presented in Tables 8.2 and 8.3.

Table 8.2. *Calculated and experimental values of the equilibrium volume and bulk modulus of InV_6S_8. The LDA+U results are obtained with U=5.95 eV and J=0.95 eV. [274].*

Method	V_0(Å^3)	B_0(GPa)
LDA	219.21	142.9
GGA	236.60	88
LDA+U	228.3	108.6
Expt.[a]	241.80	110.2

[a]From Ref.[275].

Table 8.3. *Calculated values of the lattice constants of InV_6S_8 using the LDA+U approximation (with U=5.95 eV and J=0.95 eV). [274].*

Pressure	Method	a_0(Å)	c_0(Å)
Ambient			
	LDA+U	9.1	3.2
	Expt.[a]	9.1711	3.2972
11.3 GPa			
	LDA+U	8.787	3.109
	Expt.[a]	8.953	3.254

[a]From Ref.[275].

We have concluded that, to take into account the correlation effects properly, the Hubbard like correction with the correct choice of U parameter, is very important to investigate the complex electronic structure and mechanical properties of this compound. We have also calculated the extensive band structures of this material, which were suggested by Hochheimer *et al.* [276] and found that the nesting of energy bands reduces with compression.

9. Conclusions

This thesis presents the applications of *ab initio* self-consistent total energy calculations and *ab initio* molecular dynamics simulations, based on density functional theory to characterize and explore the materials properties at ambient and high pressures.

Hydrogen is fascinating to physicists and one of the most studied materials due to predicted possibility of metallization and high temperature superconductivity. Recently hydrogen was claimed to be conductive at ambient temperature and at pressure around 260 GPa, but in contrast the other studies suggested it insulator at very same conditions. In such a scenario, we have performed *ab initio* molecular dynamics simulations to explore the phenomena possibly causing the disagreement between these findings and our results have suggested that the recent claim of conductive hydrogen by experiments might be explained by the diffusion of hydrogen.

The search for alternate and renewable energy resources is required because of exponential growth in world population, limited conventional fossil fuel resources, and to meet the increasing demand of clean and environment friendly substitutes. The efficient use of energy and development of such systems that can help to save the energy consumption is also important. In this thesis, we are presenting our studies on hydrogen storage materials, Li and Mg based cathode materials for rechargeable batteries and *MAX* phase materials, which are important to overcome the recent and future energy requirements.

We have studied the structural and electronic properties of some of the chemical hydrides, complex hydrides and functionalized nanostructures. We have analyzed the desorption of hydrogen mechanism and diffusion of hydrogen in promising hydrogen storage materials, which can lead to understand and improve the kinetics and thermodynamics of these materials and play an important role to limit the difficulties in the storage of hydrogen at favorable conditions.

Another active field relating to energy storage is rechargeable batteries. We have studied the detailed crystal and electronic structures of Li based phosphate and sulphate materials, Mg based materials and calculated the average intercalation voltage of the corresponding batteries of Na_2FePO_4F, Li_2FePO_4F, $LiNaFePO_4F$, $LiFeSO_4F$, $Mg_2Mo_6S_8$ and $MgCuMo_6S_8$. Our results are in good agreement with available experimental data and we have made new predictions too. We have also performed molecular dynamics simulations to study the diffusion of lithium in $LiFeSO_4F$, and found it to be three dimensional which is a clear advantage over other promising cathode materials, like,

$LiFePO_4$. In an effort to combine battery and fuel-cell technologies, we have calculated that transition metal doped- MgH_2 nanocluster is a material to use efficiently not only in batteries but also in fuel-cell technologies.

MAX phase materials have one application among many others to be used to develop the systems to save the energy consumption. We have studied the structural, electronic, and mechanical properties of Ti_2AlN, Ti_2AlC, V_2AlC, Nb_2AlC, Ta_2AlC, V_2GeC, Ti_3SiC_2, and Ti_4AlN_3, using the hybrid functional HSE06. Our results are comparable with the experiments, and we have suggested that HSE06 functional can be used as a predictive tool to study the properties of *MAX* phases. Further, we suggest that the proper treatment of correlation effects is important for the correct description of Cr_2AlC and Cr_2GeC. We have also presented a new type of *MAX* phases, consisting of hydrides in their composition instead of carbon or nitrogen.

In most cases amorphous materials have the superior electronic, mechanical, magnetic and optical properties than common materials. Therefore, we have constructed the amorphous structures of oxide materials such as, $YCrO_3$, $Gd_3Ga_5O_{12}$ and V_2O_5 and analyzed the corresponding characteristics. We have found disorder induced ferromagnetism above room temperature upon amorphization in perovskite $YCrO_3$. Our calculated density of states and optical properties of the amorphous structures of $Gd_3Ga_5O_{12}$ at extreme pressures are in good agreement with experimental findings. Our calculated density of states of amorphous structure of V_2O_5, are also in close agreement with experiments, which is a potential candidate for Li-ion cathode materials and smart windows. We have also calculated the electronic, structural, mechanical and optical properties of potential oxide materials such as In_2O_3, Y_2O_3, $PbTiO_3$, ZrW_2O_8, which are important for industrial point of view.

Phase change memory (PCM) materials are pomising for rewritable data storage devices, such as CD-RW, DVD-RW and DVD-RAM. We have modeled the amorphous structure of gallium doped indium oxide and analyzed the electronic properties of amorphous and crystalline structures. We have found the band gap closure in amorphous structure that is correspond to semiconductor to metallic transition in this material upon amorphization. Based on our results, we have proposed that Ga-In_2O_3 is a potential candidate for phase change memory devices. We have also calculated the electronic and optical properties of another promising phase change memory material: $Ge_2Sb_2Te_5$.

To study the spintronics materials, we have conducted the high pressure calculations of Mn doped $CdGeP_2$ and analyzed the volume, transport and magnetic properties, which is an important material for spintronics applications. Finally, we have also employed the high pressure calculations to compute the structural parameters, electronic structure and band structures of superconducting material InV_6S_8. We find that the correct choice of Hubbard like correction is necessary to take into account the correlation effects in this material, which are important for the correct description of this compound. Furthermore, we

could not find any anomaly in the lattice constants of InV_6S_8 in the high pressure calculations at extended range of pressures.

10. Sammanfattning på Svenska

Denna avhandling beskriver tillämpningen av första-princips själv-konsistenta total-energi beräkningar och första princips molekyldynamiksimuleringar, baserat på täthetsfunktionalteori för att karaktärisera och undersöka materialegenskaper vid normala samt höga tryck.

Väte är fascinerande för fysiker och ett av de mest studerade materialen på grund av den förutspådda möjligheten för metallisering och hög temperatur supraledning. Nyligen påstods väte vara ledande vid rumstemperatur och ett tryck runt 260 GPa, men i motsats föreslog andra studier att det är en isolator vid samma förhållanden. I ett detta scenario har vi utfört första-princips molekyldynamiksimuleringar för att utforska de fenomen som möjligen kan orsaka oenigheten mellan dessa olika resultat och våra resultat har föreslagit att den senaste tidens påståenden om ledande väte i experiment kan förklaras av väte-diffusion.

Sökandet efter alternativa och förnybara energikällor är nödvändig på grund av den exponentiella tillväxten i världens befolkning, begränsade mängder konventionella fossila bränslen, samt för att möta den ökade efterfrågan på rena och miljövänliga alternativ. Mer effektiv energianvändning och utveckling av system som kan bidra till att spara energi är också viktigt. I denna avhandling presenterar vi våra studier på vätelagringsmaterial, Li- och Mg-baserade material för katoden i uppladdningsbara batterier och MAX-fas material, som är viktiga för att övervinna de nutida och framtida energibehoven.

Vi har studerat de strukturella och de elektroniska egenskaperna hos några kemiska hydrider, komplexa hydrider och funktionaliserade nanostrukturer. Vi har analyserat mekanismen för väte-desorption samt diffusion av väte i lovande vätelagringsmaterial, vilket kan leda till bättre förståelse och förbättringar av kinetik och termodynamik för dessa material vilket spelar en viktig roll för att begränsa svårigheterna av väte-lagring vid gynnsamma förhållanden.

Ett annat aktivt fält inom energilagring är uppladdningsbara batterier. Vi har studerat den detaljerade kristall och elektroniska strukturen för Li baserade fosfat- och sulfat-materialet och Mg-baserade material för att beräkna den genomsnittliga spänningen vid infogande i de motsvarande batterierna Na_2FePO_4F, Li_2FePO_4F, $LiNaFePO_4F$, $LiFeSO_4F$, $Mg_2Mo_6S_8$ och $MgCuMo_6S_8$. Våra resultat är i god överensstämmelse med tillgängliga experimentella data och vi har gjort nya förutsägelser också. Vi har även utfört molekyldynamiksimuleringar för att studera diffusion av litium i $LiFeSO_4F$, och funnit att den är tredimensionell, vilket är en klar fördel jämfört med andra lovande katodmaterial, såsom $LiFePO_4$. I en ansträngning att kombinera batteri och bränslecellsteknik, har vi beräknat att det övergångsmetalls-dopade nanoklustret, MgH_2,

är ett material som kan användas effektivt inte bara i batterier utan även i bränsleceller.

En applikation av MAX fas material bland många andra är användning inom system för att spara energi. Vi har studerat de strukturella, elektroniska och mekaniska egenskaper av Ti_2AlN, Ti_2AlC, V_2AlC, Nb_2AlC, Ta_2AlC, V_2GeC, Ti_3SiC_2 och Ti_4AlN_3, med hjälp av hybrid-funktionalen HSE06. Våra resultat är jämförbara med experiment, och vi har föreslagit att HSE06 funktionalen kan användas som ett prediktivt verktyg för att studera egenskaperna hos MAX faser. Vidare föreslår vi att en korrekt behandling av korrelations effekter är viktigt för en korrekt beskrivning av Cr_2AlC och Cr_2GeC. Vi har också presenterat en ny typ av MAX faser, där sammansättningen består av hydrider istället för kol eller kväve.

I de flesta fall har amorfa material överlägsna elektroniska, mekaniska, magnetiska och optiska egenskaper över vanliga material. Därför har vi konstruerat amorfa strukturer av olika oxid material såsom, $YCrO_3$, $Cd_3Ga_5O_{12}$ och V_2O_5 och analyserat motsvarande egenskaper. Vi har funnit att oordning inducerar ferro-magnetism vid temperaturer över rumstemperatur i amorf perovskit $YCrO_3$. Vår beräknade elektronstruktur och de optiska egenskaperna hos de olika amorfa strukturerna av $Cd_3Ga_5O_{12}$ vid extrema tryck är i god överensstämmelse med de experimentella resultaten. Vår beräknade elektronstruktur i amorf V_2O_5, är också i nära överensstämmelse med experiment, vilket är en potentiell kandidat för Li-jon katod material och smarta fönster. Vi har också beräknat de elektroniska, strukturella, mekaniska och optiska egenskaper hos potentiella oxidmaterial såsom In_2O_3, Y_2O_3, $PbTiO_3$, ZrW_2O_8, som är viktiga ur industriell synvinkel.

Fas-bytes minnesmaterial (PCM) är lovande material för återskrivbara lagringsmedier, t.ex. CD-RW, DVD-RW och DVD-RAM. Vi har modellerat den amorfa strukturen av gallium dopad indiumoxid och analyserat de elektroniska egenskaperna hos de amorfa och kristallina strukturerna. Vi har hittat en reducering av elektron-bandgapet i den amorfa strukturen som motsvarar övergång från halvledare till metall i detta material vid övergång till amorf struktur. Baserat på våra resultat, har vi föreslagit att $Ga-In_2O_3$ är en potentiell kandidat för fas-bytes minnes enheter. Vi har också beräknat de elektroniska och optiska egenskaper hos ett annat lovande fas-bytes minnesmaterial: $Ge_2Sb_2Te_5$.

För att studera spinntronik material, har vi genomfört beräkningar under högt tryck för Mn dopat $CdGeP_2$ vilket är ett viktigt material för applikationer inom spinntronik, där vi analyserat volym, transport och magnetiska egenskaper. Slutligen har vi även använt beräkningar under högt tryck för att beräkna de strukturella parametrarna och elektronisk strukturen av det supraledande materialet InV_6S_8. Här finner vi att rätt val av en Hubbard lik korrigering är nödvändig för att ta hänsyn till korrelations-effekter i materialet, vilket är viktiga för att få en korrekt beskrivning av denna förening. Dessutom kunde vi inte

hitta någon anomali i gitterkonstanterna av InV_6S_8 vid högtrycksberäkningar med större omfattning av tryck.

Acknowledgements

First and foremost, all praises are due to Almighty Allah, The Most Gracious and The Most Merciful, Who has blessed me with uncountable gifts, i.e., health, knowledge, strength, patience etc.. All my devolutions and tributes to His Holy Prophet Muhammad (peace be upon him) for teaching us to recognize our Lord.

First of all I would like to express my sincere gratitude to my supervisor Professor Rajeev Ahuja, who accepted me as a PhD student in his research group and always treated me like a family member. His support, encouragement and guidance have been very important not only for my studies but also for all aspects of my life. I would also like to take this opportunity to thank my co-supervisor Nelson Theethayi, for his unconditional support during my studies. I owe my deepest gratitude to senior most Professor Börje Johansson and Professor Rajeev Ahuja for creating a wonderful research environment.

I would also like to express my gratitude to all my colleagues in Condensed Matter Theory Group and Division of Materials Theory. Special thanks to Ralph, Moyses, Anden, Peter, Peng, Zakia, and Jawad for helping me during early days of my PhD studies. Ralph and Moyses, I learned a lot from you, thank you so much! Thanks Anden for providing me with your MD script, which helped me to analyze my molecular dynamics simulation results. Sebastien! we did a lot of collaborative work and I learned a lot from you. Thank you so much for your unlimited help in research related issues. I really enjoyed your collaboration and I always considered you as my co-supervisor. Thanks Cecilia for your wonderful research collaboration during last year of my PhD studies. Heartiest thanks to Professor Anatoly for teaching me molecular dynamics. I also appreciate your nice and fruitful collaboration.

Many thanks to my past and current colleagues (Ralph, Moyses, Sebastien, Anden, Anatoly, Wei Luo, Zakia, Anton, Sergiu, Duck Young, Pornjuk, Jariyanee, Peter, Jawad, Thanayut, Tanveer, Fredrik, Cecilia, Abir, Sudip, Puspamitra, Myskal, Yunguo, Henrik, Weiwei, Zhao, Baochang, Raghuveer, Peng, and Raphael), who have made this journey so much more interesting and acknowledgeable for me. My indebtedness towards Sebastien, Moyses, Ralph, Khalid, and Sudip for proofreading and valuable suggestions during my thesis write-up. I would also like to thank Henrik for helping me with the "Swedish summary".

Too many thanks to Higher Education Commission of Pakistan (HEC) for providing me with a scholarship to pursue my PhD studies in Sweden. In this regard, I would also like to thank my supervisor Professor Rajeev Ahuja for his financial support during last years of my studies.

I would also like to thank Maroof Usmani (late), Khalid Bhutta, Younis Qureshi, Syed Faseih Iqbal, Raja Amin, Aftab Ahmed, Muhammad Tahir, Kamal Farid, Kaleem Durrani, Saleem Durrani, and Muhammad Akhtar, for their continued support and guidance since my childhood. Many thanks to Ejaz Chohan, Saif-Ullah Awan, Noor Akhtar, M. D. Jamal, M. Rafique, M. Asif, and M. Iqbal for encouraging me to pursue for higher education.

I would also like to thank all of my Pakistani friends in Uppsala, M. Rauf Alvi, M. K. K. Niazi, Zahid Abbass, M. Akhtar Ali, Mazhar-ul-Haq, Jawad Nisar, Hafiz Sohaib, Muneeb, Murad, Shezi, Shehzad, Tanvir, Imran, Shakeel, Salman Toor, Tahir Babar, Shahid Abro, Rizwan Qaisar, Qaisar Abbass, Aamir Razzaq, M. Taqi, Usman Arif, Tanveer Hussain, Nadeem Shehzad Akbar, M. Aqib, Mohsin Goraya, Khurram, Uzair, Adnan, Babar, Yasir, Azhar, Afridi, Kashif, Zubair, Aslam Mazari, Abdul Ghafoor, Allah Rakha, Rehmat shah, Ubaid, Mohsin and many more, for arranging parties, wonderful gatherings, playing indoor and outdoor cricket, and discussions on different topics. I never felt home sickness in your company. My special thanks to Khalid, Mazhar, Zahid, Sohaib, Murad, Muneeb, Abro, Aqib and Ubaid for providing me with a learning environment.

I have no words to express my heartiest gratitude to my parents, wife, brothers, sisters, and relatives for their great love, continuous support, and encouragement throughout my life. The patience of my wife during my busiest schedule is admirable. Especially, the smiles of my daughter Fatima, provided me with the strength and will to complete this job successfully.

References

[1] A. B. Belonoshko, M. Ramzan, H. K. Mao, and R. Ahuja, Nature Scientific. Reports **3** : 2340 (2013), DOI: 10.1038/srep02340.
[2] E. Wigner, and H. B. Huntington, J. Chem. Phys. **3**, 764 (1935).
[3] N. W. Ashcroft, Phy. Rev. Lett. **21**, 1748 (1968).
[4] R. J. Hemley, and H. K. Mao, Phys. Rev. Lett. **61**, 857 (1988).
[5] H. K. Mao, and R. J. Hemley, Science **244**, 1462 (1989).
[6] J. H. Eggert *et al.*, Phys. Rev. Lett. **66**, 193 (1991).
[7] J. S. Tse, and D. D. Klug, Nature **378**, 595 (1995).
[8] V. Natoli, R. M. Martin, and Ceperley, Phys. Rev. Lett. **74**, 1601 (1995).
[9] C. Narayana *et al.*, Nature **393**, 46 (1998).
[10] H. Kitamura *et al.*, Nature **404**, 259 (2000).
[11] P. Loubeyre, F. Occelli, and R. LeToullec, Nature **416**, 613 (2002).
[12] E. Babaev, A. Sudbo, and N. W. Ashcroft, Nature **431**, 666 (2004).
[13] S. A. Bonev *et al.*, Nature **431**, 669 (2004).
[14] C. J. Pickard, and R. J. Needs, Nature Phys. **3**, 473 (2007).
[15] Y. Akahama *et al.*, Phys. Rev. B **82**, 060101 (2010).
[16] M. I. Eremets, and A. Troyan, Nat. Mater. **10**, 927 (2011).
[17] W. J. Nellis, A. L. Ruoff, and I. F. Silvera, *arXiv:1201.0407* (2012)
[18] C. Zha, Z. Liu, and R. J. Hemley, Accepted in Phys. Rev. Lett.
[19] R. T. Howie, C. L. Guillaume, T. Scheler, A. F. Goncharov, and E. Gregoryanz, Phys. Rev. Lett. **108**, 125501, (2012).
[20] P. Jena, J. Phys. Chem. Lett. **2**, 206 (2011).
[21] J. Yang, A. Sudik, C. Wolverton, and D. J. Siegel, Chem. Soc. Rev. **39**, 656 (2010).
[22] A. Gutowska *et al.*, Angew. Chem. Int. Ed. **44**, 3578 (2005).
[23] A. F. Voter, F. Montalenti, and T. C. Germann, Annu. Rev. Mater. Res. **32**, 321 (2002).
[24] J. W. Long, B. Dunn, D. R. Rolison and H. S. White, Chem. Rev. **104**, 4463 (2004).
[25] J. Chen and F. Y. Cheng, Acc. Chem. Res. **42** 713 (2009).
[26] M. Winter and R. J. Brodd, Chem. Rev. **104**, 4245 (2004).
[27] P. G. Bruce, B. Scrosati and J. M. Tarascon, Angew. Chem., Int. Ed. **47**, 2930 (2008).
[28] M. G. Kim and J. Cho, Adv. Funct. Mater. **19**, 1497 (2009).
[29] J. M. Tarascon and M. Armand, Nature **414**, 359 (2001).
[30] A. S. Arico, P. Bruce, B. Scrosati, J. M. Tarascon and W. Van Schalkwijk, Nat. Mater. **4**, 366 (2005).
[31] K. S. Kang, Y. S. Meng, J. Breger, C. P. Grey and G. Ceder, Science **311**, 977 (2006).

[32] D. Deng, M. G. Kim, J. Y. Lee and J. Cho, Energy Environ. Sci. **2**, 818 (2009).
[33] V. Etacheri, R. Marom, R. Elazari, G. Salitra, and D. Aurbach, Energy Environ. Sci. **4**, 3243 (2011).
[34] A. K. Padhi, K. S. Nanjundaswamy, and J. B. Goodenough, J. Electrochem. Soc. **144**, 1188-1194(1997).
[35] A. K. Padhi, K. S. Nanjundaswamy, Masqudier, S. Jkada , J. B. Goodenough, J. Electrochem. Soc. **144**, 1609(1997).
[36] H. Huag, S.C. Yin and L.F. Nazar, Electrochem. Solid State lett. **4**, A170 (2001).
[37] C. Delacourt, P. Poizot, J. M. Tarascon, and C. Masquelier, Nature Mater., **4**, 254 (2005).
[38] T. Maxisch, F. Zhou, and G. Ceder, Phys. Rev. B **73**, 104301 (2006).
[39] A. Yamada, H. Koizumi, S. Nishimura, N. Sonoyama, R. Kanno, M. Yonemura, T. Nakamura, and Y. Kobayashi, Nature Mater., **5**, 357 (2006).
[40] B. L. Ellis, L. K. Perry, D. H. Ryan, L. F. Nazar, J. Am. Chem. Soc. **128**, 11416 (2006).
[41] B. L. Ellis, W. R. M. Makahnouk, Y. Makimura, K. Toghill and L. F. Nazar, Nature Mater., **6**, 749 - 753 (2007).
[42] N. Recham, J-N. Chotard, L. Dupont, C. Delacourt, W. Walker, M. Armand, and J-M. Tarascon, Nature Mat. **10**, 1 (2009).
[43] J-M. Tarascon, N. Recham, M. Armand, J-N. Chotard, P. Barpanda, W. Walker, and L. Dupont, Chem. Mater., **22** ,724 (2010).
[44] P. Barpanda, N. Recham, J-N. Chotard, K. Djellab, W. Walker, M. Armand, and J-M. Tarascon, J. Mater. Chem. **20**, 1659 (2010).
[45] Y. Oumellal, A. Rougier, G. A. Nazri, J. M. Tarascon, and L. Aymard, Nat. Mat. **7**, 916 (2008).
[46] M. W. Barsoum, Prog. Solid State Chem. **28**, 201 (2000).
[47] M. W. Barsoum and T. El-Raghy, Am. Sci. **89**, 334 (2001).
[48] G. N. Greaves, and S. Sen, Advances in Physics **56**, 1 (2007).
[49] B. N. Pal, B. M. Dhar, K. C. See, and H. E. Katz, Nat. Mater. **8**, 898 (2009).
[50] S. Beke, Thin Solid Films **519**, 1761 (2011).
[51] C. Navone, R. Baddour-Hadjean, J. P. Pereira-Ramos and R. Salot, J. Power Sources **152**, A1790 (2005).
[52] A. M. Andersson, C. G. Granqvist and J. R. Stevens, Appl. Opt. **28**, 3295 (1989).
[53] A. Talledo and C. G. Granqvist, J. Appl. Phys. **77**, 4655 (1995).
[54] M. S. Burdis, Thin Solid Films, **311**, 286 (1997).
[55] R. Maik, J. Scherer, L. Li, P.M.S. Cunha, O.A. Scherman and U. Steiner, Adv. Mater., **24**, 1217 (2012).
[56] J. Liu, X. Wang, Q. Peng and Y. Li, Adv. Mater. **17**, 764 (2005).
[57] H. K. Kang, Y. H. Han, H. J. Shin, S. Moon and T. H. Kim, J. Vac. Sci. Technol. B **21**, 1027 (2003).
[58] S. Raoux, W. Wełnic, and D. Ielmini, Chem. Rev. **110**, 240 (2010).
[59] H. Ohno, Science **281**, 951 (1998).

[60] T. Dietl *et al.*, Science **287**, 1019 (2000).
[61] Y. M. *et al.*, Science **291**, 854 (2001).
[62] P. Hogenberg and W. Kohn, Phys. Rev. **136**, B864 (1964).
[63] W. Kohn and L. Sham, Phys. Rev. **140**, A1133 (1965).
[64] R. M. Driezler and E. K. U. Gross, Density Functional Theory An Approach To The Quantum Many-Body Problem (Springer-Verlag, Berlin, 1990).
[65] Richard M. Martin, Electronic Structure Basic Theory and Practical Methods (Cambridge University Press, 2004).
[66] D. M. Ceperley and B. J. Alder, Phys. Rev. Lett. **45**, 566 (1980).
[67] A. D. Becke, Phys. Rev. A **38**, 3098 (1988).
[68] J. P. Perdew and Y. Wang, Phys. Rev. B **45**, 13244 (1992).
[69] J. P. Perdew, K. Burke and M. Ernzerhof, Phys. Rev. Lett. **77**, 3865 (1996).
[70] J. P. Perdew, M. Ernzerhof, and K. Burke, J. Chem. Phys. **105**, 9982 (1996).
[71] J. Heyd, G. E. Scuseria, and M. Ernzerhof, J. Chem. Phys. **118**, 8207 (2003).
[72] J. Heyd and G. E. Scuseria, J. Chem. Phys. **121**, 1187 (2004).
[73] J. Heyd, G. E. Scuseria, and M. Ernzerhof, J. Chem. Phys. **124**, 219906 (2006).
[74] N. W. Ashcroft and N. David Mermim, Solid State Physics, Saunders College Publishing, 1976.
[75] P. E. Blöchl, Phys. Rev. B **50**, 17953 (1994).
[76] G. Kresse and J. Hafner, Phys. Rev. B **47**, R558 (1993).
[77] G. Kresse and D. Joubert, Phys. Rev. B **59**, 1758 (1999).
[78] D. Vanderbilt, Phys. Rev. B **41**, 7892 (1990).
[79] S. Cottenier, Density Functional Theory and the family of (L)APW-method a step-by-step introduction (Instituut voor kern-en Stralingsfysica, K. U. Leuven, Belgium), 2002, ISBN 90-807215-1-4 (to be found at http://www.wien2k.at/reg-user/textbooks).
[80] M. Gajdos, K.Hummer, and G.Kresse, Phys .Rev B **73**, 045112 (2006).
[81] P. P. Edwards and F. Hensel, Nature **388**, 621 (1997).
[82] I. F. Silvera and J. W. Cole, Journal of Physics: Conference Series **215**, 012194 (2010).
[83] J. Yang, A. Sudik, C. Wolverton and D. J. Siegel, Chem. Soc. Rev. **39**, 656 (2010).
[84] F. H. Stephens, V. Pons and R. Tom Baker, Dalton Trans. **25**, 2613 (2007).
[85] A. C. Stowe, W. J. Shaw, J. C. Linehan, B. Schmid, and T. Autrey, Phys. Chem. Chem. Phys. **9**, 1831 (2007).
[86] Z. Xiong, C. K. Yong, G. Wu, P. Chen, W. Shaw, A. Karkamkar, T. Autrey, M. O. Jones, S. R. Johnson, P. P. Edwards and W. I. F. David, Nat. Mater. **7**, 138 (2008).
[87] H. Wu, W. Zhou and T. Yildirim, J. Am. Chem. Soc. **130**, 14834 (2008).

[88] A. T. Luedtke, A. T. and T. Autrey, Inorg. Chem. **49**, 3905 (2010).
[89] H. V. K. Diyabalanage, R. P. Shrestha, T. A. Semelsberger, B. L. Scott, M. E. Bowden, B. L. Davis and A. K. Burrell, Angew. Chem., Int. Ed. **46**, 8995 (2007).
[90] H. V. K. Diyabalanage, T. Nakagawa, R. P. Shrestha, T. A. Semelsberger, B. L. Davis, B. L. Scott, A. K. Burrell, W. I. F. David, K. R. Ryan, M. O. Jones and P. P. Edwards, J. Am. Chem. Soc. **132 (34)**, 11836 (2010).
[91] K. Shimoda, K. Doi, T. Nakagawa, Y. Zhang, H. Miyaoka, T. Ichikawa, M. Tansho, T. Shimizu, A. K. Burrell and Y. Kojima, J. Phys. Chem. C **116**, 5957 (2012).
[92] R. V. Genova, K. J. Fijalkowski, A. Budzianowski and W. Grochala, J. Alloys. Compd. **499**, 144 (2010).
[93] Q. Zhang, C. Tang, C. Fang, F. Fang, D. Sun, L. Ouyang and M. Zhu, J. Phys. Chem. C **114**, 1709 (2010).
[94] Y. Guo, G. Xia, Y. Zhu, L. Gao and X. Yu, Chem. Commun. **46**, 2599 (2010).
[95] H. L. Chu, G. T. Wu, Z. T. Xiong, J. P. Guo, T. He and P. Chen, Chem. Mater. **22**, 6021 (2010).
[96] G. Soloveichik, J. H. Her, P. W. Stephens, Y. Gao, J. Rijssenbeek, M. Andrus and J. C. Zhao, Inorg. Chem. **47**, 4290 (2008).
[97] Y. Guo, H. Wu, W. Zhou, and X. Yu, J. Am. Chem. Soc. **133**, 4690 (2011).
[98] H. Wu, W. Zhou, F. E. Pinkerton, M. S. Meyer, Q. Yao, S. Gedipelli, T. J. Udovic, T. Yildirim and J. J. Rush, Chem. Commun. **47**, 4102 (2011).
[99] K. J. Fijalkowski, R. V. Genova, Y. Filinchuk, A. Budzianowski, M. Derzsi, T. Jaron, P. J. Leszczynski and W. Grochala, Dalton. Trans. **40**, 4407 (2011).
[100] Y. S. Chua, Z. Wu, Z. Xiong, A. Karkamkar, J. Guo, M. Jian, M. W. Wong, T. Autrey and P. Chen, Chem. Commun. **46**, 5752 (2010).
[101] Y. S. Chua, Z. Wu, Z. Xiong, T. He and P. Chen, Chem. Mater. **21**, 4899 (2009).
[102] M. Ramzan, F. Silvearv, A. Blomqvist, R. H. Scheicher, S. Lebègue, and R. Ahuja, Phys. Rev. B **79**, 132102 (2009).
[103] R. F. W. Bader, ``Atoms in Molecules: A Quantum Theory (International Series of Monographs on Chemistry''), edited by Clarendon Press, Oxford (1990).
[104] G. Henkelman, A. Arnaldsson, and H. Jonsson, Comp. Mat. Science **36**, 354 (2006).
[105] E. Sanville, S. D. Kenny, R. Smith, and G. Henkelman, J. Comp. Chem. **28**, 899 (2007).
[106] A. D. Becke and K. E. Edgecombe, J. Chem. Phys. **92**, 5397 (1990).
[107] W. L. Mao. and H. K. Mao, Proc. Natl. Acad. Sci. USA. **101**, 708-710 (2004).
[108] M. Ramzan, T. Hussain, and R. Ahuja, Appl. Phys. Lett. **101**, 111902 (2012).

[109] M. Ramzan and R. Ahuja, J. Phys. Chem. Sol. **71**, 1137 (2010).
[110] W. T. Klooster, T. F. Koetzle, P. E. M. Siegbahn, T. B. Richardson, and R. H. Crabtree, J. Am. Chem. Soc. **121**, 6337 (1999).
[111] N. J. Hess, G. K. Schenter, M. R. Hartman, L. L. Daemen, T. Proffen, S. M. Kathmann, C. J. Mundy, M. Hartl, D. J. Heldebrant, A. C. Stowe, and T. Autrey, J. Phys. Chem. A, **113**, 19, 5723-5735 (2009).
[112] Y. Lin, W. L. Mao, V. Drozd, J. Chen, and L. L. Daemen, J. Chem. Phy. **129**, 234509 (2008).
[113] Muhammad Ramzan, Fredrik Silvearv, Sèbastien Lebègue, and Rajeev Ahuja, J. Phys. Chem. C **114**, 20036 (2011).
[114] Muhammad Ramzan and Rajeev Ahuja, J. Phys. Chem. C **116**, 17351 (2012).
[115] C. F. Hoon, and E. C. Reynhardt, J. Phys. C **16**, 6137 (1983).
[116] M. E. Bowden, G. J. Gainsford, and W. T. Robinson, Aust. J. Chem. **60**, 149 (2007).
[117] J. B. Yang, J. Lamsal, Q. Cai, W. J. James, and W. B. Yelon, Appl. Phys. Lett. **92**, 091916 (2008).
[118] L. Schlapbach and A. Zuttel, Nature (London) 414, 23 (2001).
[119] G. W. Crabtree, M. S. Dresselhaus, and M. V. Buchanan, Phys. Today **40**, 39 (2004).
[120] W. Grochala and P. P. Edwards, Chem. Rev. (Washington, D.C.) **104**, 128 (2004).
[121] B. C. Hauback, H. W. Brinks, C. M. Jensen, K. Murphy, and A. J.Maeland, J. Alloys Compd. **358**, 142 (2003).
[122] A. Zuttel, P. Wenger, S. Rentsch, P. Sudan, P. Mauron, and C. Emmenegger, J. Power Sources **118**, 1 (2003).
[123] J. K. Kang, S. Y. Kim, Y. S. Han, R. P. Muller, and W. A. Goddard, Appl. Phys. Lett. **87**, 111904 (2005).
[124] H. Smithson, A. Marianetti, D. Morgan, A. Van der Ven, A. Predith, M. Ceder, Phys. ReV. B **66**, 144107 (2002).
[125] A. Zuttel, A. Borgschulte, S. Orimo, I. Scr. Mater., 56, 823 (2007).
[126] A. Borgschulte, A. Zuttel, P. Hug, A.-M. Racu, and J. Schoenes, J. Phys. Chem. A **112**, 4749 (2008).
[127] M. Ramzan and R. Ahuja, Appl. Phys. Lett. **94**, 141903 (2009).
[128] M. Ramzan and R. Ahuja, J. Appl. Phys. **106**, 016104 (2009).
[129] J. Hout, G. Liang, S. Boily, A. Van Neste, and R. Schulz, J. Alloys Compd. **293**, 495 (1999).
[130] G. Liang, J. Hout, S. Boily, A. Van Neste, and R. Schulz, J. Alloys Compd. **292**, 247 (1999).
[131] J. L. Bobet, B. Cheavlier, B. Darriet, and J. Etourneau, J. Alloys Compd. **336**, 292 (2002).
[132] N. Hanada, T. Ichikawa, and H. Fujii, J. Phy. Chem. B **109**, 7188 (2005).
[133] P. Larsson, C. M. Araujo, J. A. Larsson, P. Jena, and R. Ahuja, PNAS **105, (24)**, 8227 (2008).
[134] S. Cheung, W. Deng, Duin Act van and W. A. Goddard, J. Phy. Chem. A **109**, 851 (2005).

[135] L. H. Liang, G. W. Yang and B. Li, J. Phy. Chem. B **109**, 16081 (2005).
[136] R. Wagemans, J. H. Lenthe van, P. E. Jongh de, A. J. Dillen van and K. P. Jong de, J. Am. Chem. Soc. **127**, 16675 (2005).
[137] M. Ramzan, T. Hussain, and R. Ahuja, Appl. Phys. Lett. **94**, 221910 (2009).
[138] M. Ramzan, S. Lebègue, and R. Ahuja, Int. J. Hydrogen Energy **35**, 10373 (2010).
[139] J. O. Sofo, A. S. Chaudhari, and G. D. Barber, Phys. Rev. B **75**, 153401 (2007).
[140] D. C. Elias, R. R. Nair, T. M. G. Mohiuddin, S. V. Morozov, P. Blake, M. P. Halsall, A. C. Ferrari, D. W. Boukhvalov, A. K. Geim, and K. S. Novoselov, Science **323**, 610 (2009).
[141] G. Kim, S. Jhi, S. Lim, and N. Park, Appl. Phys. Lett. **94**, 173101 (2009).
[142] T. Hussain, B. Pathak, M. Ramzan, T. A. Maark, and R. Ahuja, Appl.Phys. Lett. **100**, 183902 (2012).
[143] T. Hussain, B. Pathak, T. A. Maark, C. M. Araujo, R. H. Scheicher, and R. Ahuja, Europhys. Lett. **96**, 27013 (2011).
[144] T. Hussain, B. Pathak, T. A. Maark, M. Ramzan and R. Ahuja, Europhys. Lett. **99**, 47004 (2012).
[145] S. Wang, H. Mao, X. Chen, and W. L. Mao, Proc. Natl. Acad. Sci. USA. **106**, 14763-14767 (2009).
[146] N. W. Ashcroft, Phys Rev Lett. **92**,187002 (2004).
[147] X. J. Chen *et al.* Proc Natl Acad Sci USA **105**, 20 (2008).
[148] M. I. Eremets, I. A. Trojan, S. A. Medvedev, J. S. Tse, Y. Yao, Science **319**, 1506 (2008).
[149] W. L. Mao, C. A. Koh, and E. D. Sloan, Physics Today, 42 (2007).
[150] W. L. Mao and H. K. Mao, Proc Natl Acad Sci USA **101** 708 (2004).
[151] T. A. Strobel, M. Somayazulu, and R. J. Hemley, Phys. Rev. Lett. **103**, 065701 (2009).
[152] M. Ramzan, S. Lebègue, and R. Ahuja, Phys. Rev. B **81**, 233103 (2010).
[153] Sèbastien Lebègue, C. Moysés Araújo, D. Y. Kim, Muhammad Ramzan, H.-K. Mao and Rajeev Ahuja
Proc. Natl. Acad. Sci. USA (PNAS) **109**, 9766 (2012).
[154] H. Liu, L. Zhu, W. Cui, and Y. Ma, J. Chem. Phys. **137**, 074501 (2012).
[155] B. Baranowski, Physica B **16**, 265 (1999).
[156] R. W. Kates, W. C. Clark, R. Correll, J. M. Hall, C. C. Jaeger, and I. Lowe, Science **292**, 641 (2001).
[157] N. Armaroli and V. Balzani, Angew. Chem., Int. Ed. **46**, 52 (2007).
[158] A. G. Nazri and G. Pistoia, Lithium Batteries: Science and Technology (Kluwer Academic/Plenum, Boston), 496 (2004).
[159] A. K. Padhi, K. S. Nanjundaswamy, and J. B. Goodenough, J. Electrochem. Soc. **144**, 1188 (1997).
[160] J. Barker and M. Y. Saidi, U. S. Pat. **5**, 866 (1999).

[161] M. Dutreilh, C. Chevalier, C. M. El-Ghozzi, and D. Avignant, J. Solid State Chem. **142**, 15 (1999).
[162] J. Barker, M. Y. Saidi, and J. L. Swoyer, Electrochem. Solid-State Lett. **6**, A1 (2003).
[163] S. C. Yin, R. Edwards, N. Taylor, P. S. Herle, and L. F. Nazar, Chem. Mater. **18**, 1745 (2006).
[164] B. L. Ellis, W. R. M. Makahnouk, Y. Makimura, K. Toghill and L. F. Nazar, Nature Mat. **6**, 749 (2007).
[165] M. Ramzan, S.Lebègue, and R. Ahuja, Appl. Phys. Lett. **94**, 151904, (2009).
[166] Muhammad Ramzan and Rajeev Ahuja, Eurphys. Lett. **87**, 18001 (2009).
[167] Muhammad Ramzan, Sèbastien Lebègue, Peter Larsson and Rajeev Ahuja, J. Appl. Phys. **106**, 043510 (2009).
[168] N. Recham, J-N. Chotard, L. Dupont, C. Delacourt, W. Walker, M. Armand, and J-M. Tarascon, Nature Mat. **9**, 68 (2010).
[169] M. Ramzan, S.Lebègue, and R. Ahuja, Phys. Rev. B **82**, 125101 (2010).
[170] Muhammad Ramzan, Sèbastien Lebègue, Tae W. Kang and Rajeev Ahuja, J. Phys. Chem. C **115**, 2600 (2011).
[171] V. L. Chevrier, S. P. Ong, R. Armiento, M. K. Y. Chan, and G. Ceder, Phys. Review B **82**, 075122 (2010).
[172] M. Hayashi, H. Arai, H. Ohtsuka and Y. Sakurai. J. Power Sources **119**, 617 (2003).
[173] P. Novak, R. Imhof and O. Haas, Electrochim. Acta **45**, 351 (1999).
[174] J. M.Tarascon and M. Armand, Nature, **414**, 359 (2001).
[175] T. S. Arthur, N. Singh and M. Matsui, Electrochem. Commun. **16**, 103 (2012).
[176] D. Aurbach, Z. Lu, A. Schechter, Y. Gofer, H. Gizbar, R. Turge- man, Y. Cohen, M. Moshkovich, and E. Levi, Nature **407**, 724 (2000).
[177] N. Singh, T. S. Arthur, C. Ling, M. Matsui and F. Mizuno, Chem. Commun. **49**, 149 (2013).
[178] M. A. Pietzka and J. C. Schuster, J. Phase Equilib. **15(4)**, 392 (1994).
[179] M. W. Barsoum, L. Farber, I. Levin, A. Procopio, T. El-Raghy, and A. Berner, J. Am. Ceram. Soc. **82**, 2545 (1999).
[180] B. Holm, R. Ahuja, and B. Johansson, Appl. Phys. Lett. **79**, 10 (2001).
[181] P. Finkel, B. Seaman, K. Harrell, J. Palma, J. D. Hettinger, S.E. Lofland, A. Ganguly, M. W. Barsoum, Z. Sun, S. Li, and R. Ahuja, Phys. Rev. B **69**, 1 (2004).
[182] M. W. Barsoum, A. Murugaiah, S. R. Kalidindi, and T. Zhen, Phys. Rev. Lett. **92**, 255508 (2004).
[183] S. Li, R. Ahuja, M. W. Barsoum, P. Jena, and B. Johansson, Appl. Phy. Lett. **92**, 221907 (2008).
[184] M. Ramzan, S.Lebègue, and R. Ahuja, Appl. Phy. Lett. **98**, 021902 (2011).
[185] W. B. Pearson, The Crystal Chemistry and Physics of Metals and

Alloys (Wiley-Interscience, New York, 1972), pp. 502 and 518.
[186] P. Finkel, M. W. Barsoum and T. El-Raghy, J. Appl. Phy., **87**, 1701-1703 (2000).
[187] B. Manoun, F. X. Zhang, S. K. Saxena, T. El-Raghy, and M. W. Barsoum, J. of Phys. and Chem. of Solids, **67**, 2091-2094 (2006).
[188] A. Onodera, H. Hirano, T. Yuasa, N. F. Guo, and Y. Miyamoto, Appl. Phy. Lett. **74**, 3782 (1999); Abstracts, AIRAPT- 17th International Conference on High Pressure Science and Technology, Honolulu, Hawai, July 25-30 (1999).
[189] M. W. Barsoum, C. J. Rawan, T. El-Raghy, and A. T. Procopio, W. D. Porter, H. Wang, and C. R. Hubbard, J. Appl. Phy., **87**, No.12 (2000).
[190] B. Manoun, R. P. Gulve, S. K. Saxena, S. Gupta, M. W. Barsoum, and C. S. Zha, Phys. Rev. B, **73**, 024110 (2006).
[191] B. Manoun, S. Amini, S. Gupta, S. K. Saxena, and M. W. Barsoum, J. Phys. Condens. Matter., **19**, 456218 (2007).
[192] Y. Zhou and Z. Sun, Mat. Res. Innovat., **3**, 286-291 (2000).
[193] W. Jeitschko and H. Nowotny, Monatsch Chem., **98**, 329 (1967).
[194] J. D. Hettinger, S. E. Lofland, P. Finkel, T. Meehan, J. Palma, K. Harrel, S. Gupta, A. Ganguly, T. El-Raghy, and M. W. Barsoum, Phys. Rev. B, **72**, 115120 (2005).
[195] M. Ramzan and R. Ahuja, Appl. Phy. Lett. **96**, 261906 (2010).
[196] M. Ramzan, S.Lebègue, and R. Ahuja, Phys. Status Solidi (RRL) **5**, 122 (2011).
[197] M. Ramzan, S.Lebègue, and R. Ahuja, Solid Stat. Commun. **152**, 1147 (2012).
[198] N. A. Phatak, S. R. Kulkarni, V. Drozd, S. K. Saxena, L. Deng, Y. W. Fei, J. Z. Hu, W. Luo, and R. Ahuja, J. Alloys Compd. **463**, 220 (2008).
[199] L. Huang, M. Ramzan, L. Vitos, B. Johansson, and R. Ahuja, J. Phys. Chem. Sol. **71**, 1065 (2010).
[200] V. L. Moruzzi and J. F. Janak, and K. Schwarz, Phys. Rev. B **37**, 790 (1988).
[201] A. Amézaga, E. Holmström, R. Lizárraga, E. Menendez-Proupin, P. Bartolo-Perez and P. Giannozzi, Phys. Rev. B **81**, 014210 (2010).
[202] R. Lizárraga, E. Holmström, A. Amézaga, N. Bock, T. Peery, E. Menendez-Proupin and P. Giannozzi, J. Mater. Sci. **18**, 5071 (2010).
[203] R. Lizárraga, E. Holmström, C. Parker and C. Arrouvel, Phys. Rev. B **83**, 094201 (2011).
[204] C. Århammar, A. Pietzsch, N. Bock, E. Holmström, C. M. Araujo, J. Gråsjö, S. Zhao, S. Green, T. Peery, F. Hennies, S. Amerioun, A. Föhlisch, J. Schlappa, T. Schmitt, V. N. Strocov, G A. Niklasson, D. C. Wallace, J.-E. Rubensson, B. Johansson and R. Ahuja, Proc. Natl. Acad. Sci. U.S.A., **108**, 6355 (2011).
[205] N. Bock, E. Holmström, T. B. Peery, R. Lizárraga, E. D. Chisolm, G. De Lorenzi-Venneri and D. C. Wallace, Phys. Rev. B **82**, 144101 (2010).
[206] R. Lizàrraga, M. Ramzan, C. M. Araújo, A. Blomqvist, R. Ahuja and

E. Holmström, Eur. Phys. Lett. **99**, 57010 (2012).
[207] M. Stromme, R. Ahuja and G. A. Niklasson, Phys. Rev. Lett. **93**, 206403/1 (2004).
[208] G. A. Niklasson, R. Ahuja and M. Stromme, Mod. Phys. Lett. B **20**, 863 (2006).
[209] J.W. Palko, W.M. Kriven, S.V. Sinogeikin, J.D. Bass, A. Sayir, J. Appl. Phys. **89**, 7791 (2001).
[210] T. Tomiki, J. Tamashiro, Y. Tanahara, A. Yamada, H. Fukutani, T. Miyahara, H. Kato, S. Shin, M. Ishigame, J. Phys. Soc. Jpn. **55**, 4543 (1986).
[211] M. Ramzan, Y. Li, R. Chimata, R. Ahuja, Comp. Mater. Sci. **71**, 19 (2013).
[212] J. Ederth, P. Johnsson, G. A. Niklasson, A. Hoel, A. Hultåker, P. Heszler, C. G. Granqvist, A. R. van Doorn, M. J. Jongerius, D. Burgard. Phys. Rev. B **68**, 155410 (2003).
[213] G. Burns and B. A. Scott, Phys. Rev. Lett. **25**,167 (1970).
[214] J. A. Sanjurjo, E. López-Cruz, and G. Burns, Phys. Rev. B **28**, 7260 (1983).
[215] G. Shirane, S. Hoshino, and K. Suzuki, Phys. Rev. **80**, 1105 (1950).
[216] M. E. Lines and A.M.Glass, Principles and Applications of Ferroelectrics and Related Materials (Clarendon Press, Oxford, 1977).
[217] K. Uchino, Piezoelectric Acutuators and Ultrasonic Motors (Kluwer Academic, Boston, 1996).
[218] P. E. Janolin, P. Bouvier, J. Kreisel, P. A. Thomas, I. A. Kornev, L. Bellaiche, W. Crichton, M. Hanfland, and B. Dkhil, Phys. Rev. Lett. **101** (2008).
[219] D. Cahen and J. A. Ibers, J. Catal. **31**, 369 (1973).
[220] N. Seriani, W. Pompe, and L. C. Ciacchi, J. Phys. Chem. B **110**, 14860 (2006).
[221] K. Kuribayashi and S. Kitamura, Thin Solid Films **400**, 160 (2001).
[222] M. H. Kim, T. S. Park, D. S. Lee, and E. Yoon, J. Mater. Res. **14**, 634 (1999).
[223] W. J. Moore and L. Pauling, J. Am. Chem. Soc. **63**, 1392 (1941).
[224] J. Waser and E. D. McClanahan, J. Chem. Phys. **19**, 413 (1951).
[225] N. A. Shishakov, Sov. Phys. Crystallogr. 2, 677 (1957).
[226] O. Muller and R. Roy, J. Less Common Met. **16**, 129 (1968).
[227] M. P. H. Fernandez and B. L. Chamberland, J. Less Common Met. **99**, 99 (1984).
[228] K.-J. Range, F. Rau, U. Klement, and A. M. Heyns, Mater. Res. Bull. **12**, 1541 (1987).
[229] K. C. Hass and A. E. Carlsson, Phy. Rev. B **46**, 4246 (1992).
[230] K. T. Park, D. L. Novikov, V. A. Gubanov, and A. J. Freeman, Phy. Rev. B **49**, 4425 (1994).
[231] R. Ahuja, S. Auluck, B. Johansson, M. Khan, Phy. Rev. B **50**, 2128 (1994).
[232] Jamal Uddin, Juan E. Peralta, and Gustavo E. Scuseria, Phy. Rev. B

71, 155112 (2005).
[233] N. Seriani, Z. Jin, W. Pompe and L. Colombi Ciacchi, Phy. Rev. B **76**, 155421 (2007).
[234] R. K. Nomiyama, M. J. Piotrowski and J. L. F. Da Silva, Phy. Rev. B **84**, 100101(R) (2011).
[235] T. Kaewmaraya, Muhammad Ramzan, W. Sun, M. Sagynbaeva and Rajeev Ahuja, Comput. Mater. Sci. 10.1016/j.commatsci.2013.07.021.
[236] J.S.O.Evans, Z.Hu, J.D.Jorgensen, D.N.Argyriou, S.Short and A.W.Sleight, Science 275, 61 (1997).
[237] A.W.Sleight, Current Opinion in Solid State and Materials Science 3, 128 (1998).
[238] F. R. Drymiotis, H. Ledbetter, J. B. Betts, T. Kimura, J. C. Lashley, A. Migliori, A. Ramirez, G. Kowach, J. Van Duijn, Phys. Rev. Lett. 93, 025502 (2004).
[239] J.S.O.Evans, W.I.F.David and A.W.Sleight, Acta Cryst. B55, 333 (1999).
[240] T.A.Mary, J.S.O.Evans, T.Vogt and A.W.Sleight, Science 272, 90 (1996).
[241] G.Ernst, C.Broholm, G.R.Kowach and A.P.Ramirez, Nature 396, 147 (1998).
[242] A.P.Ramirez and G.R.Kowach, Phys. Rev. Lett. 80, 4903 (1998).
[243] C.A.Perottoni and J.A.H. da Jornada, Science 280, 886 (1998).
[244] A.K.A.Pryde, K.D.Hammonds, M.T.Dove, V.Heine, J.D. Gale and M.C.Warren, J.Phys.:Condens. Matter 8, 10973 (1996).
[245] R.Mittal and S.L.Chaplot, Phys. Rev. B60, 7234 (1999).
[246] N.L.Allan, G.D.Barrera, J.A.Purton, C.E.Sims and M.B.Taylor, Phys. Chem. Chem. Phys. 2, 1099 (2000).
[247] T.R.Ravindran, A.K.Arora and T.A.Mary, Phys. Rev. B67, 064301 (2003).
[248] D.Cao, F.Bridges, G.R.Kowach and A.P.Ramirez, Phys. Rev. Lett. 89, 215902 (2002).
[249] D.Cao, F.Bridges, G.R.Kowach and A.P.Ramirez, Phys. Rev. B68, 014303 (2003).
[250] M. Ramzan, W. Luo, R. Ahuja, J. Appl. Phys. **109**, 033510 (2011).
[251] M. Wuttig, Nat. Mater. **4**, 265 (2005).
[252] M. H. R. Lankhorst, B. W. S. M. M. Ketelaars, and R. A. M. Wolters, Nat. Mater. **4**, 347 (2005).
[253] A. L. Greer and N. Mathur, Nature (London) **437**, 1246 (2005).
[254] H. F. Hamann, M. O. Boyle, Y. C. Martin, M. Rooks, and H. K. Wickramasinghe, Nat. Mater. **5**, 383 (2006).
[255] S. L. Wang, C. Y. Chen, M. K. Hsieh, W. C. Lee, A. H. Kung, and L.H. Peng, Appl. Phys. Lett. 94, 113503 (2009).
[256] Muhammad Ramzan, T. Kaewmaraya, and R. Ahuja, Appl. Phys. Lett. **103**, 072113 (2013).
[257] Thanayut Kaewmaraya, Muhammad Ramzan, H. Lofas, and Rajeev Ahuja, J. Appl. Phys. **113**, 033510 (2013).

[258] J. W. Park, S. H. Eom and H. Lee, Phys. Rev. B **80**, 115209 (2009).
[259] B. S. Lee, J. R. Abelson, S. G. Bishop, D. H. Kang, B. K. Cheong, and K. B. Kim, J. Appl. Phys. **97**, 093509 (2005).
[260] J. Sinova and I. Zutić, Nature Mater. **11**, 368 (2012).
[261] T. Dietl, Nature Mater. **9**, 965 (2010).
[262] I. Zutić, J. Fabian, and S. Das Sarma, Rev. Mod. Phys. **76**, 323 (2004).
[263] D. D. Awschalom and M. E. Flatté, Nature Phys. **3**, 153 (2007).
[264] H. Ohno, Science **281**, 951 (1998).
[265] M. Csontos, G. Mihály, B. Jankó, et al. Nature Mater. **4**, 447 (2005).
[266] M. Csontos, T. Wojtowicz, X. Liu, et al. Phys. Rev. Lett. **95**, 227203 (2005).
[267] M. Gryglas-Borysiewicz, et al. Phys. Rev. B **82**, 153204 (2010).
[268] F. Gronwold, H. Haraldsen, B. Pedersen, T. Tufle, Rev. Chim. Mine´ral **6** 215 (1969).
[269] A.B. de Vries, F. Jellinek, Rev. Chim. Mine´ral **11**, 624 (1974).
[270] T. Othani, S. Onoue, Mater. Res. Bull. **21**, 69 (1986).
[271] M. R. Harrison and M. G. Francesconi, Coord. Chem. Rev. **255**, 451 (2011).
[272] R. Münch, H. D. Hochheimer, A. Werner, G. Materlik, A. Jayaraman and K. V. Rao, Phys. Rev. Lett. **50**, 1619 (1983).
[273] H. D. Hochheimer and R. Münch, Phil. Mag. B **63**, 979 (1991).
[274] Muhammad Ramzan and Rajeev Ahuja, Appl. Phys. Lett. **99**, 221904 (2011).
[275] A. B. Garg, V. Vijayakumar, B. K. Godwal, T. Ohtani, B. R. Martin and H. D. Hochheimer, Solid State Commun. **132**, 731 (2004).
[276] H. D. Hochheimer, C. F. Miclea, P. Modak, A. K. Verma, R. S. Rao and T. Ohtani, J. Phys: Conference Series **121**, 032013 (2008).

Acta Universitatis Upsaliensis

Digital Comprehensive Summaries of Uppsala Dissertations from the Faculty of Science and Technology 1062

Editor: The Dean of the Faculty of Science and Technology

A doctoral dissertation from the Faculty of Science and Technology, Uppsala University, is usually a summary of a number of papers. A few copies of the complete dissertation are kept at major Swedish research libraries, while the summary alone is distributed internationally through the series Digital Comprehensive Summaries of Uppsala Dissertations from the Faculty of Science and Technology.

Distribution: publications.uu.se
urn:nbn:se:uu:diva-205243

ACTA
UNIVERSITATIS
UPSALIENSIS
UPPSALA
2013